Design and Evaluation of Bispecific T cell Engaging Antibodies for the Treatment of Neuroblastoma

Alyssa Noll

A dissertation submitted in partial fulfillment of the requirements for the degree of

Doctor of Philosophy

University of Washington

2024

Reading Committee:

James Olson, Chair

Mark Headley

Jonathan Cooper

Program Authorized to Offer Degree:

Molecular and Cellular Biology

University of Washington

Abstract

Design and Evaluation of Bispecific T cell Engaging Antibodies for the Treatment of Neuroblastoma

Alyssa Noll

Chair of the Supervisory Committee:

James Olson

Department of Molecular and Cellular Biology

Neuroblastoma, a cancer of the sympathetic nervous system, is the most common extracranial solid tumor in children, representing 10% of all pediatric malignancies. Despite aggressive treatment with intensive multi-modal therapies, most children with high-risk neuroblastoma will relapse, so novel therapeutic approaches are desperately needed. Immunotherapies have risen to the forefront of cancer treatments, exemplified by the ability of checkpoint inhibitors to induce anti-tumor responses in adult cancers refractory to conventional treatments. However, children with cancer, including those with neuroblastoma, have failed to benefit from these advances, attributed to intrinsic mechanisms of immune evasion. Thus, neuroblastoma presents a challenge that may serve as a model for the application of immunotherapies for other “immunologically cold” pediatric tumors.

Bispecific T cell engaging antibodies are engineered proteins designed to simultaneously bind a tumor specific antigen and CD3 on T cells, thereby instructing

endogenous lymphocytes to destroy the bridged tumor cell. Bispecific T cell Engagers (BTEs) are a rapidly evolving approach to treating cancer, with the number of clinically approved BTEs jumping from 1 to 8 since 2022. Although one BTE, blinatumomab, has improved outcomes in pediatric leukemia, the application of BTEs to pediatric solid tumors has proved challenging in part due to a scarcity of tumor-specific antigens.

To identify potential neuroblastoma antigens suitable for BTE immunotherapy, we screened a diverse panel of neuroblastoma cell lines and identified B7H3, a surface protein with reported roles in immune evasion, as a candidate target. B7H3 overexpression was validated in high-risk neuroblastoma patient samples compared to adjacent peripheral tissues.

Although there are over 100 distinct BTEs in preclinical development, few published works have directly compared different BTE designs and CD3 engagers. We designed, produced, and evaluated a suite of unique B7H3-CD3 BTEs to investigate the role of BTE architecture and CD3 affinity on the function of BTEs in vitro. We found that IgG-like BTEs with anti-CD3 scFvs linked to the carboxy-termini of the IgG light chains mediated potent anti-tumor activity in vitro, attributed to their bivalency for both B7H3 and CD3. This format, termed IgG-L-scFv, demonstrated an increase in potency with an increase in CD3 affinity, and yet demonstrated strictly target-dependent activity. From these studies, we identified a $B7H3^{MGA271}$-$CD3^{ADI24}$ IgG-L-scFv as the lead candidate BTE. Despite the promising potency of this molecule in functional assays, in neuroblastoma xenograft models, we found that efficacy was limited by insufficient recruitment of T cells in circulation. This finding highlights a crucial barrier to the application of BTEs and other T-cell targeting immunotherapies to neuroblastoma and by extension other pediatric solid tumors. A deeper understanding of the mechanisms regulating T cell trafficking may guide future development of immunotherapeutic strategies for children with high-risk neuroblastoma.

Table of Contents

Table of Figures

List of Supplemental Tables

Acknowledgements

I feel incredibly fortunate to have several mentors who have contributed to my growth as a scientist, future physician, and as a person. Dr. Olson, thank you for taking me in as a student. Your encouragement to pursue interesting and impactful scientific questions and seek understanding for its own sake has shaped me as a scientist. Our discussions constantly challenged me to think more critically. Dr. Vitanza, thank you for your continued mentorship and invaluable guidance. I appreciate that you have always kept your door open to me and that you encourage my involvement in DMG research. I look forward to continuing to work and learn from you. Dr. Michelle Monje, although I have graduated from your lab, you continue to inspire me. Thank you for encouraging me as a young college student to pursue this path. You are a fantastic model for women physician-scientists, and I am lucky to have learned from you directly. To my committee members, thank you all for your helpful feedback and encouragement. I also would like to thank each member of the Olson Lab, past and present. Shelli, from the first day I stepped foot in the lab, you have always taken the time to teach me. Thank you for teaching me so much of what I have learned; this PhD would have been immeasurably more difficult without you. You are a selfless and patient teacher and an exemplary scientist. Matt and Ken, thank you both for your willingness to share your knowledge and expertise, I always enjoy learning from you. Kristina, thank you for teaching me how to produce proteins and for making the lab such an enjoyable place to hang out, learn, and fail together. There is no one I would rather split 96 T225 flasks in one day with. Jason P, thank you for always looking over my designs and providing feedback and hilarious conversations. Emily, thank you for being so generous with your time, I look up to you as a model of scientific efficacy. I would also like to directly thank every person who contributed data to this thesis, Alison, Akinsola, Bianka, Chunfeng, Ray, Kristina, Jason, Steven, thank you for your help with protein productions. Emily, Lisa, and Heather, thank you for always providing help with in vivo studies. You three made the vivarium an enjoyable place to be. Dr. Erin Crotty, thank you for your advice and friendship, you exemplify the qualities I wish to

become as a physician. Thank you to the entirety of the MSTP and MCB programs for making graduate school and positive and productive experience. I also want to thank my family, my parents and sister who have always been steadfast supporters throughout my life, I am lucky to always be able to count on you. And finally, I want to thank my husband Jordan, for always encouraging me to dream big.

1. B7H3 is a Promising Target for Bispecific T cell Engager Immunotherapy for Neuroblastoma

Abstract

Children with high-risk neuroblastoma face poor outcomes despite treatment with intensive multi-modal therapies. While Anti-GD2 monoclonal antibodies have shown clinical efficacy in neuroblastoma by relying on Fc-dependent activation of the innate immune system, this therapy is associated with dose-limiting pain and is not curative. T cell-engaging bispecific antibodies have shown clinical potential in pediatric hematological malignancies but have yet to demonstrate success in pediatric solid tumors. The development of novel bispecific T cell engagers (BTEs) for the treatment of pediatric solid tumors has been hampered in part by the limited number of differentially expressed surface antigens that can be safely targeted. Here, we identify B7H3 as a candidate immunotherapeutic target in neuroblastoma. We demonstrate that B7H3 is highly expressed on most neuroblastomas and minimally expressed in normal pediatric tissues. In addition, we provide evidence that loss of B7H3 expression slows the growth of neuroblastoma cultures in vitro and that diminished B7H3 expression is associated with a more favorable histology in patient tissue samples. This work serves as a foundation for the development of B7H3-directed bispecific T cell engaging antibodies for the treatment of neuroblastoma.

Introduction

Neuroblastoma: an overview

Epidemiology

Neuroblastoma, the most common extracranial solid tumor in children, is a neuroendocrine tumor that arises from sympathoadrenal progenitor cells. With over 600 new cases diagnosed each year, neuroblastoma represents 8-10% of all pediatric malignancies, and 15% of pediatric cancer-driven mortality[1]. Neuroblastoma is the most common cancer diagnosed in infants, with an incidence rate of 58 cases per 1 million[2]. The prevalence of neuroblastoma decreases with increasing age, rarely occurring in children older than 15 years[1,3].

Pathophysiology

Neuroblastoma develops from neural crest-derived progenitor cells that undergo malignant transformation[4]. The neural crest is a collection of multipotent stem cells located in the neural tube. During neurulation, these cells migrate throughout the embryo, giving rise to a diverse array of cell types. A subset of neural crest cells commits to a sympathoadrenal lineage and differentiates into either adrenal chromaffin cells, which establish the adrenal medulla, or sympathetic ganglia, which are distributed bilaterally from the spinal cord[5]. Consequently, neuroblastoma tumors may form in any of these locations, causing a wide range of clinical presentations that can make differential diagnosis of the disease challenging.

The adrenal medulla is the most common primary tumor site (40%)[1,6]. While adrenal tumors may be asymptomatic at the time of diagnosis, they may also cause symptoms of hypertension, abdominal distension, and pain[1,6]. The next most common locations are in sympathetic ganglia of the abdomen (25%), thorax (15%), cervical spine (5%) and pelvis (5%)[1,6]. Vessel and nerve compression at these sites can cause distressing and urgent symptoms such as Horner's syndrome, respiratory distress, urinary retention, or paralysis[6]. While low-grade tumors may be straightforwardly removed through surgery, high-grade tumors are extremely

infiltrative and difficult to fully resect. Half of patients at the time of diagnosis present with metastatic disease[1]. Neuroblastomas metastasize through lymphatic and hematopoietic spread to bone marrow (71%), cortical bone (56%) lymph nodes (30-35%), and liver (11-30%), which are associated with their own constellations of presenting symptoms[1,7,8].

Like other pediatric solid tumors, neuroblastoma is associated with few genetic alterations that drive pathophysiology. The most commonly observed genetic aberration is amplification of the oncogene *MYCN* (defined as >10 copies), which occurs in 40% of high-grade patients and 5% of low-grade patients[3]. Somatic mutations in anaplastic lymphoma kinase (ALK) are found in an additional 10% of cases[9]. Other identified genetic changes include loss of function mutations in *ATRX* (10%) and *TERT* (25%)[9,10]. Of these molecular abnormalities, *MYCN* is considered the predominant driver of disease progression, and correlates independently with decreased survival[11–13].

Clinical management

Neuroblastoma is an incredibly heterogeneous disease. Clinical presentation and disease course vary extensively, influenced heavily by patient age, tumor site(s), *MYCN* status, and extent of metastatic spread. Outcomes range from spontaneous remission, differentiation to a benign neoplasm, or instead, progression to aggressive, metastatic disease resulting in death. While neuroblastoma in infants < 18 months of age is often curable and associated with favorable outcomes (4-year event-free survival (EFS) 82 +/- 1%), neuroblastoma in older children is associated with a significantly poorer prognosis (4-year EFS 42 +/- 1%)[14]. Older children are more likely to be diagnosed with high-risk neuroblastoma, a group representing 50% of those diagnosed. Children with high-risk (HR) neuroblastoma have an overall long-term survival rate of <50% despite treatment with intensive multimodal therapies, including surgical resection, chemotherapy, radiation, hematopoietic stem cell transplantation, cis-retinoic acid, and immunotherapy[1,15–17]. The long-term effects of these therapies are not well characterized, in part

due to the low number of HR neuroblastoma survivors. Post-treatment, patients may experience lasting side effects, including symptoms of ototoxicity, renal dysfunction, and infertility[16]. In addition, 1-8% of survivors develop secondary neoplasms, attributed largely to radiation and chemotherapy exposures[18,19]. The dismal prognosis and high prevalence of toxic side effects among children with HR neuroblastoma highlights the urgent need for novel treatment approaches that reduce toxicity and improve long term outcomes.

Dinutuximab: the first targeted immunotherapy for neuroblastoma

Targeted immunotherapies have increasingly become incorporated into cancer care. For example, monoclonal antibodies (mAbs) are one of the largest classes of novel drugs approved for the treatment of cancer in the last decade[20]. These agents specifically target an epitope present on cancer cells, and work via a variety of immune and non-immune mediated mechanisms. Dinutuximab (Unituxin, ch14.18) is a monoclonal antibody targeting GD2, a neuroblastoma-associated disialoganglioside. In 2015, this drug became the first antibody therapy to be FDA-approved for use in any pediatric solid tumor[21]. The addition of dinutuximab in combination with GM-CSF and IL-2 to cis-retinoic acid maintenance therapy resulted in the most significant improvement in neuroblastoma outcomes in recent years, improving two-year EFS by 20% compared to patients receiving cis-retinoic acid therapy alone (2 year-EFS; 66 vs 46%, p = 0.01)[22]. While the survival benefit provided by dinutuximab represents significant progress, dinutuximab is not curative[15,22–25]. 40% of patients will ultimately relapse within 5 years[25]. Outcomes for relapsed/refractory disease following dinutuximab treatment are dismal.

The substantial yet unsatisfactory clinical effects of dinutuximab have sparked increased interest in the development of novel immunotherapeutic approaches for neuroblastoma. The mechanism of action of dinutuximab is thought to be four-fold: induction of apoptosis, antibody-dependent cell-mediated cytotoxicity (ADCC), antibody-dependent cellular phagocytosis (ADCP), and complement-dependent cytotoxicity (CDC)[26,27]. Notably, dinutuximab does not directly

engage with the adaptive immune system. Several T-cell directed therapies that stimulate an adaptive immune response have demonstrated success in treating hematological malignancies. T cell-mediated immunotherapies that target a cancer-associated antigen have the potential to enable selective killing of tumor cells while leaving normal tissues unharmed. Activation of tumor-specific T cell clones may also spark lasting immunological memory, lowering the risk of future recurrence.

Mechanisms of immune evasion in neuroblastoma

Neuroblastoma presents unique challenges to redirected T cell immunotherapies. In general, pediatric solid tumors are characterized by unique intrinsic mechanisms of immune evasion that are not observed in adult malignancies. First, a growing number of whole-genome sequencing studies demonstrate that high-risk neuroblastomas are associated with a low frequency of somatic mutations compared to adult cancers[9,28]. The paucity of mutations in protein-coding genes results in limited expression of targetable neoepitopes and subsequently, a dearth of T cell clones that recognize tumor-specific antigens. Additionally, downregulation of MHC class I (MHC-I) on neuroblastomas is common[29,30]. The combination of limited generation of neoepitopes and lack of antigen-presenting machinery in neuroblastoma cells may weaken the reactivity of tumor-infiltrating lymphocytes.

Immune checkpoint inhibitors were some of the first T-cell directed immunotherapies evaluated for the treatment of neuroblastoma. Expression of immune checkpoint molecules such as PD-L1 in the solid tumor microenvironment substantially limits cytotoxic functions of tumor-infiltrating lymphocytes. Monoclonal antibodies blocking binding of these checkpoint proteins to their receptors have mediated substantial therapeutic efficacy in adult cancers. Unfortunately, this therapeutic class has yet to show a clinical benefit in neuroblastoma[31,32]. This discrepancy may be due to low tumor immunogenicity or perhaps differences in the developing immune system.

Additionally, published studies have disagreed on the extent and prognostic significance of PD-L1 expression in neuroblastoma[32–35]. Thus, alternative strategies are needed.

Chimeric Antigen Receptor T cell (CAR-T) adoptive cell therapy is slowly revolutionizing cancer treatment, mediating dramatic efficacy in pediatric leukemia patients with minimal toxicities[36,37]. CAR-T therapy involves collecting a patient's lymphocytes and genetically engineering T cells to express a CAR protein that can recognize a cancer antigen independently of MHC complexes. CAR constructs contain an extracellular target antigen-binding domain, a hinge region, a transmembrane domain, and one or more intracellular signaling domains that induces CAR-T cell activation[38]. Most CAR-T trials for neuroblastoma have shown limited efficacy[39] with the recent exception of a third-generation GD2-directed CAR T cell (NCT03373097) that induced a response in 63% of patients[40]. Due to a growing demand for CAR-T products nationwide and a limited manufacturing capability, cancer patients may face prolonged wait times for CAR-T cells[41]. In addition, lack of standardized manufacturing protocols and differences in CAR designs may contribute to differences in patient outcomes.

Bispecific T cell Engaging antibodies: a novel immunotherapeutic approach

An alternative approach is to leverage the presence of a patient's own T cells with a bispecific T cell engaging antibody. Bispecific T cell engagers (BTEs) represent a growing class of targeted immunotherapies developed for the treatment of cancer. BTEs are designed to bind a tumor associated antigen and a T cell activating receptor, often CD3, on T cells simultaneously (**Figure 1.1**).

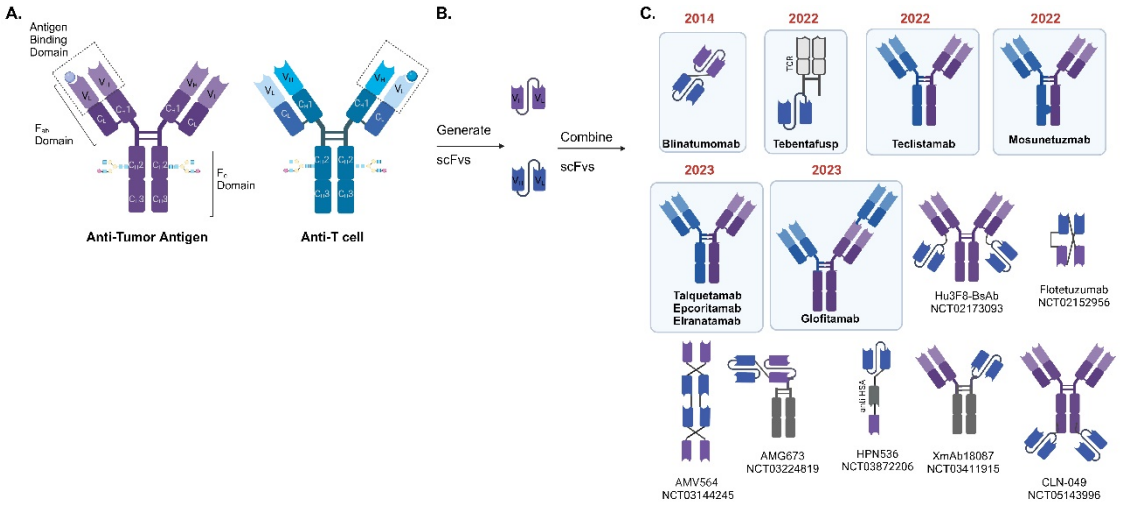

Figure 1.1: *Schematic overview of the generation of bispecific T cell engaging antibodies.*

(A) Monoclonal human IgG1 antibodies are composed of F_{ab} and F_c domains that bind antigens and Fc receptors, respectively.
(B) Single chain variable fragments (scFvs) are generated by combining variable heavy chain (V_H) and variable Light chain (V_L) sequences with amino acid linkers.
(C) Illustration of the diverse range of bispecific T cell engaging antibodies currently under evaluation in clinical trials or clinically approved (indicated by blue boxes). Year of drug approval is denoted by red text.

This dual engagement drives the formation of an immunologic synapse, phosphorylation of intracellular CD3 domains and induction of T cell mediated tumor cell death[42–44]. In contrast to canonical stimulation of T cells, BTE-mediated activation occurs independently of MHC complexes and holds the capability to activate polyclonal populations of both CD4 and CD8 cells (**Figure 1.2**)[44,45]. Additionally, in contrast to adoptive cell therapies, BTE therapy is an "off-the shelf" approach that can be immediately administered to patients with no time lost waiting for cellular engineering.

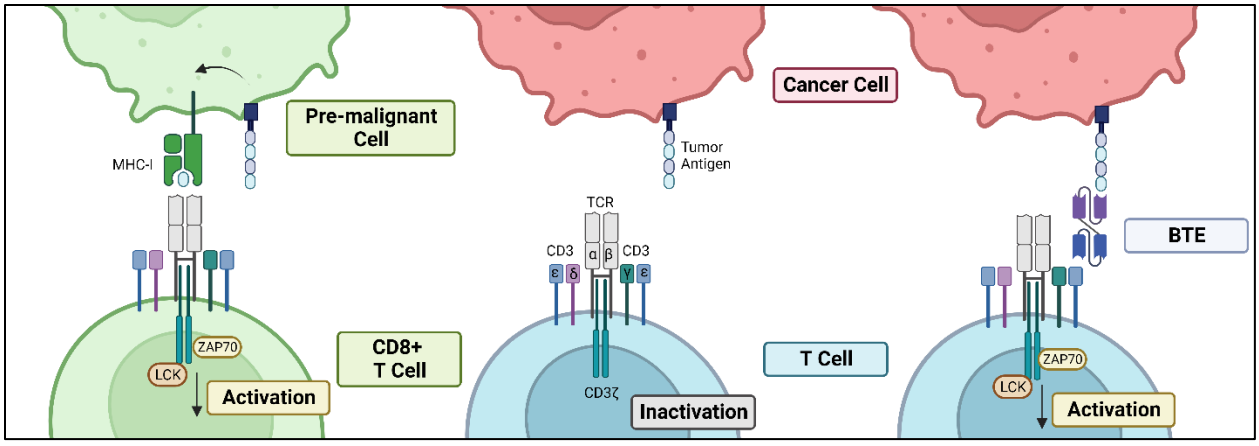

Figure 1.2: *Bispecific T cell Engagers (BTEs) induce the formation of an immunologic synapse between T cells and cancer cells.*

(left) Cytotoxic CD8+ T cells in the healthy immune system identify pre-malignant cells through antigen presentation on MHC-I molecules. Antigen binding to an antigen-specific T cell Receptor (TCR) results in the clustering of CD3 proteins and intracellular signal transduction.
(middle) In neuroblastoma, MHC-I is often absent, allowing cells to evade detection.
(right) Bispecific T cell engaging antibodies (BTEs) bind tumor associated antigens and CD3 on T cells, directly eliciting CD4+ and CD8+ T cell activation independently of MHC-I.

Blinatumomab (Blincyto®)[46], a bispecific CD19-directed CD3-engaging antibody, became the first clinically approved BTE in 2014 for the treatment of adult relapsed/refractory precursor B-cell acute lymphoblastic leukemia (B-ALL)[47]. Following the clear evidence of its clinical benefit in adults, the safety and efficacy of blinatumomab was quickly established in pediatric populations[48–51]. A large open-label single arm study of children diagnosed with CD19-positive B-ALL demonstrated an impressive complete response rate of 63% after only two treatment cycles[48]. Subsequently, in 2016, the FDA granted accelerated approval of blinatumomab for pediatric B-ALL patients with relapsed or refractory disease. Today, blinatumomab remains the only BTE FDA-approved for the treatment of a pediatric malignancy.

The development of BTEs for the treatment of pediatric cancers is a new and rapidly evolving field of research. So far, the majority of pediatric clinical trials have restricted to hematological malignancies (75%, n=12/16). Of the 8 BTEs in clinical trials for children, half target antigens present on solid tumors (50%, n=4/8) (**Supplementary Table 1**). Two GD2-CD3

targeting BTEs have been evaluated in human clinical trials enrolling neuroblastoma patients. In the first study, patients, including 7 with neuroblastoma (58%, n=7/12), were dosed with biweekly infusions of GD2-CD3 BTE-armed autologous lymphocytes. The maximally tolerated dose was not reached, yet evidence of BTE-mediated activity was observed in 4/12 individuals (33%), including one patient who exhibited a complete bone marrow response (NCT02173093)[52]. A more recent Phase I trial evaluated the safety and efficacy of a GD2-CD3 BTE in a cohort of 11 children, 7 with neuroblastoma (64%). The maximally tolerated dose of BTE was not reached, and 9 patients (82%) showed evidence of disease progression (NCT03860207).

The potential to engineer a BTE with a limited toxicity profile makes this modality an attractive option for use in children. Childhood development is a dynamic and delicate process. Conventional chemotherapies, which non-discriminately target cycling cells, have lasting negative impacts on postnatal development. Chemotherapy-related cognitive impairment is a debilitating neurological syndrome characterized by impaired attention and executive functioning that significantly impacts activities of daily living[53]. Blinatumomab has been used to safely treat children who have a high risk of chemotherapy-related adverse events as well as those suffering from severe chemotherapy-associated toxicities[54], suggesting that BTEs when designed optimally, may represent an innocuous treatment approach.

However, a significant challenge in developing targeted immunotherapies for pediatric solid tumors is the fact that solid tumor antigens are often co-expressed on by non-malignant cells. Therefore, antigen selection is crucial step in the design of BTEs to not only maximize therapeutic efficacy but also to minimize “on-target off-tumor” toxicities. BTEs for hematological malignancies largely target antigens that are also expressed by normal B and plasma cells (CD19, CD20, CD22, BMCA). BTE-mediated depletion of these cells is largely tolerable. However, this is unlikely to be the case for most solid tumor antigens. For instance, dinutuximab causes dose-limiting pain due to antibody-mediated complement activation of GD2-expressing peripheral neurons[22,55,56]. One approach to minimize harm to normal tissue is to target a tumor-

restricted neoantigen. Neoantigens are generated by tumor-intrinsic mutations that drive the expression of either altered cell surface proteins, oncofetal antigens, or aberrant post-translational modifications. However, as discussed, neoantigens are rare in neuroblastoma due to their low mutational burden.

Patients with high-risk neuroblastoma are in dire need of novel therapeutic approaches to improve outcomes. Bispecific T cell Engaging antibodies have shown clinical efficacy in hematological malignancies, but their potential to treat solid tumors has not been fully explored. Here, we explore potential neuroblastoma-associated antigens that could be targeted with a BTE and identify B7H3 as a promising candidate antigen.

Methods

Patient Derived Cell Cultures

LAN-1, IMR-32, SK-N-SH, and SK-N-BE2 cells were obtained from American Type Culture Collection. Cells were cultured in RPMI media supplemented with 10X/20mM GlutaMAX (ThermoFisher, #35050061) and 10% fetal bovine serum (ThermoFisher, #1043806). CHLA-255 cells were generously shared by the laboratory of Dr. Dean Lee (Abigail Wexner Research Institute, Nationwide Children's Hospital). Other patient-derived neuroblastoma cell lines were obtained from Children's Oncology Group and cultured in RPMI media supplemented with 20% fetal bovine serum, 10X/20 mM GlutaMAX, 10X Insulin-Transferrin-Selenium (ThermoFisher, #51500056), 10X and Antibiotic-Antimycotic (ThermoFisher, #15240062). All cultures were maintained in a 5-8% CO_2 buffered incubator at 37ºC. All cell lines are described in **Supplementary Table 2.**

Evaluation of Surface Antigen Expression by Flow Cytometry

Samples were stained with the following APC- or PE-conjugated antibodies according to manufacturer's instructions, resuspended in a final solution containing DAPI (ThermoFisher,

#D3571, 1 ug/mL) and analyzed on a NovoCyte 3000 Flow Cytometer: APC mouse IgG1k isotype control (BioLegend, #400142), APC anti-human GD2 (BioLegend, #357306), APC anti-human CD24 (BioLegend, #311118), APC anti-CD56/NCAM (BioLegend, #362504), APC anti-human PD-L1/CD274 (BioLegend, #329708), APC anti-human ROR1 (BioLegend, #357806), APC anti-human B7H3/CD276 (BioLegend, #351006), PE mouse IgG1k isotype control (Biolegend, #400114), PE anti-human B7H3/CD276 (BioLegend, #351004).

Generation of Kaplan-Meier Curves

B7H3 expression and clinical data of neuroblastoma patients deposited in Cangelosi (GEO ID: GSE62564, Kocak (GEO ID: GSE45547), and SEQC (GEO ID: GSE49710) datasets were analyzed using the R2: Genomics Analysis and Visualization Platform software (https://hgserver1.amc.nl/cgi-bin/r2/main.cgi). The optimal B7H3 expression cutoff with maximal sensitivity was determined for each dataset using the "Survival ROC" function. Based on this expression level, patients were classified as having high- or low- B7H3 expression. Analysis was restricted to patients with Stage IV neuroblastoma. Kaplan-Meier overall survival curves were plotted in R2.

Quantification of B7H3 Expression by Flow Cytometry

Cells were stained with a saturating concentration (10 ug/mL) of PE-conjugated anti-human CD276 antibody (Clone MIH42, Catalog #351004, BioLegend; San Diego, Ca, USA) per manufacturers instruction. Stained samples were analyzed on a NovoCyte 3000 Flow Cytometer. Cell surface antigen expression was quantified using the BD Quantibrite PE Quantitation kit (BD Biosciences, #340495) following the manufacturers protocol.

Immunohistochemistry of Tissue Microarrays

Neuroblastoma tissue microarrays were generously shared by Seattle Children's Hospital Department of Pathology. Normal Mixed Adult/Pediatric Tissue microarrays were purchased from BioMax (FDA999w1, BE01014a). The normal Pediatric Tissue Microarray was generously shared

by the Maris Lab (Children's Hospital of Philadelphia, Philadelphia, PA). IHC was performed using the Ventana Discovery Ultra IHC/ISH Auto-Stainer. Following deparaffinization, antigen retrieval was performed with CC1 (Roche-Ventana, #950-500) for 32 min (37°C). After blocking, incubation with Anti-CD276/B7H3 antibody (LS Bio, #LS-C743430) was performed for 40 min (37°C). Primary antibody detection was accomplished with an anti-rabbit HQ/anti-HQ-HRP system (Roche-Ventana, #760-4815, #760-4820) paired with a ChromoMap DAB Kit (Roche Ventana, #760-159). Identification of DAB positive cells and quantification of DAB average optical density was performed using Halo Image Analysis Software (Indica Labs). For staining optimization, OVCAR3 flank xenografts were used as a positive control. Human tonsil tissue and mouse splenic tissue were used as negative controls. B7H3 expression was quantified as an H-score, calculated as: (% DAB+ cells) x (average DAB optical density).

Generation of Isogenic B7H3 Knock-out Cell Lines

sgRNAs targeting B7H3 were designed using the Synthego CRISPR Gene Knock-Out Design Tool and purchased from Synthego. sgRNA sequences are listed in **Supplementary Table 3**. RNP complexes were prepared by reconstituting sgRNA and Cas9 2NLS nuclease (Synthego) and adding to complete SF Cell Line Nucleofector Solution (Lonza, #V4XC-2032) to a final volume of 25uL. This mixture was incubated at room temperature for 15 minutes to promote RNP complex formation. For nucleofection, $0.2x10^5$ cells were harvested, washed with PBS, resuspended in 20uL of the RNP solution, and transferred to a 16-well Nucleocuvette Strip ((Lonza, #V4XC-2032). Nucleofection was performed using the 4D-Nucleofector TM X Unit (Lonza) using the program CA-168. Nucleofected cells were harvested 48hr later and expanded in culture. To isolate single cell clones, cells were diluted and 1 cell/well was plated into a 96 well plate and cultured. Clones were screened for target antigen expression by flow cytometry using a NovoCyte 3000 Flow Cytometer. Genomic DNA was extracted (Qiagen, #69504) from clones displaying loss of surface antigen expression. Genomic regions surrounding the CRISPR target gene were PCR amplified

using Phusion Polymerase (ThermoFisher, #F531S). Following size verification by agarose gel electrophoresis, PCR products were column purified (Machery-Nagel, #740609) and submitted for Sanger sequencing (GeneWiz) using unique sequencing primers. See **Supplementary Table 4** for PCR and sequencing primers used. Sanger Sequencing trace files for wild-type and edited cells were analyzed using the Interference of CRISPR Edits (ICE) tool[57].

Statistical Analysis

Preliminary data analysis was performed using Excel version 16.0.16130.20806 (Microsoft). GraphPad Prism (version 10.1.0) was used to conduct statistical analysis and generate graphs. Statistical comparisons were made using either unpaired, two-tailed, *t*-tests when comparing two experimental groups, or one-way ANOVA with a multiple comparison correction when comparing three or more conditions. For all statistical analysis, $p < 0.05$ was set as the threshold for statistical significance. P values are denoted with asterisks: $p > 0.05$, non-significant (ns); $*p < 0.05$; $**p < 0.01$; $***p < 0.001$; and $****p < 0.0001$.

Results

Neuroblastoma cells express several targetable surface antigens

To identify potential targets for BTE immunotherapy, we screened a panel of neuroblastoma cell lines by flow cytometry and compared surface expression of selected candidate antigens (**Figure 1.3**). A diverse panel of patient derived cultures (n=13) was selected to reflect the heterogeneity of this disease (**Supplementary Table 2**). Of the 7 antigens evaluated, CD56 had the highest median expression (expression detected on n=13/13, median MFIR = 163.5). While elevated surface expression is desirable, we found that CD56 expression was

unacceptably high on normal pediatric tissues as well (data not shown). Due to a suspected lack of a therapeutic window, we eliminated CD56 as a suitable option.

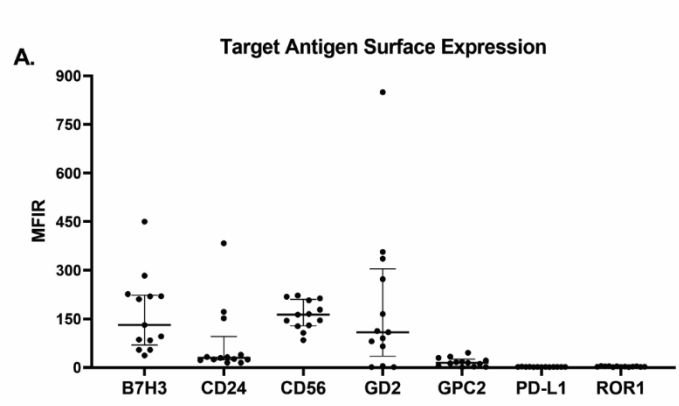

B.

Function of Selected Antigens in Neuroblastoma	
B7H3	Immune checkpoint ligand, roles in invasion, angiogensis
CD24	Roles in invasion, proliferation, suppression of innate immunity.
CD56	Roles in migration, invasion, and prognosis
GD2	Roles in invasion, proliferation, suppression of innate immunity.
GPC2	Oncofetal antigen with limited post-natal expression
PDL1	Immune checkpoint ligand
ROR1	Roles in migration and proliferation

Figure 1.3: *Surface expression of targetable surface antigens on neuroblastoma cell lines*

(A) Flow cytometry evaluation of a panel of human neuroblastoma cell lines (n=13) was performed to evaluate expression of targetable surface antigens. Each data point represents an individual cell line. MFIR (mean fluorescence intensity ratio) was calculated by dividing mean fluorescent intensity of the sample by that of the corresponding isotype control. For each plot, the median expression is indicated by the center line. Error bars represent the interquartile range (25^{th} and 75^{th} percentiles).
(B) Selected functions of antigens evaluated in (A).

Of the remaining candidates, B7H3 had the next highest median expression (expression detected on n=13/13, median MFIR = 131.3). CD24 and GPC2 were each expressed on >90% of cell lines evaluated but had significantly lower expression levels (median MFIR = 29.9 and 14.4 respectively) compared to B7H3. PD-L1 and ROR1 had even lower or absent levels of expression, with median MFIRs of 1.6 and 2.7 respectively. Given that B7H3 was expressed highly and

homogenously on each of the neuroblastoma cell lines screened (**Figure 1.4**), we further evaluated the potential of B7H3 as a target antigen for bispecific T cell engager therapy.

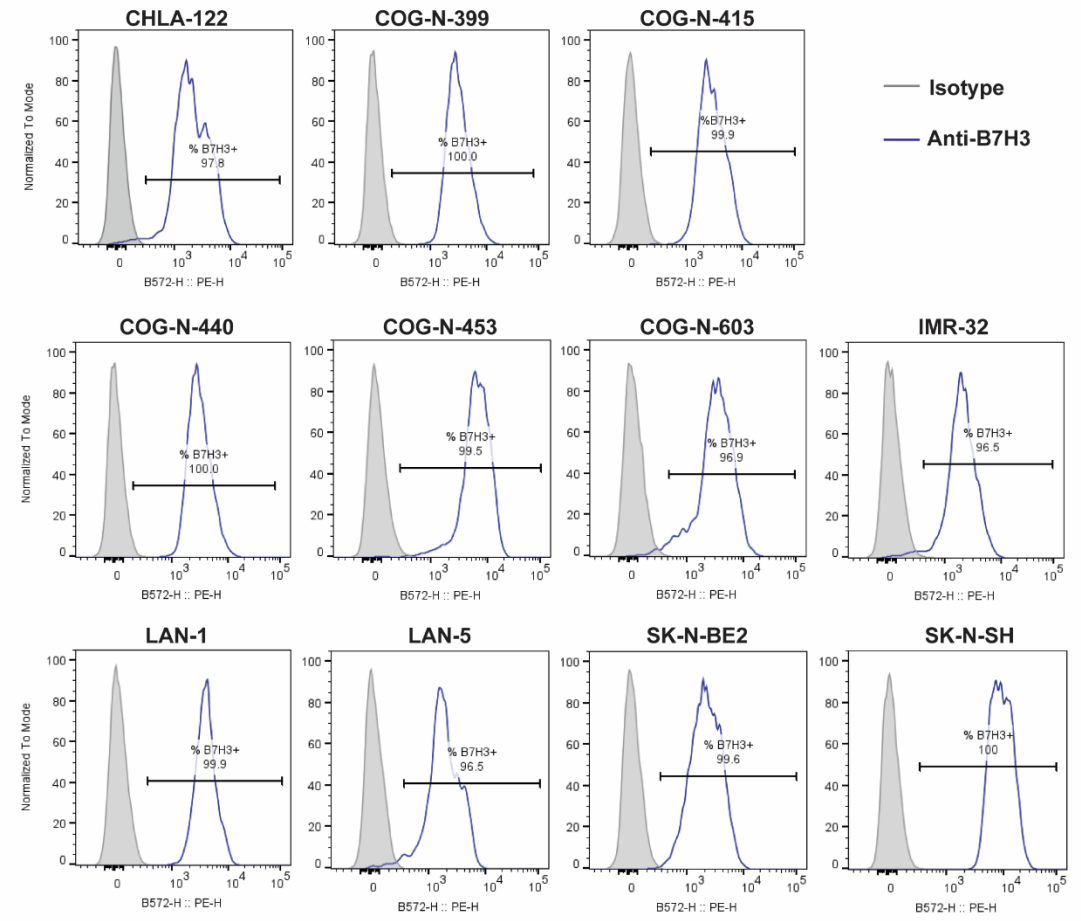

Figure 1.4: *B7H3 is homogenously expressed in neuroblastoma cell lines.*

Surface expression of B7H3 on neuroblastoma cell lines as determined by flow cytometry analysis.

<u>B7H3 (CD276) is highly and homogenously expressed on neuroblastoma tumors.</u>

B7H3 (CD276) is a member of the B7 family of immune-regulatory ligands, whose members bind co-stimulatory or co-inhibitory receptors on lymphocytes. Other characterized B7 family proteins include B7.1 (CD80), B7.2 (CD86), ICOS-L (B7H2, CD278), PD-L1 (B7H1, CD274), PD-L2 (CD273), and B7H4[58]. The human B7H3 gene (*B7H3, CD276, B7RP-2*) is located on chromosome 15q24[59]. B7H3 is a type I transmembrane protein consisting of 316 amino acids[60,61]. The extracellular domain of human B7H3 consists of 4 Ig-like domains. Although it

shares 88% sequence similarity with murine B7H3, no reported anti-B7H3 monoclonal antibodies cross-react between the two species[62]. This is thought to be due in part to species-specific glycosylation patterns[63,64]. The intracellular domain of B7H3 is short and lacks a known signaling domain[62]. Like PD-L1, B7H3 inhibits adaptive immune responses and anti-tumor immunity[62,63]. Although multiple studies have affirmed B7H3 binding to T cells, the corresponding receptor has not yet been identified[58,61,62].

B7H3 expression is elevated in multiple pediatric solid tumors, including neuroblastoma[65–68]. B7H3 promotes tumorigenesis through immune and non-immune mediated mechanisms[62], summarized in **Figure 1.5A**. In neuroblastoma, knockdown of B7H3 suppresses tumor cell proliferation and induces cell cycle arrest[69], while over-expression may confer chemoresistance to doxorubicin[70]. We found a correlation between increased levels B7H3 mRNA and poorer outcomes in Stage IV neuroblastoma (**Figure 1.5B**), consistent with prior publications[69]. Quantitative flow cytometry analysis confirmed surface expression of B7H3 on all evaluated neuroblastoma cultures and highlighted the variable degrees of expression present (**Figure 1.5C**). Expression of B7H3 was confirmed on patient neuroblastoma samples of various stages and locations by immunohistochemistry (IHC) analysis of tissue microarrays (**Figure 1.5D**). Of 129 tumor samples analyzed, 104 (95.4%) demonstrated moderate to high levels of B7H3 staining (H score > 2). Treatment regimens for neuroblastoma patients are determined based on tumor categorization as low-, intermediate-, or high- risk. Risk status is methodically determined by a combination of factors including age, *MYCN* status, and histopathologic classification. The International Neuroblastoma Pathology Classification (INPC) system categorizes neuroblastoma tumors as either “favorable” or “unfavorable” based on the degree of differentiation, mitotic-karyorrhexis index, and age[71]. In the analyzed tissue microarrays, increased B7H3 expression correlated with unfavorable histologic grading (favorable, mean H Score = 4.98; unfavorable, mean H score = 20.03) ($p < 0.0001$)(**Figure 1.5E**). To evaluate the potential therapeutic window, expression of B7H3 was also evaluated on normal adult and pediatric tissues. Weak to moderate

staining was observed on some normal tissues, including the adrenal gland, skin, brain, spinal cord, kidney, and stomach (**Figure 1.5F, G**).

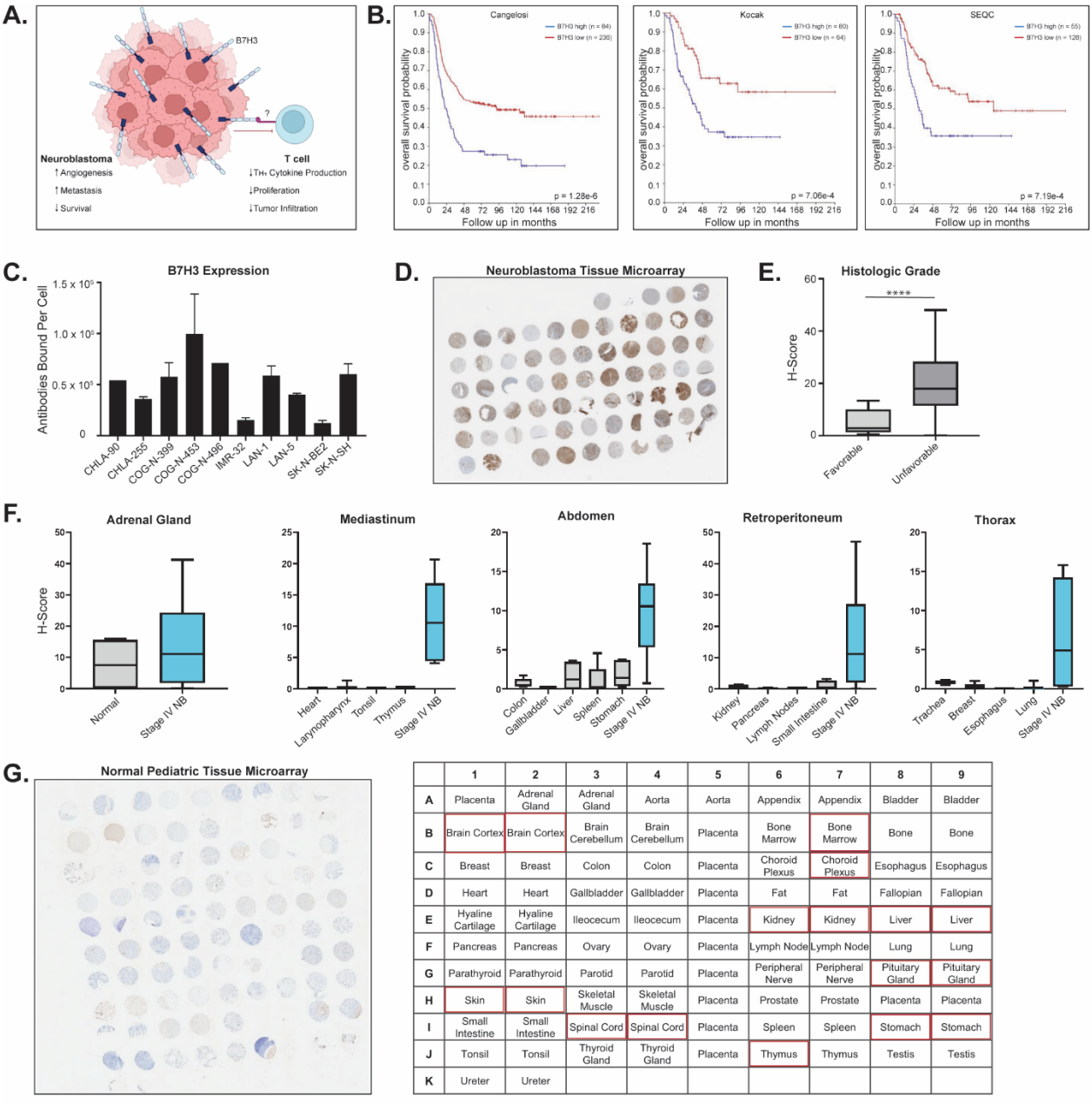

	1	2	3	4	5	6	7	8	9
A	Placenta	Adrenal Gland	Adrenal Gland	Aorta	Aorta	Appendix	Appendix	Bladder	Bladder
B	Brain Cortex	Brain Cortex	Brain Cerebellum	Brain Cerebellum	Placenta	Bone Marrow	Bone Marrow	Bone	Bone
C	Breast	Breast	Colon	Colon	Placenta	Choroid Plexus	Choroid Plexus	Esophagus	Esophagus
D	Heart	Heart	Gallbladder	Gallbladder	Placenta	Fat	Fat	Fallopian	Fallopian
E	Hyaline Cartilage	Hyaline Cartilage	Ileocecum	Ileocecum	Placenta	Kidney	Kidney	Liver	Liver
F	Pancreas	Pancreas	Ovary	Ovary	Placenta	Lymph Node	Lymph Node	Lung	Lung
G	Parathyroid	Parathyroid	Parotid	Parotid	Placenta	Peripheral Nerve	Peripheral Nerve	Pituitary Gland	Pituitary Gland
H	Skin	Skin	Skeletal Muscle	Skeletal Muscle	Placenta	Prostate	Prostate	Placenta	Placenta
I	Small Intestine	Small Intestine	Spinal Cord	Spinal Cord	Placenta	Spleen	Spleen	Stomach	Stomach
J	Tonsil	Tonsil	Thyroid Gland	Thyroid Gland	Placenta	Thymus	Thymus	Testis	Testis
K	Ureter	Ureter							

Figure 1.5: *B7H3 (CD276) is overexpressed in neuroblastoma.*

(A) B7H3 plays roles in tumor progression and immune evasion.
(B) Prognostic significance of B7H3 mRNA expression in patients with Stage IV neuroblastoma across multiple datasets.
(C) Quantification of B7H3 surface expression across neuroblastoma cell lines.

(D) Neuroblastoma tumor microarrays were evaluated for B7H3 expression by IHC. Representative TMA is shown.
(E) Unfavorable histology classification is associated with increased B7H3 expression. (n=76, unpaired, two-tailed Student's *t*-test, ****$p<0.0001$).
(F) B7H3 expression in neuroblastoma compared to adjacent normal tissues. H-scores were generated by multiplying the %B7H3+ cells by the average DAB intensity of tissue microarray samples across neuroblastoma TMAs (n=2) and normal mixed adult/pediatric TMAs (n=2). In the box and whisker plots, the center line denotes the median H-score, while the outer limits of the box denote the 25th and 75th percentiles. Whiskers denote minimum and maximum data points.
(G) A normal pediatric tissue microarray (n=1) was evaluated for B7H3 expression by IHC (left). Corresponding sample key is depicted on the right. Samples identified as B7H3+ are indicated by red boxes.

Loss of B7H3 expression inhibits neuroblastoma growth in vitro

While targeted immunotherapies can allow some otherwise refractory patients to reach a state of remission, recurrence remains a risk. Increasing data from children treated with either blinatumomab or CD19-targeting CAR-T cells suggests that downregulation of CD19, a process termed antigen escape, is a common mechanism of resistance. In a pediatric clinical trial of blinatumomab, 22% (n= 4/18) of patients who relapsed post-treatment had CD19-negative disease[72]. The incidence of antigen escape is even higher post CAR-T cell treatment, with studies showing rates of CD19 antigen loss in 70% to 93% of relapsed patients[73,74]. Given that solid tumors classically display heterogenous expression of surface antigens[75], it is likely that selection and expansion of cells with low target expression will be observed in solid tumors treated with a BTE.

The early investigations of relapses following CD19-targeted therapies illustrate the importance of selecting a target antigen that not only exhibits differential patterns of expression but also minimizes the risk of antigen escape. We aimed to evaluate if neuroblastoma cell cultures are dependent on B7H3 for survival and growth. Using CRISPR-Cas9, we knocked out the B7H3 gene in three neuroblastoma cultures: LAN-1, SK-N-BE2, and SK-N-SH (**Figure 1.6A**). In SK-N-SH cells, loss of B7H3 resulted in cell death, precluding further analysis. In LAN-1 and SK-N-BE2 cells, loss of B7H3 significantly reduced the doubling time of cultures (**Figure 1.6B, 1.6C**). This observation provides support for the postulated role of B7H3 in neuroblastoma cell proliferation[69].

Interestingly, we observed that lower B7H3 expression in neuroblastoma tumors is associated with a more favorable histologic grading, characterized by lower mitotic indexes (**Figure 1.5E**). Together, these results suggest that B7H3 plays a role in neuroblastoma cell growth and thus, this antigen may be less susceptible to antigen escape.

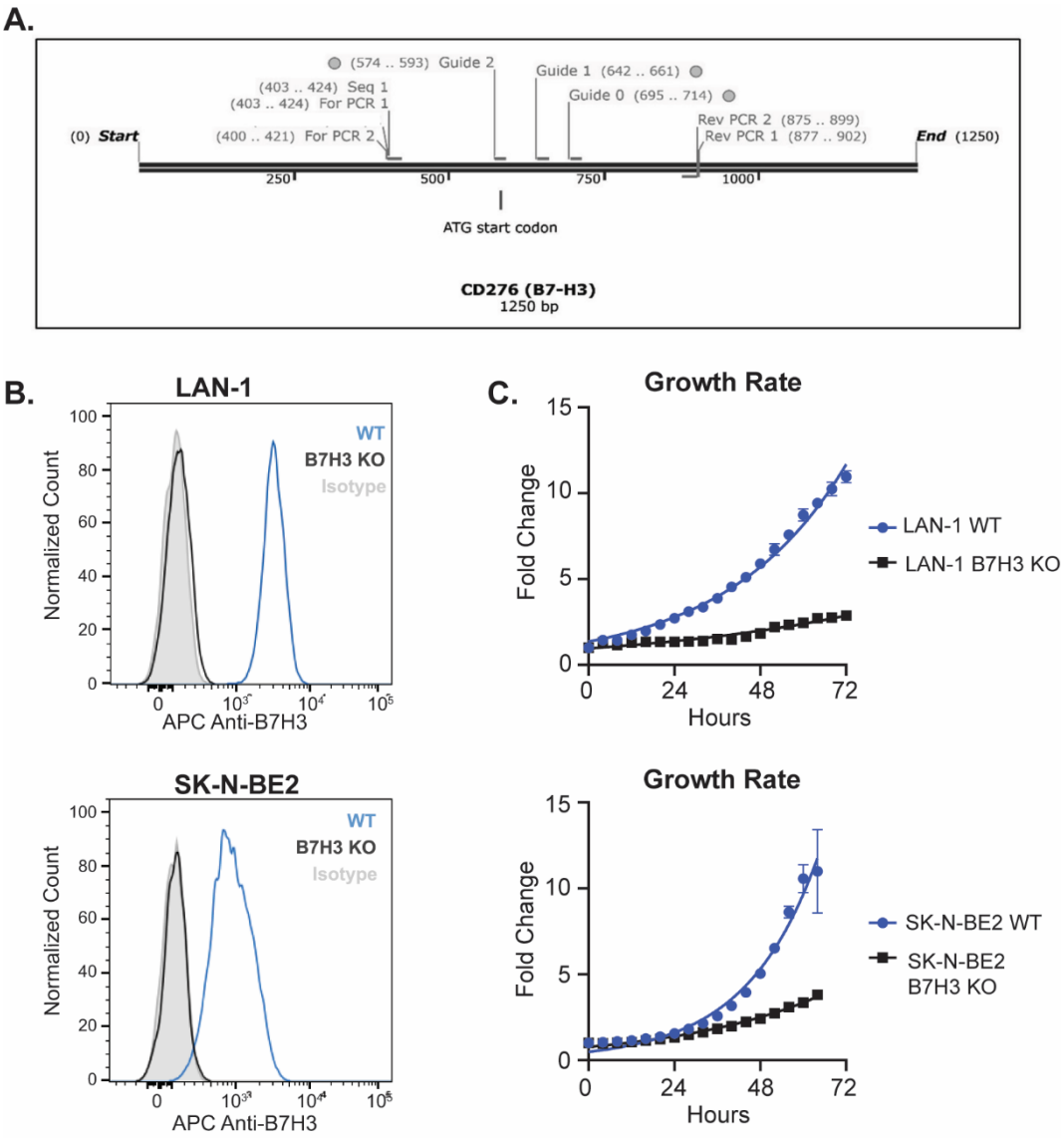

Figure 1.6: *Loss of B7H3 hinders neuroblastoma cell growth in vitro.*

(A) B7H3/CD276 gene map displaying locations of single guide RNAs and PCR amplifying and sequencing primers.
(B) FACs histograms comparing B7H3 expression in neuroblastoma wildtype (WT) (blue) and B7H3 knock-out (KO) cells (black). Cell staining with an isotype control antibody was used a control (gray).

(C) Fold change in WT and B7H3 KO neuroblastoma cell counts over time. Data is shown as mean +/- SD, n = 3 technical replicates.

Discussion

Patients with relapsed high-risk neuroblastoma have few therapeutic options. While CD19-targeting bispecific T cell engaging antibodies have shown promising efficacy in pediatric B-ALL, additional research is needed to evaluate whether BTEs are a suitable approach for pediatric solid tumors such as neuroblastoma. As is the case for other targeted immunotherapies, selection of a suitable target antigen is a major challenge. On-target off-tumor toxicity is a significant concern, which may be overcome by selecting a tumor-associated antigen that is minimally expressed in normal tissues.

Here, we identified clinically relevant targets expressed by neuroblastoma cell cultures and tissue samples that could be targeted with a bispecific T cell engaging antibody. We show that neuroblastoma cell cultures and patient tissue samples express the B7 family protein B7H3 (CD276) on their surfaces, providing a tractable target for a bispecific T cell engager approach. Recently published work showed that B7H3 is expressed by GD2-low and GD2-negative neuroblastoma bone marrow aspirates, suggesting that a B7H3-targeted BTE could be a potential therapeutic option for patients who do not respond to dinuximab[76]. Through IHC analysis, we demonstrate that neuroblastoma tissues express higher levels of B7H3 compared to normal pediatric tissues. However, it is important to note that even low levels of target antigen expression may be sufficient to mediate cytotoxicity against non-malignant cells. Intrinsic characteristics of BTEs will influence the potential for on-target off-tumor cytotoxicity, such as the specific tumor epitope targeted and the affinity of the target:BTE interaction. Factors that influence BTE activity will be discussed in greater depth in the following chapter.

A review of current literature suggests there may be a therapeutic window for B7H3-targeted therapies, although the tolerability any therapeutic window can only be properly

evaluated through systematic clinical trials. In syngeneic neuroblastoma mouse models, B7H3-targeting CAR-T cells mediated tumor control without causing overt toxicity[64]. In addition, no overt neurotoxicity was observed in neuroblastoma patients receiving intrathecal doses of a radio-iodinated monoclonal B7H3 antibody, despite B7H3 expression on neural tissues[77]. Enoblituzumab (MGA271, MacroGenics)[78], a humanized anti-B7H3 monoclonal antibody, induced measurable anti-tumor responses in a phase I study of adults with solid tumors[79]. This antibody is currently under evaluation in children with solid tumors, and thus far, no significant toxicities have been reported (NCT02982941). The scFv of MGA271 has also been leveraged to create novel B7H3-targeting CAR-T cells[80,81]. Early phase clinical trials of B7H3-targeted CAR-T cells in solid tumor patients may provide additional insights into potential toxicity of B7H3-targeted therapies (NCT04185038, NCT04483778, NCT04897321).

2. Bispecific T cell Engager Design and Production

Abstract

Bispecific T cell Engaging Antibodies (BTEs) are engineered proteins that simultaneously engage cytotoxic T cells and tumor cells through binding to CD3 and a tumor-associated antigen, resulting in T cell-mediated destruction of cancer cells. Although there are over 100 distinct BTEs in preclinical development, few published works have directly compared different BTE designs. Here, we designed a panel of 15 unique BTEs that recognize the neuroblastoma tumor antigen B7H3 and bind CD3 through one of 5 unique anti-CD3 single chain variable fragments, with the goal of investigating the roles of BTE architecture and CD3 affinity on BTE function. Structural BTE variants were constructed and ranked based on their ability to be readily produced and purified as well as their potency in functional assays. Our results demonstrate that BTEs in the IgG-L-scFv architecture potently induce T cell-mediated destruction of neuroblastoma cells in vitro, and this potency is potentiated by increasing affinity to CD3. The association between increased CD3 binder affinity and potency was not observed in BTE architectures with monovalent binding to both targets. These results provide insight into the optimization of BTE design and function.

Introduction

Bispecific T cell engaging antibodies vary widely, with over 100 unique architectures and numerous distinct production methods described. In order to understand the rationale underlying BTE designs, it is necessary to first understand the role of native antibody structure on function.

Structure and functions of conventional human IgG antibodies

Immunoglobulin G (IgG) is the most common type of antibody found in human serum, accounting for 75% of plasma immunoglobulins[82,83]. Each IgG antibody recognizes a unique foreign antigen, and following binding, activates the humoral immune system. Of the 4 subtypes of IgG (IgG1-IgG4), IgG1 is the most abundant, representing 60% of all IgGs[82]. As shown in **Figure 2.1**, human IgG1 antibodies are composed of 4 polypeptide chains: two identical light chains and two identical heavy chains that are connected by disulfide bonds[82]. Each heavy chain consists of an N-terminal variable domain (V_H) and a constant domain comprising three constant regions (C_H1, C_H2, C_H3). A flexible 15-amino acid chain termed the “hinge” connects the two heavy chains between C_H1 and C_H2, creating a symmetrical structure. The light chains are shorter in length and are each composed of one N-terminal variable domain (V_L) and one C-terminal constant domain (C_L). The light chain together with the V_H and C_H1 regions form the fragment antigen binding (Fab) domain, which contains the antigen recognition site. Binding to antigens is mediated by the variable fragment (Fv) domain (V_H and V_L). The portion of the antibody consisting of the C_H2 and C_H3 domains below the hinge is termed the fragment crystalline (Fc) domain. Residues in the C_H2 region mediate the main effector functions of IgG1s, including binding to C1q and Fc receptors (FcyRs). Binding of C1q to IgG1 Fc is mediated by three loops located on C_H2: residues 266-272, 294-300 and residues 325-441, and results in activation of the classical complement cascade[84]. A highly conserved N-linked glycosylation site located at the N297 residue of all IgG subclasses mediates binding to FcyRs on immune effector cells, mediating

phagocytosis or antibody-dependent cell-mediated cytotoxicity[82,84]. Nearby, histidine residues H310 and H435 are responsible for binding to the neonatal Fc receptor (FcRn), which promotes antibody recycling and is responsible for the long serum half-life of IgGs[84–86].

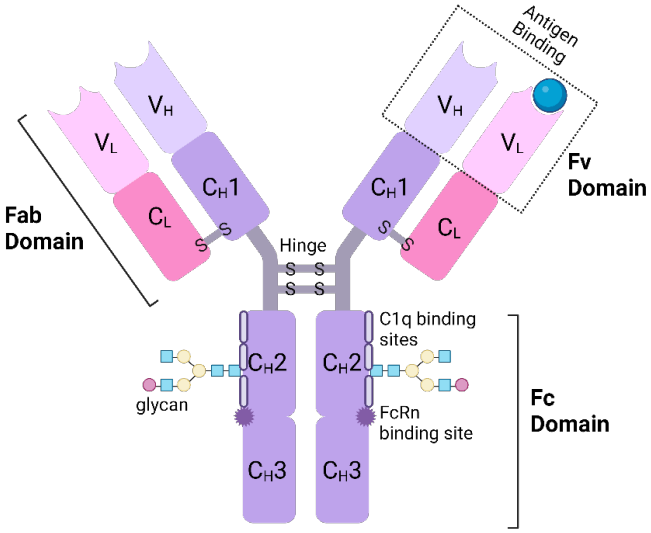

***Figure 2.1**: Structure and functions of human IgG1 antibodies.*

Light chains (L) are highlighted in pink and heavy chains (H) are highlighted in purple. C: constant domain; V: variable domain; S-S: disulfide bond; Fab: fragment antigen binding; Fc: fragment crystallizable; Fv: fragment variable; C1q: complement component 1q; FcRn: neonatal Fc Receptor.

The other subclasses of IgG (IgG2, IgG3, and IgG4) share over 90% of their amino acid sequences with IgG1, and therefore are structurally similar[82]. Sequences variations are concentrated in the hinge regions and C_H2 domains, which predominantly impacts the capacity of these isotypes to invoke Fc-mediated effector functions. Thus, each subtype of IgG is classified based on their distinct hinge region, number and locations of inter-chain disulfide bonds, and capacity to induce Fc-effector functions.

IgG2 antibodies (32% of IgGs) are produced in response to bacterial-derived polysaccharides and only bind one subset of FcγRs, FcγRII[82]. IgG3 antibodies (4% of IgGs) are characterized by their uniquely long hinge region (62 amino acids) that greatly increases the flexibility of the Fab arms. IgG3 antibodies are the most potent activators of Fc effector functions,

binding C1q and all classes of activating FcγRs with the highest affinity[82]. IgG4s (4% of IgGs) are produced in response to chronic antigen stimulation. Of all the IgG isotypes, IgG4s have the lowest affinity for activating FcγRs and are unable to bind C1q[82,83,87]. IgG4s carry a unique amino acid (S228) in the hinge region and an unusual CH3 domain that weakens binding between the two heavy chains. Under reducing conditions, Fab arm exchange can occur, allowing the dissociation of heavy chains and subsequent exchange of two halves of IgG4 (each consisting of one heavy and one light chain), resulting in the natural formation of bispecific IgG4 molecules[87–89].

Bispecific T cell Engaging antibodies: principles of design

The term "bispecific antibody" refers to an antibody that can recognize two distinct epitopes. Bispecific T cell engaging antibodies (BTEs) are bispecific antibodies that have been engineered to simultaneously bind a tumor associated antigen and T cells, thereby promoting T-cell mediated destruction of cancer cells. Broadly, the structure of BTEs can be classified into two groups, those with Fc domains (IgG-like) and those that lack an Fc domain (Fv-like).

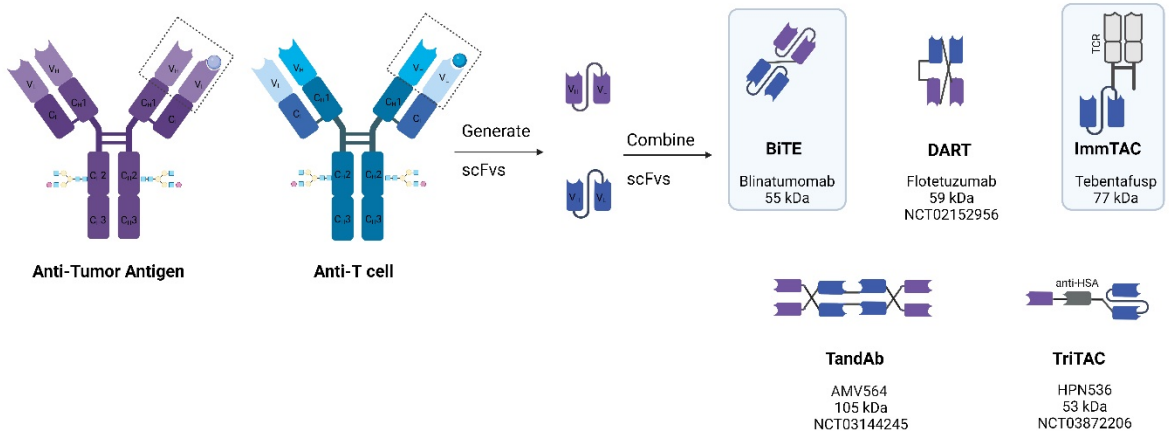

***Figure 2.2**: Fv-like bispecific T cell engaging antibodies.*

Fv: variable fragment; scFv: single chain variable fragment; BiTE: bispecific T cell engager; DART: Dual-affinity re-targeting molecules; ImmTAC: Immune-mobilizing monoclonal T cell receptors against cancer;

TCR: T cell receptor; TandAb: Tandem diabodies; TriTAC: Tri-specific T cell-Activating Construct; HSA: human serum albumin. Clinically approved BTE are denoted by blue boxes.

Fv-like BTEs

Single chain variable fragments (scFvs) are generated by connecting the variable regions of the heavy (V_H) and light (V_L) immunoglobulin chains of the antibody of interest with a short amino acid linker (**Figure 2.2**). This results in a single polypeptide that retains specificity and affinity for the original epitope but lacks effector functions. With a molecular weight of 25-30 kDa, the scFv is the smallest immunoglobulin-based protein that retains functional native variable regions. Given their simplified structure and small size, scFvs are extremely modular and can be easily incorporated into various structures to generate multi-specific antibodies (**Figure 2.2**) There have been several Fv-like BTE designs that have entered clinical trials including BiTEs, DARTs, ImmTACs, TandAbs, and TriTACs (**Figure 2.2**). The most common and well-characterized Fv-like BTE architecture is the Bispecific T cell Engager (BiTE).

BiTEs

The Bispecific T cell Engager (BiTE) format is exemplified by blinatumomab, the first-in-class bispecific antibody approved as a cancer treatment in the United States[46,47]. BiTEs are created by connecting two scFvs with a flexible amino acid linker, thereby creating a single polypeptide with one N and one C terminus. The small size of BiTEs (~55 kDa) offers several advantages. For example, BiTEs bring T cells and tumor cells in close enough proximity to form an immunologic synapse that is an optimal distance to promote cytotoxicity[45]. In addition, monovalent engagement of CD3 prevents systemic activation of T cells in the absence of target engagement[44]. Furthermore, their small structure permits BiTEs to penetrate solid tumors effectively[90]. However, the compact nature of BiTEs carries a cost. Plasma proteins smaller than 60 kDa are quickly filtered out of circulation through the renal glomeruli[91]. Due to their small molecular weight and inability to bind FcRns, BiTEs are rapidly eliminated from systemic circulation through a combination of renal excretion and catabolism with a serum half-life of 1.25

hours[92,93]. Consequently, a 28-day continuous infusion of blinatumomab is required to maintain therapeutic drug concentrations in the blood[93].

DARTs

Dual-affinity re-targeting molecules (DARTs) were engineered as a more stable alternative to BiTEs. DARTs separate Fvs onto isolated polypeptide chains that are then covalently bonded with a disulfide linkage placed at the carboxyl termini (**Figure 2.2**). The DART structure is purported to better mimic natural IgG:antigen interactions and improve stability[94]. Flotetuzumab (MGD006) is an anti-CD123/CD3 DART that is under evaluation for the treatment of acute myeloid leukemia, Hodgkin's lymphoma, and T-ALL[95] (NCT04582864, NCT04158739, NCT04681105). However, at 59 kDa, DARTs share some of the same pharmacokinetic limitations as BiTEs, with a half-life of approximately 3.5 hours[95].

ImmTACs

Immune-mobilizing monoclonal T cell receptors against cancer (ImmTACs) are a unique class of Fv-based BTEs that consists of an anti-CD3 scFv bound to the beta chain of a T cell Receptor (TCR)[96] (**Figure 2.2**). By using a soluble TCR to mediate binding to tumor cells, the repertoire of targetable antigens is expanded to encompass any tumor-associated cell surface or intracellular protein that is presented as a short peptide on Human Leukocyte Antigens (HLA) present on the target cell surface. In early 2022, the FDA approved tebentafusp (IMCgp100, KIMMTRAK®), a bispecific gp100 peptide-HLA-directed T cell engaging ImmTAC, for the treatment of unresectable or metastatic uveal melanoma[97]. This approval was based on the results of a randomized phase III clinical trial which showed evidence that tebentafusp provided a significant overall survival benefit[98,99]. Although tebentafusp was well-tolerated, on-target off-tumor toxicity was observed - 83% of patients exhibited grade >2 rashes, attributed to T cell targeting of normal melanocytes. Although the half-life of tebentafusp is 7.5 hours, it is sufficiently potent to permit weekly dosing as a single 20-minute continuous infusion[99].

A major disadvantage of ImmTACs is their limited scope of application. Due to the specificity inherent to TCRs, use of tebentafusp is restricted to patients with an HLA-A*02:01 serotype. Only half of patients screened for the aforementioned phase III clinical trial met this eligibility requirement. Because the prevalence of HLA types varies by race and ethnicity, ImmTACs may exacerbate existing inequities that affect access to cancer treatment[100]. For instance, the HLA-A*02:01 allele is found more frequently in individuals of European descent (27% allele frequency) and is less common in those of African American (11.9%) and Asian and Pacific Islander ancestry (6.5%)[100]. A cross-sectional retrospective analysis of clinical trials involving HLA-restricted therapeutics demonstrated that that likelihood of being enrolled was highest for individuals of European ancestry (50.3% chance of enrollment) and lowest for people of African American descent (33% chance of enrollment). The concerns surrounding access to ImmTACs could be addressed by expanding the TCR repertoire of these drugs. However, there may be insufficient financial incentives for pharmaceutical companies to do so. Other ImmTACs currently in clinical development are also restricted to the HLA-A*02:01 serotype (NCT03973333, NCT04262466). While ImmTACs expand potential targetable antigens to include intracellular oncoproteins, this type of BTE is less applicable for pediatric solid tumors, which frequently downregulate HLA and express few neoepitopes.

TandAbs

Tandem diabodies (TandAbs) are composed of 4 Fv domains linked in succession to form a linear molecule (**Figure 2.2**). The dual bivalency of this structure increases avidity for both targets, enhancing binding to both T cells and tumor cells. With a molecular weight of approximately 105 kDa, intact TandAbs cannot pass though the glomerular filter and thus have a longer serum half-life compared to other Fv-based designs, approximately 20 hours[101]. AMV564 is a TandAb bispecific antibody that targets CD33 and CD3 and is currently being evaluated for AML, myelodysplastic syndromes, and solid tumors (NCT03516591, NCT04128423).

TriTACs

One approach to increase the half-lives of Fv-like BTE designs is to incorporate an anti-albumin binding fragment, which extends serum half-life to between 49-113 hours[102]. Investigation of the utility of this Tri-Specific T Cell-Activating Construct (TriTAC) format is being spearheaded by Harpoon Therapeutics[102] (**Figure 2.2**). HPN536 is a MSLN-CD3 targeting TriTAC that is currently in phase I clinical testing in patients with MSLN-positive solid tumors (NCT03872206).

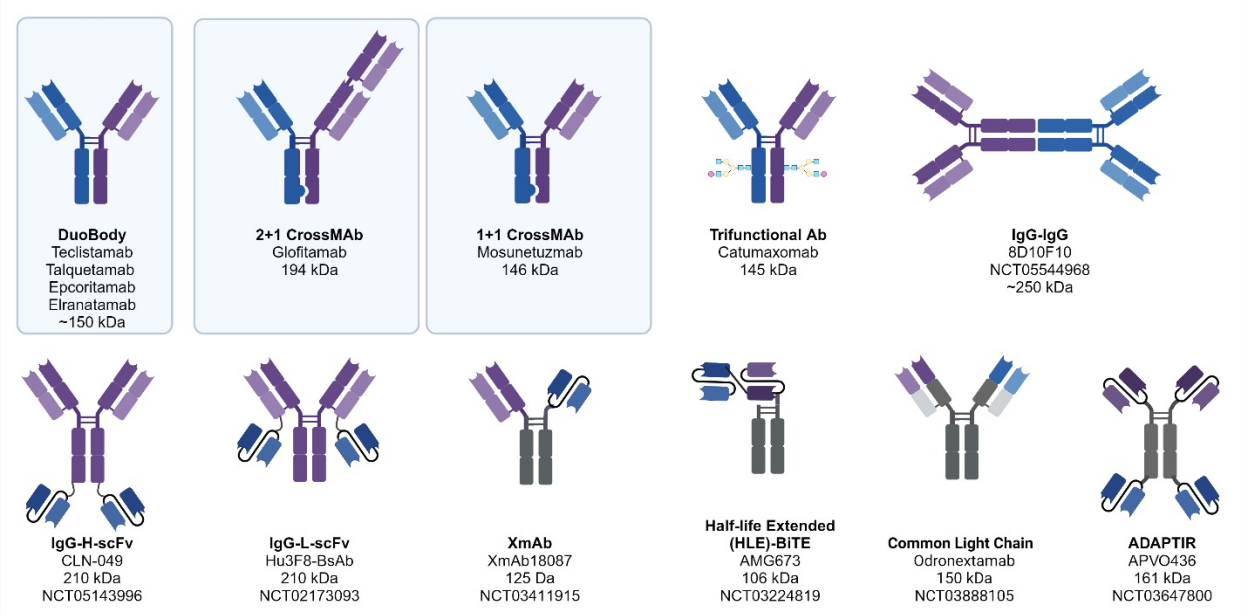

Figure 2.3: *IgG-like bispecific T cell-engaging antibodies.*

Overview of IgG-like formats of bispecific T cell-engaging antibodies designed for the treatment of cancer that are currently under evaluation in clinical trials or clinically approved (denoted by blue boxes).

IgG-like BTEs

In contrast to Fv-like BTEs, IgG-like BTEs contain a Fc domain, which creates a significant pharmacokinetic advantage. IgGs are too large (150 kDa) to undergo first-pass renal excretion. Furthermore, Fc-FcRn mediated antibody recycling extends the serum half-life of human IgGs to 18-21 days[85]. IgG-like BTEs have a similarly long half-life and are typically administered through either weekly subcutaneous or intravenous injections. However, in the context of BTE therapies,

Fc-mediated immune effector functions are undesired, as they may trigger nonspecific immune activation.

Catumaxomab (Removab) is an EpCAM-CD3 BTE that was approved in the European Union in 2009 for treatment of malignant ascites. This rat/mouse hybrid IgG-like BTE was designed with a fully functional Fc domain (**Figure 2.3**). In clinical trials, the maximal tolerated dose of catumaxomab was quickly reached due to cytokine release syndrome. The intact Fc domain was heavily speculated to reduced tolerability of this drug, potentially mediating cross-linking of T cells in the absence of tumor cell engagement[103]. Catumaxomab has since been voluntarily withdrawn from the European market. Due to the documented experience with Catumaxomab, IgG-like BTEs now commonly introduce mutations to the Fc domain to abrogate Fc-mediated immune stimulation and reduce activation of the complement cascade[104]. L234A, L235A, and P329G ("LALAPG") mutations are commonly utilized to inhibit binding to FcγR and C1q while leaving FcRn binding unaffected[104]. Elimination of IgG effector functions can also be achieved through ablation of the N297 glycosylation site by substituting in alanine, glutamine, or glycine[104,105]. The N297A Fc mutation has no demonstrable effect on binding to human or murine neonatal Fc receptors[86], and may even improve biodistribution of IgG-like BTEs by preventing myeloid-mediated depletion of T cells[105].

FDA-approved IgG-like BTEs

Six IgG-like BTEs have been approved by the FDA since 2022, each for the treatment of adult hematological malignancies (**Figure 2.3**)(**Supplementary Table 5**). Teclistamab (JNJ-64007957, TECVAYLI)[106] and Talquetamab (JNJ-64407564, TALVEY ®)[107] are Duobody BTEs approved for the treatment of multiple myeloma, targeting BCMA and GPRC5D respectively. Both drugs are administered as weekly subcutaneous injections and are well-tolerated. In late 2022, Mosunetuzumab (RG7828, Lunsumio) a humanized CD20-CD3 CrossMAb received approval for the treatment of follicular lymphoma[108,109]. So far, 2023 has brought the approval of three

additional BTEs. Glofitamab (COLUMVI™)[110] and Epcoritamab (GEN3013, ELREXFIO™)[111] co-target CD20 and CD3, and are approved for the treatment of adult diffuse large B cell lymphoma. However, Glofitamab, is a CrossMab BTE designed with 2:1 valency for CD20:CD3 while Epcoritamab is a more traditional DuoBody with a 1:1 valency (**Figure 2.3**). All of these drugs contain silencing Fc mutations. See **Figure 2.3** for additional IgG-like constructs undergoing clinical evaluation. At this time, there are no IgG-like or Fv-based BTEs approved for the treatment for pediatric solid tumors. Methods utilized to produce IgG-like BTEs often vary, which will be discussed next.

Methods of BTE Expression and Production

Prokaryotic expression systems for antibody production

Therapeutic proteins are produced using "host" cells that have been genetically engineered to express genes encoding a desired protein product. However, proper synthesis of the encoded polypeptide does not guarantee the formation of a functional final product. To produce a functional protein, polypeptides must fold into their correct conformation, often guided by chaperone proteins, and receive any necessary post-translational modifications within the host cell.

E coli is one of the most established hosts used for protein expression, owing to their simplicity and cost-effectiveness. *E coli* expression platforms have been leveraged to generate simple scFvs and Fv-like BTEs, although production of full-length IgG-like molecules is also possible[112,113]. While production of BTEs in *E coli* is feasible, the relatively complex structure of BTEs creates production challenges. As a prokaryotic organism, *E coli* lacks post-translational machinery and essential chaperone proteins. Consequently, antibody fragments produced in *E coli* suffer from high rates of misfolding and insolubility[113]. Additionally, the cytoplasm of *E coli* is a highly reducing environment, which inhibits the formation of disulfide bridges, which are often needed to ensure correct folding[114]. Several groups have published adjusted protocols to improve

folding and solubility of bispecific antibodies in *E coli*, including development of mutant strains that facilitate disulfide bond formation, intentional engineering of hyper-stable Fvs, and co-expression of molecular chaperone proteins[114–117].

Pharmaceutical-grade proteins manufactured in *E coli* require additional purification steps post-production before they can be safely administered to human patients[118]. Lipopolysaccharide endotoxins are ubiquitously present in the outer membrane of gram-negative bacteria, and if administered to humans, can induce life-threatening septic shock. The presence of contaminating endotoxins in therapeutic proteins produced in *E coli* must therefore be closely monitored and carefully removed. Of the 157 FDA-approved therapeutic antibodies, 5% are produced in *E coli*[119]. Of the 8 currently approved BTEs, only tebentafusp is produced in *E coli* host cells[119,120] (**Supplementary Table 5**).

Non-human mammalian expression systems for antibody production.

The majority of approved therapeutic bispecific and monoclonal antibodies are produced though recombinant expression in mammalian cell systems[119]. Unlike prokaryotic hosts, mammalian cells can express, fold, post-translationally modify, and secrete proteins in a manner more analogous to that of human cells. This translates to improved yields of Fv-like and IgG-like BTEs. Today, the non-human mammalian cell line, Chinese Hamster Ovary (CHO), is predominantly used to manufacture therapeutic antibodies, as they are readily and stably transfected and are capable of secreting large quantities of protein[121,122]. For these reasons, 7/8 (87.5%) of approved BTEs and 76% of therapeutic antibodies are produced in CHO cells[119] (**Supplementary Table 5**).

Although CHO cells largely produce proteins with human-compatible post-translational modifications, use of non-human host cells carries a risk of inciting immunogenicity against non-human glycosylation patterns. For example, the monoclonal antibody cetuximab (Erbitux) is commercially manufactured using the murine myeloma cell line SP2/0. SP2/0 cells express the

enzyme α-1,3-galactosyltransferse that catalyzes the formation of galactose-α-1,3-galactose on Fab heavy chains[123]. Patients with pre-existing IgE antibodies against this oligosaccharide experience severe hypersensitivity reactions in response to cetuximab. The incidence of this infusion reaction varies geographically, occurring in 3-22% of patients[123]. Subclones of CHO cells have been identified that share expression of the galactosyltransferase responsible for inducing hypersensitivity to cetuximab[124]. Likewise, the presence of galactose-α-1,3-galactose has been documented on the CHO-produced therapeutic antibody abatacept (Orencia)[123]. Due to the risk of creating immunogenic proteins, non-human cells are less than ideal hosts for BTE production.

Human cell expression systems

While CHO cells are considered the workhorse expression system for manufacturing therapeutic antibodies, human cells such as human embryonic kidney 293 (HEK293) cells are growing in popularity. HEK293s impart human glycosylation profiles onto generated antibodies which reduces immunogenicity and enhances potency, stability, and half-life[125,126]. HEK293s are easily transfected cells that grow well in serum-free media in suspension, making them an attractive option for pre-clinical BTE discovery campaigns[121,127]. HEK293 cells can also be used to produce antibodies on larger scales, most commonly through transient expression methods[128]. Several bispecific antibodies currently in clinical development are produced in this manner, including cibistamab (NCT04826003) and RO7122290 (NCT04826003)[128]. However, transient expression methods are costly and time intensive. We have developed a lentiviral-based protocol for protein expression termed “Deadalus” that rapidly generates stable HEK293 Freestyle cells without the need for clonal selection[129]. This method ensures efficient genomic integration of transgenes while bypassing the need for large-scale preparations of high-quality DNA and time-intensive transfection protocols[130,131]. A significant advantage of HEK293 cells is their ability to produce complex proteins that carry human post-translational modifications. However, use of human host cells theoretically carries an increased risk of pathogen transmission due to the lack

of a cross-species barrier. However, current best manufacturing processes include steps to inactive and clear viral pathogens[132]. Currently, there are no FDA-approved monoclonal or therapeutic antibodies produced in human expression platforms[119]; however, a few other therapeutic proteins are produced in human host cells, including recombinant factor VII-Fc fusion protein efmoroctocog alfa (ELOCTA®)[132].

Strategies to improve BTE production.

The production of bispecific antibodies presents considerably more challenges compared to the manufacture of standard monospecific antibodies. Asymmetric IgG-like BTEs are composed of two different heavy chains and two unique light chains. Working under the assumption that these four polypeptides undergo a process of random recombination, the number of possible IgG-like products can be calculated. For an IgG, there are 2 heavy chains, with 2 unique options available for each position, creating a total of 2 x 2 = 4 possible heavy chain configurations. The same is true for the light chains, 2 x 2 = 4 possible light chain configurations. In total, random recombination will generate a total of (2 x 2) x (2 x 2) = 16 possible IgG-like molecules, of which 12.5% (2/16) represent the desired bispecific IgG (**Figure 2.4**)[133]. This low yield is far from optimal. Undesired pairings between heavy and light chains are referred to the "heavy and light chain problems". In comparison to IgG-like BTEs, production of Fv-like BTEs is relatively straightforward as the short linkers utilized prevents intrachain paring of V_H and V_L domains.

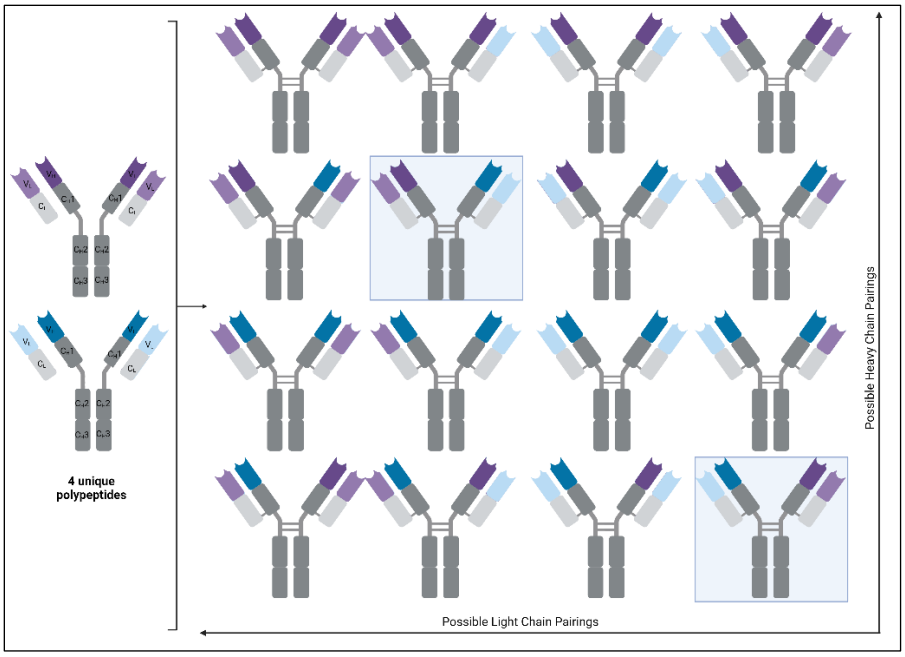

Figure 2.4: *Illustration of the heavy and light chain problems.*

Schematic showing all combinations of heavy and light chains possible when combining two distinct parental antibodies.

To avoid heavy and light chain mispairings, the first IgG-like BTEs relied on clumsy methods involving chemical hetero-conjugation[134,135]. However, this protocol places stringent limitations on BTE architecture and is plagued by high rates of unfolding and aggregation. Today, co-expression in stable cells is the predominant approach used for BTE production. Several strategies to improve the yield of IgG-BTEs have been documented. Here, I will discuss approaches that have been used to produce clinically approved BTEs including quadromas, knobs-into-holes, CrossMAb and DuoBody platforms.

Quadromas

A hybridoma is a B-cell/myeloma hybrid cell that produces a single monoclonal antibody. The earliest IgG-like BTEs were generated by fusing two antibody-producing hybridomas into a single quadroma cell that consequently expresses two heavy chains and two light chains. As previously discussed, the resulting recombination of heavy and light chains yields a blend of IgGs

as well as free heavy chains, free light chains, and various other undesirable side products. To simplify production, a combination of hybridomas producing parental antibodies of different species (mouse IgG2a and rat IgG2b) was used to generate catumaxomab[103]. While preferential species-specific pairing reduced the number byproducts, the intensive purification process and low final protein yields has relegated quadroma technology nearly obsolete with the advancements in alternative methods.

Addressing the heavy chain problem

To foster proper chain pairing, clever genetic engineering strategies have been employed. To address the heavy chain problem, “knobs-into-holes” mutations can be introduced to favor the formation of heavy chain heterodimers over homodimers. This is achieved by introducing a large tryptophan into the C_H3 region of one heavy chain (T366Y) that can fit into a “hole” created by replacing a larger residue with a smaller amino acid (Y407T) on the alternate $C_H3$domain[136]. These substitutions reduce the number of unique potential products from 10 to 4, with the desired BTE composing 25% of the pool (**Figure 2.5**). Additional C_H3 mutations have been described that further enhance heavy chain heterodimerization and introduce additional disulfide bonds to increase conformational stability[137]. In spite of these alterations, hole-hole homodimers may form, which can be overcome through selective purification methods.

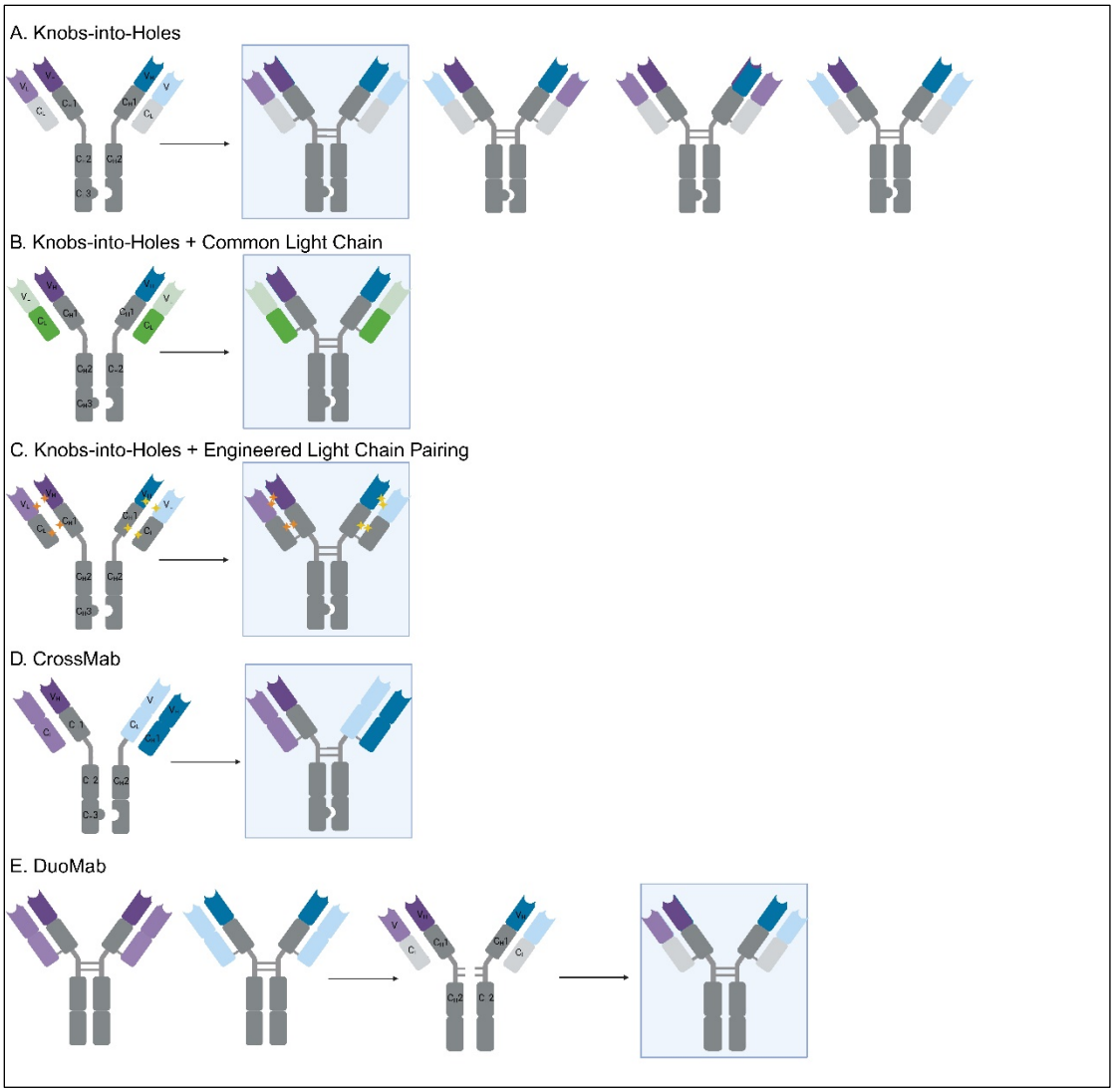

Figure 2.5: *Approaches to reduce heavy and light chain mispairings.*

Overview of strategies commonly utilized to limit undesired heavy and light chain pairings.

Addressing the light chain problem

While the knobs-into-holes approach greatly improved heavy chain pairing, mispairing of light chains remained a limitation. Overcoming this issue proved more challenging, as the molecular interfaces between Fab arms are identical, complex, and significantly stabilize IgGs. To avoid light chain mispairing, BTEs can be designed with a single common light chain (**Figure 2.5**). This strategy leverages the fact that most of an antibody's specificity stems from the complementary-determining regions (CDRs) present in the V_H domains. However, this method requires

identification of two parental monoclonal antibodies that share the same light chain. This can only be accomplished through use of novel antibody libraries with limited light chain diversity[137] or though antibody discovery campaigns in transgenic animals that express a single light chain[138]. The latter option is becoming increasingly common as the number of transgenic models has grown. Options available for licensing include ATX-CLC mice (Alloy), OmniFlic rats and chickens (Omni Ab), RenLite mice (RenMab) and KY-CLC mice (Kyinno Bio). However, immunization campaigns are extremely expensive, time-intensive, and do not guarantee successful generation of antibodies with the desired functional characteristics. An alternative approach that involves heavily engineering pre-existing distinct light chains can be used in combination with knob-into-holes mutations to better favor desired light chain pairings. This approach places strategic mutations in the V_H-V_L and C_H1-C_L interfaces (**Figure 2.5**)[139,140]. However, these sequence changes are inherently destabilizing and can affect the affinity of the final molecule.

The CrossMAb platform is an alternative solution to the light chain problem developed by Roche[141]. This method uses knobs-in-holes mutations to ensure heavy chain pairing but additionally swaps the C_H1 and C_L domains of one Fab (**Figure 2.5**). This "cross-over" effectively prevents chain mispairings, as pairing of the free light chain can only occur with the desired V_H1-C_H1-C_H2-C_H3 peptide or free V_H1-C_H1 heavy chain. The latter byproduct can be easily purified out based on size. Thorough preclinical evaluation of CrossMAbs suggests that this method does not drastically alter the affinities of the final product compared to parental antibodies[141]. Several iterations of this protocol have been described to create diverse array multi-specific antibodies[142].

DuoBody BTEs are generated using a method based on Fab arm exchange that naturally occurs between IgG4 antibodies[88,89,143]. In this process, the C_H3 sequences of the each monospecific IgGs are modified, one with a K409R substitution and one with a F405L mutation[143]. Next, each monospecific IgG is produced in separate CHO cell cultures. Post-purification, the two IgGs are recombined under reducing conditions, which disrupts disulfide bonds and drives

controlled Fab-arm exchange. Following reoxidation, the resulting final product contains >95% bispecific antibody (**Figure 2.5**)[143].

Symmetric IgG-like BTEs

Several of the BTEs presented in **Figure 2.3** circumvent the light chain issue by fusing scFvs to Fc scaffolds in lieu of Fabs. scFvs can also be appended onto the heavy or light chains of monospecific IgGs to make the final molecule bispecific (IgG-L-scFv, IgG-H-scFv, **Figure 2.3**). Because these designs attain bispecificity through chain extension rather than by introducing novel chains, there are fewer undesirable byproducts. However, for symmetric IgG-like BTEs, intentional engineering of the introduced linkers and domains is critical for minimizing aggregation[144,145].

Structural Determinants of BTE function

The function and by extension, the clinical applicability, of bispecific T cell engaging antibodies is heavily influenced by protein structure. In the following subsections, we highlight crucial structural determinants of BTE function including epitope selection, affinity, and avidity.

Tumor-targeting epitope

Two antibodies that target the same antigen at distinct epitopes can mediate distinct downstream effects. For example, rituximab binding concentrates CD20 tetramers into lipid rafts, eliciting robust binding of C1q and inducing complement-dependent cytotoxicity. In contrast, tositumomab, which targets an alternative epitope on CD20, does not affect CD20 membrane localization. As a result, tositumomab does not activate the complement cascade, and instead mediates tumor cell death by blocking cell cycle progression[146,147]. Likewise, pertuzumab and trastuzumab, two clinically approved anti-HER2 monoclonal antibodies, target distinct epitopes located in the extracellular domain of HER2. Pertuzumab blocks a region of the extracellular domain required for HER2 heterodimerization, resulting in blockade of HER2 intracellular signaling pathways, whereas trastuzumab binds an epitope closer to the cell

membrane and primarily mediates antibody-dependent cellular cytotoxicity[147,148]. Clinical evidence suggests that these drugs are synergistic, emphasizing the distinct, complementary mechanisms of action of these two antibodies[149].

The exact tumor-associated epitope targeted can also influence on-target off-tumor toxicity. Dinutuximab, a GD2-targeting monoclonal antibody used to treat neuroblastoma, is associated with dose-limiting allodynia attributed to GD2 expression on normal peripheral nerves[55,56]. A recent study demonstrated that an antibody specific to the 9-O-aceylated form of GD2, clone 8B6, binds neuroblastoma cells but not normal peripheral neurons[150]. Anti-tumor activity of 8B6 was similar to that of a conventional anti-GD2 mAb, suggesting that targeting of an alternative GD2 epitope may reduce a major dose-limiting toxicity.

The size of the tumor antigen and location of the targeting epitope impact BTE function by influencing the size of the immunological synapse formed. Growing evidence suggests that membrane proximal tumor epitopes promote smaller, more effective immunological synapses compared to membrane-distal epitopes[151,152]. To develop a novel BTE targeting melanoma chondroitin sulfate proteoglycan (MCSP), a group of researchers produced a panel of BTEs in the BiTE format, pairing an anti-$CD3^{L2K}$ scFv with various anti-MCSP scFvs[151]. Unexpectedly, results showed that while all anti-MCSP scFvs shared similar affinities for MCSP, clones that recognized epitopes located closer to the tumor cell membrane were more potent. To ensure this phenomenon was not unique to MCSP, the authors engineered CHO cells to express EpCAM fusion proteins of various lengths. Using the clinical-stage EpCAM-CD3 BiTE MT110, they showed a clear correlation between antigen size and BTE potency[151]. Another group recapitulated these findings using IgG-like BTEs, further demonstrating that targeting membrane proximal epitopes promotes superior immunologic synapse formation between tumor cells and T cells, characterized by increased exclusion of CD45 and target clustering at the cell:cell interface[152]. Altogether, epitope selection is crucial for the design of BTEs, and can have direct effects on

mechanisms of tumor cell death, on-target off-tumor toxicity, as well as the formation of BTE-driven immunologic synapses, and by extension, potency of BTEs.

Affinity to tumor antigens

The strength of the binding interaction between an Fv and an antigen is termed affinity. The affinity of tumor-targeting variable domains heavily influences the functional activity of BTEs. For example, complementary studies using HER2-CD3 BTEs as model systems demonstrated that increased affinity for HER2 correlated with increased cytotoxicity in vitro independently of HER2 expression levels[153,154]. This relationship also extended to anti-tumor efficacy in mouse xenograft models[153]. However, pre-clinical evaluation of HER2-CD3 BTEs in cynomolgus monkeys found that increased affinity of the HER2 binding domains resulted in symptoms of cytokine-release syndrome as well as damage to normal HER2+ organs[154]. Thus, the optimal affinity of tumor-targeting scFvs or Fabs will need to balance anti-tumor efficacy with on-target, off-tumor cytotoxicity.

The impact of anti-tumor antigen affinity on toxicity is also evident from preclinical work using GD2-targeting CAR-T cells. Several reports showed that anti-GD2 CAR-T cells were well-tolerated in xenografts mouse models[155,156]. However, a subsequent study demonstrated that enhancing the affinity of the anti-GD2 scFv dramatically increased mortality, attributed to a combination of on-target off-tumor neurotoxicity and general cytokine-mediated toxicities[156,157]. Increasing the affinity of the anti-tumor Fvs in a BTE would likely mediate similar effects. Tumor antigen binding affinity can also influence BTE biodistribution. Using affinity-tuned variants of an anti-HER2 monoclonal antibody, one study showed that moderate binding affinity for HER2 was associated with improved antibody accumulation into solid tumors. In contrast, low and high affinity variants showed minimal intra-tumoral accumulation. The low affinity HER2 antibody exhibited a broad biodistribution, while the high-affinity variant concentrated in the perivascular outer region of tumors[158].

These studies illustrate that anti-tumor binding properties critically influence the functional activity and tolerability of bispecific T cell engaging antibodies. However, in the context of developing a novel BTE for pediatric solid tumors, underlying target antigen biology (antigen size, location of targeted epitope, antigen membrane localization, antigen dependency, intracellular signaling) likely also influences the extent to which antigen affinity influences BTE function.

Affinity to CD3

The role of CD3 affinity on BTE function is less thoroughly characterized. One pre-clinical study showed that increasing BTE affinity for CD3 increases BTE potency of BTEs only in the context of low target antigen expression[153]. In contrast, another study showed that CD3 affinity had no effect on BTE efficacy in vitro or in mouse xenograft models[154]. However, in cynomolgus monkeys, the high-CD3 affinity BTE was not well-tolerated[154]. High levels of pro-inflammatory cytokines were noted, consistent with cytokine release syndrome. Preclinical work suggests that for anti-CD3 antibodies, increased affinity is associated with undesirable polyreactivity and consequently, poorer pharmokinetic profiles[159]. Novel CDR engineering approaches can be employed to decrease polyreactivity and thereby improve the clinical utility of high affinity CD3 binders[159].

Growing evidence suggests that the affinity of anti-CD3 binding domains heavily influences the safety and efficacy of BTEs. Fine tuning the affinities of both tumor cell-engaging and T cell-engaging binders is likely necessary to ensure a tolerable therapeutic index. However, the impact of BTE affinity is likely extremely context-dependent, and the effect of CD3 affinity on safety and efficacy in human patients is not yet clear.

Avidity

Affinity and avidity together drive antibody-mediated functions. Avidity is defined as the "accumulated binding strength of multiple affinities contributed by individual non-covalent interactions in cross-linking events"[160]. For canonical IgGs, single antibody-antigen binding

interactions are low affinity and insufficient to trigger effector functions. However, avidity instilled by bivalency towards the target antigen drives clustering of multiple IgGs on target cell membranes. Once a certain threshold number of IgGs bound to target cells is met, effector functions are triggered[160].

BTEs are hypothesized to elicit T cell activation through an analogous manner termed "cross-arm binding". The initial binding to a tumor associated antigen anchors BTEs to tumor cells, creating an opportunity for T cells to bind multiple BTEs. Successive BTEs bound to tumor cell membrane continually engage CD3 until a minimum threshold is met that triggers T cell activation. Cross-arm binding of BTEs is influenced by BTE valency, target antigen expression levels and crosslinking efficacy of the BTE[161]. A complex relationship between affinity and efficacy exists that is tied to the level of antigen expression, as avidity is poorer when antigen levels are low and influenced by the nature of then antigen itself.

The manipulation of avidity is an important design principle for engineering novel bispecific antibodies. One way to modulate avidity of a BTE is to alter the valency of the anti-tumor binders. A study of affinity-tuned HER2-CD3 BTEs showed that a dual monovalent HER2-CD3 BTE had minimal anti-tumor activity in vitro. However, the potency of this molecule could be substantially increased by incorporating a second anti-HER2 binder[162]. The avidity instilled by bivalent low affinity binding improved the selectivity of this molecule, greatly favoring targeting of HER2 overexpressing cells[162]. Likewise, the FDA-approved BTE Glofitamab (COLUMVI™) contains two anti-CD20 and one anti-CD3 binders (**Figure 2.3**). In preclinical studies, this 2+1 configuration proved more potent compared to analogous 1+1 designs[163,164]. Clinically, the bivalent binding to CD20 is postulated to help preserve Glofitamab activity in the presence of competing anti-CD20 monoclonal antibodies[164]. Altogether, these studies show that a therapeutic window can be created by leveraging avidity and affinity. However, the requirement for high target expression suggests that this method may not apply to other surface antigens.

BTE architecture heavily influences avidity. For example. A comparison of GD2-CD3 targeting BTE variants demonstrated that BTEs with bivalency for GD2 in a cis-configuration outperformed BTEs that were monovalent or contained two anti-GD2 binding domains oriented in a trans configuration[165]. Tumor antigen-specific features such as expression levels and distribution patterns may further influence the avidity of BTE interactions and consequently amplification of an anti-tumor adaptive immune response.

To better understand how selected structural features of BTEs may influence BTE function, we designed, produced, and compared a panel of BTE variants recognizing CD3 and the neuroblastoma-associated antigen B7H3.

Methods

Protein Designs

Anti-B7H3 Bispecific T cell engagers utilized V_H and V_L domains derived from the monoclonal antibody enoblituzumab (MGA271)[78]. Anti-CD3 scFv sequences were derived from OKT3, L2K[46], MM194, ADI50024 ("ADI24")[159] and ADI26906 ("ADI26")[159]. BiTE constructs were adapted from the sequence of blinatumomab[46]. MaxibAb and IgG-L-scFv constructs contained a human IgG1 backbone. Fc domains contained an additional N297A mutation to abrogate Fc effector functions. IgG-L-scFv designs contained a $(G_4S_1)_3$ linker between the CD3 scFv and the C_L domains. An additional $(G_3S_1)_4$ linker was used between the V_H and V_L domains of the anti-CD3 scFvs. Amino acid sequences were reverse translated using human codons, codon-optimized, and synthesized de novo at GenScript (New Jersey, USA). The sequences of selected constructs are provided in **Supplemental Table 6**.

High-throughput Expression and Purification of Bispecific T cell Engagers from Human Cells

The Daedalus mammalian expression platform was used to produce BTE proteins[129,130]. In the high-throughput adaptation of this protocol, a large number of unique proteins can be generated

in parallel in 96-well plates using a STARlet Liquid Handler (Hamilton) to automate pipetting steps. In this high-throughput protein expression system, HEK 293-ST cells were transfected with lentiviral vectors and DNA plasmids encoding proteins of interest. Each lentiviral vector contained a cis-linked fluorescent protein reporter (iRFP or GFP) driven by an internal ribosome entry site, allowing tracking of relative protein expression levels. Light chains or knobs were associated with the iRFP reporter. Heavy chain or holes sequences were associated with the GFP reporter. iRFP and GFP lentiviral vectors were co-transfected into HEK 293-ST cells at an equal ratio. After 3 days, supernatant containing lentivirus was collected and used to transduce suspension-adapted FreeStyle 293-F cells in 96-well plates. 3 days post-transduction, viral titers were evaluated by flow cytometry using an iQue Screener Plus Flow Cytometer (Sartorius). 7 days post-transduction, mammalian proteins were purified from 293-F conditioned media using Nuvia IMAC resin (BioRad, #700802) and subsequently undergo HPLC using SEC 2.7uM columns (Agilent, #PL1180-5301). Fractions corresponding to the monomeric proteins of interest were pooled and validated by UPLC. Protein concentrations were quantified on a Stunner instrument (Unchained Labs). Then, proteins were flash frozen in liquid nitrogen.

Patient Derived Cell Cultures

LAN-1 and SK-N-SH cells were obtained from American Type Culture Collection. Cells were cultured in RPMI media supplemented with 10X/20mM GlutaMAX (ThermoFisher, #35050061) and 10% fetal bovine serum (ThermoFisher, #1043806). All cultures were maintained in a 5-8% CO_2 buffered incubator at 37ºC. All cell lines are described in **Supplementary Table 2.**

Evaluation of Bispecific T cell Engager Binding by Flow Cytometry

Target binding of BTEs was evaluated by flow cytometry. LAN-1 cells or human ATCs were incubated with titrations of BTEs in duplicate for 30 minutes on ice. Then, cells were washed and incubated with an anti-His Tag secondary antibody (GenScript, #A01802, 0.6 ug/mL) for 30

minutes on ice. Cells were washed and resuspended in a final solution of DAPI (ThermoFisher, #D3571, 1 ug/mL). Cells were analyzed on an iQue Screener Plus Flow Cytometer (Sartorius).

Lentiviral Transduction of Neuroblastoma Cells

Using lentivirus production methods described previously[129], we generated a lentivirus encoding firefly luciferase and an iRFP fluorescent reporter. Briefly, a 12-well plate was seeded with 0.5 million cells per well at a density of 1e6/mL. Cells were transduced with 100, 300 or 500 µL of 1× lentivirus in the presence of polybrene (Sigma, #TR-10030-G, 4 µg/mL) at a final volume of 1 mL. Cells were incubated overnight at 37ºC. Then, supernatant was removed and replaced with fresh cell culture media. After 72 hours, iRFP expression was evaluated by flow cytometry. Cultures with <95% iRFP positivity were flow sorted using a MA900 Cell Sorter (Sony).

T cell Isolation and Expansion

Healthy, unstimulated human donor peripheral blood mononuclear cells (PBMCs) were obtained from Bloodworks NW (Seattle, WA, USA), frozen and stored in liquid nitrogen. T cells were isolated from a thawed PBMC aliquot using a CD3+ magnetic negative selection kit (StemCell Technologies, #7951) according to the manufacturer's instructions. Isolated cells were stained with anti-CD3 antibody and analyzed by flow cytometry to verify successful T cell isolation, defined as >95% CD3+ population. Isolated naïve T cells were activated and expanded using Human T cell anti-CD3/CD28 activating Dynabeads (ThermoFisher, #11132D) according to manufacturer's protocol. Cells were cultured in RPMI media supplemented with 25mM HEPEs (ThermoFisher, #22400105), 10X GlutaMAX (ThermoFisher, #35050061), 1X PenStrep (ThermoFisher, #10378016), 0.5X 2-mercaptoethanol (ThermoFisher, #21-985-023), human recombinant IL-2 (StemCell Technologies, #78036) and 10% heat-inactivated human serum (Valley Biomedical, #HP1022HI). After 14 days of culture, T cells were harvested. Briefly, T225 flasks were placed on a magnetic slab for 5 minutes. Supernatant was decanted into 600mL TPP bottles. Remaining beads were resuspended in media and transferred to a 15mL conical tube placed on a magnetic

stand. After 5 minutes, the cell suspension was transferred to a TPP bottle. Cells were spun down at 500xg for 20 minutes at 4ºC. Supernatant was decantated and cell pellet was resuspended and placed on a magnetic rack to remove remaining Dynabeads. After 5 minutes, cells were removed and counted on a ViCell Analyzer (Beckman Coulter). Collected T cells were phenotyped by flow cytometry and subsequently frozen in cell culture solution supplemented with 10% DMSO.

T cell Cytotoxicity Assays

In a 96-well flat bottom plate (Greiner, #655090) neuroblastoma-luc-iRFP target cells were plated in neuroblastoma culture media and allowed to adhere. Then, serially diluted concentrations of BTEs and purified human activated T cells were added to wells in T cell culture media lacking IL-2. Neuroblastoma-luc-iRFP target cells were co-cultured with purified T cells at a 5:1 Effector:Target (E:T) cell ratio. All conditions were performed in a minimum of triplicate wells. To evaluate changes in tumor cell death, iRFP+ cells were quantified using the Incucyte SX5 cell analysis system (Sartorius) every 4 hours. iRFP+ cell counts were exported to Excel (Microsoft) and percent cytotoxicity was calculated utilizing the following formula:

% Cytotoxicity = [(Mean Count of iRFP+ cells (no drug) – Mean count of iRFP+ cells (with drug)) / Mean count of iRFP+ cells (no drug)] x 100%

Fitted curves were generated by applying a Sigmoidal, 4PL, x is log(concentration) model or a [Agonist] vs response – variable slope (four parameters) model using GraphPad Prism 10.

Evaluation of T cell Activation and Exhaustion Markers by Flow Cytometry

Human ATCs were incubated with LAN-1 iRFP cells (5:1 E:T) and serially diluted equimolar concentrations of BTEs was added in triplicate. After 48 hours, cells were pelleted, and supernatant was collected and frozen at -20ºC for cytokine analysis. Cell pellets were washed and stained with the following antibodies: PE anti-human CD25 (BioLegend, #302606), PE anti-human CD69 (BioLegend, #310906), PE anti-human OX40 (BioLegend, #350004), PE anti-

human PD-1 (BioLegend, #379210) or PE mouse IgG1k isotype control antibody (BioLegend, #400114) according to manufacturer protocol. For Day 5 analysis, the experiment was repeated, but cells were co-cultured for five days and stained with the following antibodies: PE anti-human PD-1 (BioLegend, #379210), PE anti-human TIM-3 (BioLegend, #379210), PE anti-human LAG-3 (BioLegend, #369306), PE-anti human HLA-DR/DP/DQ PE (BioLegend, #361716), or PE mouse IgG1k isotype control antibody (BioLegend, #400114) according to manufacturer's instructions. Cells were acquired on a iQue Screener Plus Flow Cytometer (Sartorius). Acquired data was analyzed using GraphPad Prism 9. Fitted curves were generated by applying a Sigmoidal, 4PL, x is log(concentration) model.

Cytokine Quantification

For T cell cytotoxicity assays, supernatant was collected by spinning the assay plate at 400xg for 5 minutes, transferring supernatant to a V-bottom 96-well plate (Corning, #3363) and stored at -20ºC. Luminex cytokine detection assays were completed by the Immune Monitoring Core at Fred Hutch Cancer Center (Seattle, WA). Briefly, samples and cytokine standards were incubated with multiplexed microbeads coated with cytokine-specific capture reagents. Beads were washed, incubated with biotinylated detection reagents, washed, and stained with PE-conjugated streptavidin, washed, and analyzed on a Luminex 200 System instrument. Sample concentrations were calculated from best-fit curves generated for each analyte. Acquired data was analyzed using GraphPad Prism 10.

Statistical Analysis

Preliminary data analysis was performed using Excel version 16.0.16130.20806 (Microsoft). GraphPad Prism (version 10.1.0) was used to conduct statistical analysis and generate graphs. Statistical comparisons were made using either unpaired t-tests when comparing two experimental groups, or one-way ANOVA with a multiple comparison correction when comparing three or more conditions. For all statistical analysis, $p<0.05$ was set as the threshold for statistical

significance. P values are denoted with asterisks: $p > 0.05$, non-significant (ns); $*p < 0.05$; $**p < 0.01$; $***p < 0.001$; and $****p < 0.0001$.

Results

Design and Production of a Diverse Panel of B7H3-CD3 Targeting Bispecific T cell Engagers

Given the promising differential expression profile of B7H3, we designed a panel of B7H3-directed CD3-engaging bispecific human antibodies. Based on a review of available patents and publications, we created an anti-B7H3 scFv derived from the humanized monoclonal antibody enoblituzumab (MGA271)[78]. Enoblituzumab binds human B7H3 with relatively high affinity (K_D = 9.5 nM), demonstrates minimal binding to normal human tissues, and was well tolerated in cynomolgus monkeys[78]. The therapeutic potential of enoblituzumab to treat solid tumors is currently under evaluation (NCT01391443, NCT024275213).

We engineered a panel of n=15 B7H3-CD3 bispecific T cell engaging antibodies (BTEs), generated by combining the anti-B7H3^{MGA271} scFv with five unique anti-CD3 scFvs and arranging them into three distinct architectures (**Figure 2.6A**). The five anti-CD3 scFvs were selected for their spectrum of reported affinity to CD3εγ, ranging from 0.06 to 2500 nM[159,166]. The affinities reported in **Figure 2.6B** reference studies which measured CD3 affinity using surface plasmon resonance, specifically calculating the affinity of CD3 Fabs to recombinant CD3εγ. Notably, CD3^{OKT3} was reported to have very low affinity for the isolated CD3εγ heterodimer. This may be due to the fact that CD3^{OKT3} recognizes a particularly small epitope located on CD3ε. When CD3εγ is complexed with a TCR, the affinity of CD3^{OKT3} is higher (K_d = 1-2 x 10^{-9} M)[167,168]. CD3^{L2K} is used in blinatumomab and shares >90% sequence similarity with CD3^{OKT3}. CD3^{L2K} is reported to recognize the same epitope on CD3e as CD3^{OKT3} with 100-fold lower affinity[169]. Affinity of monomeric CD3^{L2K} to human CD3 is around 260 nM[170]. For ease of comparison, we have categorized CD3^{L2K} as low affinity, CD3^{OKT3} and CD3^{MM194} as mid-affinity, and CD3^{ADI26}, CD3^{ADI24} as high affinity T cell binders.

We aimed to compare three BTE formats that have previously demonstrated efficacy in pre-clinical models or in clinical studies: BiTE, MaxibAb, and IgG-L-scFv (**Figure 2.3**). See **Supplementary Table 6** for amino acid sequences.

A.

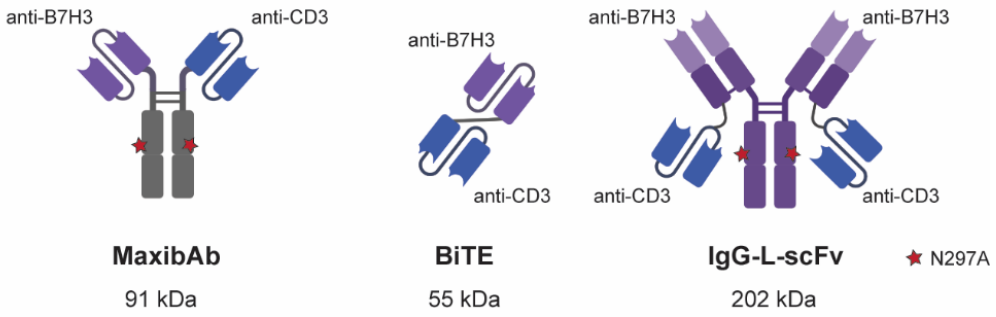

B.

CD3 binder	Fab Affinity for CD3εγ (K_D)
L2K	
OKT3	2500 nM
MM194	9 nM
ADI26906	1.1 nM
ADI50024	0.059 nM

Figure 2.6: *Development of a panel of B7H3-CD3 bispecific T cell engaging antibodies.*

(A) To generate bispecific T cell engagers (BTEs), scFvs are generated from distinct monoclonal antibodies and can be combined in a variety of different ways to generate distinct BTE architectures.
(B) Table listing anti-CD3 clones utilized in BTEs and corresponding affinities for CD3εγ.

The MaxibAb format (91 kDa) consists of a human IgG1 backbone modified with knob-and-hole mutations to facilitate heterodimerization. The anti-B7H3 scFv was connected to an Fc construct containing T366S/L368A/Y407 “hole” mutations. This was paired to an Fc construct containing a T366W “knob” mutation linked to an anti-CD3 scFv. We have previously described a highly potent PDL1-CD3 MaxibAb[130]. The BiTE format is identical to that of the FDA-approved drug blinatumomab, and consists of two scFvs linked by a short, flexible $(G_4S_1)_1$ amino acid linker. BiTEs have a molecular weight of around 55 kDa, about one third of the weight of a typical IgG antibody (150 kDa). In contrast to BiTEs and MaxibAbs, which are both dual monovalent BTEs, IgG-L-scFvs are tetravalent and larger than traditional IgGs (202 kDa). In this architecture, a bivalent IgG that recognizes a tumor-specific antigen is linked to an anti-CD3 scFv off the carboxyl

terminus of each light chain (**Figure 2.6**). This design has demonstrated efficacy when used in combination with an anti-CD3^{OKT3} and various anti-tumor antibodies (GD2[165,171,172], HER2[172,173], CD33[174], GPA33[175]). The potency of this design is attributed to several factors: bivalency for the tumor antigen, the orientation of the T cell and tumor cell binding domains in a cis-configuration, and the incorporation of an optimized anti-CD3 linker length[165]. Although it contains two anti-CD3 scFvs, T cell engagement is considered monomeric due to steric limitations that prevent non-specific activation of T cells[165]. Use of a GD2-CD3^{OKT3} IgG-L-scFv is currently in clinical trials for children and young adults with neuroblastoma and osteosarcoma (NCT02173093)[52]. Both IgG-L-scFvs and MaxibAb designs contained Human IgG1 Fc domains modified with a N297A mutation to remove a glycosylation site that mediates binding to Fc receptors required for phagocytosis and complement activation[176].

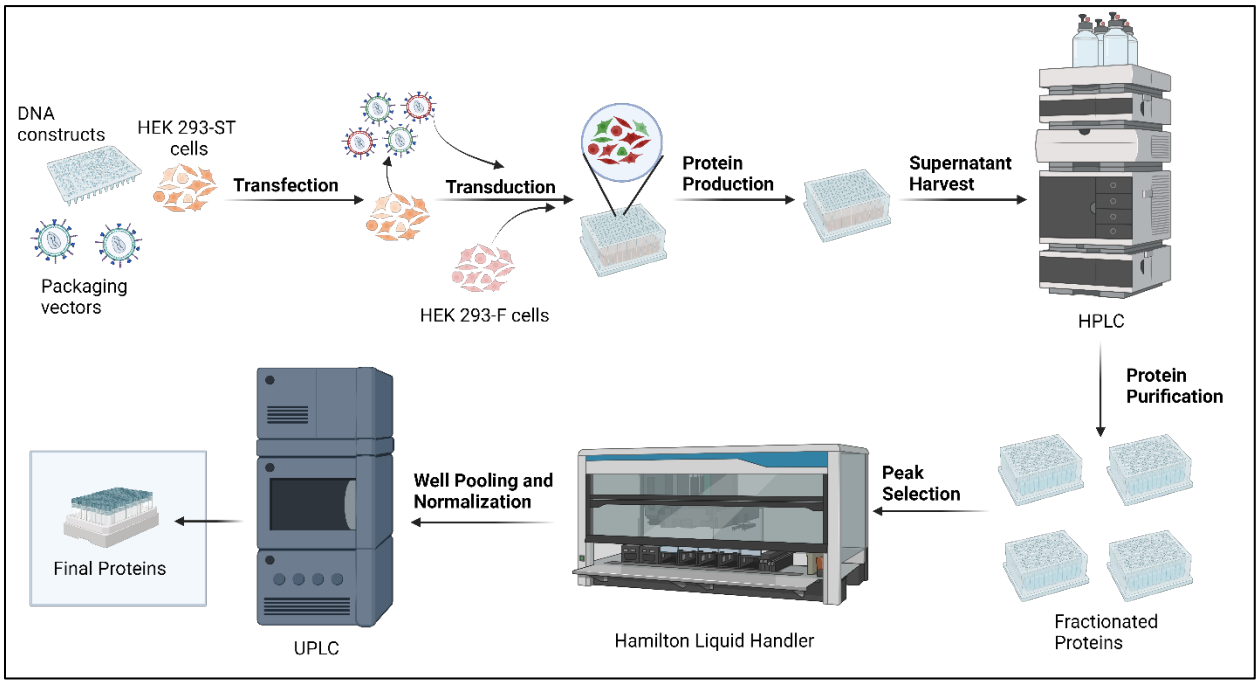

Figure 2.7: *High-throughput protein production pipeline utilized to produce BTEs.*

HEK: human embryonic kidney; HPLC: high-performance liquid chromatography; UPLC: ultra-performance liquid chromatography.

BTEs were generated using a high-throughput mammalian expression system (**Figure 2.7**). In this platform, human embryonic kidney (HEK) cells stably and robustly produce BTEs

which are subsequently purified and quantified. Ease of manufacturing is a significant consideration when designing therapeutic proteins. In our production pipeline, 93% (n =14/15) designed BTE constructs were successfully produced (**Figure 2.8**). Final UPLC traces for each construct are shown in **Figure 2.8A**. The B7H3-CD3^{OKT3} BiTE was the only molecule that failed production. In general, MaxibAb constructs were associated with the highest protein yields (**Figure 2.8B**).

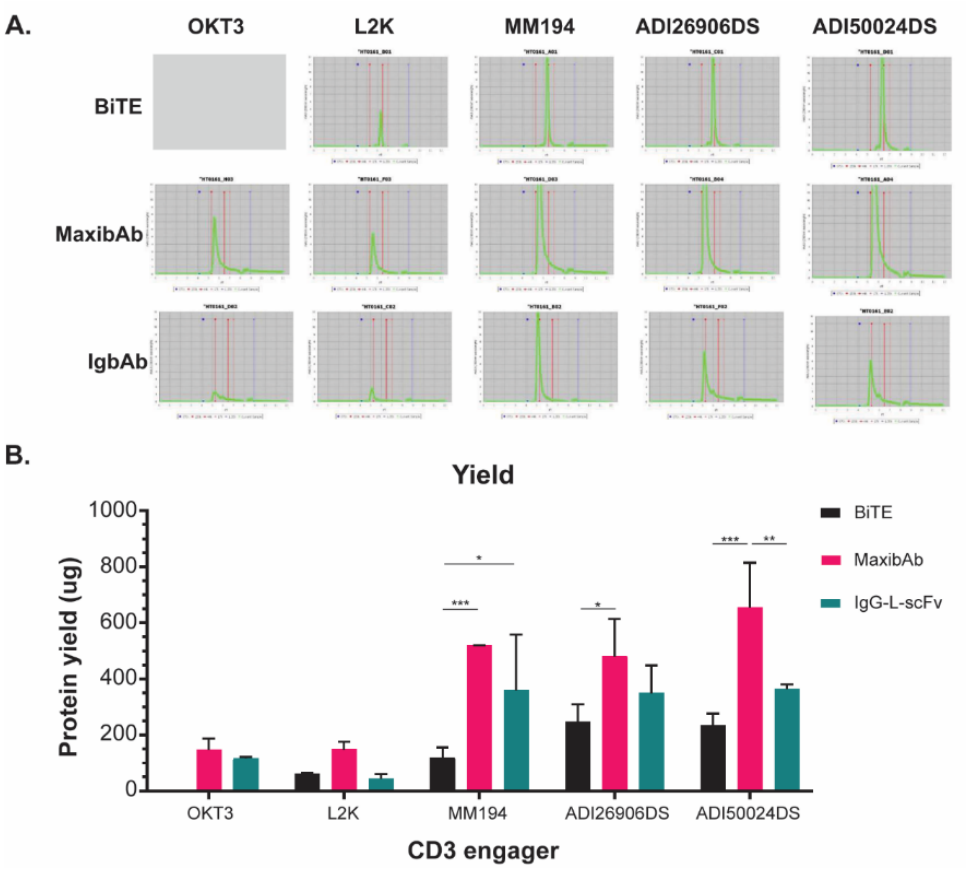

Figure 2.8: *High-throughput production of a panel of B7H3-CD3 BTEs.*

(A) Final UPLC traces for generated anti-B7H3/CD3 BTEs. Vertical red lines indicate molecular weights standards of 156 kDa (left) and 44 kDa (right).

(B) Average protein yield of individual BTEs per production run. Each construct was produced in two wells of a 96-well plate, and production was repeated once, for a total of 4 wells. (n=2, two-way ANOVA with Tukey's multiple comparisons correction, *p<0.05, **p<0.01, ***p< 0.001). Data is shown as mean +/- SD.

IgG-L-scFv molecules, despite their seemingly complex structure also yielded large quantities of purified protein. In our experience, the symmetrical architecture of the IgG-L-scFv

limited undesirable heterodimerization compared to asymmetric designs. BiTE constructs were relatively laborious to purify, primarily due the formation of BiTE-BiTE dimers that significantly reduced final yields. Comparing the impact of the anti-CD3 engagers on BTE production, we observed that anti-$CD3^{OKT3}$ and anti-$CD3^{L2K}$ scFvs were associated with the lower protein yields (**Figure 2.8B**). Interestingly, although these clones are ubiquitously used in the bispecific antibody field, we found BTEs containing either anti-$CD3^{L2K}$ or anti-$CD3^{OKT3}$ had an increased propensity to form undesirable side products. Pairing these CD3 clones with an alternative anti-B7H3 domain or optimizing linker lengths may improve production of BTEs with this scFv.

BTE structure and CD3 engager influence in vitro potency

BTE binding to antigen-expressing cells was evaluated by flow cytometry (**Figure 2.9**). The relative quantity of BTEs bound to cells was evaluated using a secondary antibody recognizing the histidine tag present on the light chain of each construct. We found that IgG-L-scFv BTEs bound most effectively to B7H3-expressing target cells (BiTE, mean MFIR = 2.57) (MaxibAb, mean MFIR = 2.44)(IgG-L-scFv, mean MFIR = 5.74)($p < 0.0001$) (**Figure 2.9A**). This result reflects the increase in avidity provided by bivalent binding to B7H3. In contrast, binding of CD3 scFvs were lower in IgG-L-scFvs compared to BiTEs and MaxibAbs (**Figure 2.10B**). This difference was most significant for higher affinity binders like ADI24 (IgG-L-$scFv^{ADI24}$, mean MFIR = 1.97) ($BiTE^{ADI24}$, mean MFIR = 8.44) ($P = 0.03$) ($MaxibAb^{ADI24}$, mean MFIR = 14.66)($p = 0.005$). However, this observation also extended to low affinity CD3 binders like L2K (IgG-L-$scFv^{L2K}$, mean MFIR = 1.01) ($BiTE^{L2K}$, mean MFIR = 3.77)($P = 0.002$)($MaxibAb^{L2K}$, mean MFIR = 4.16)($p = 0.0015$). The relatively low affinity of the IgG-L-scFv design for CD3 is consistent with prior work demonstrating that CD3 bivalency in this architecture does not translate to increased avidity for the T cell antigen[165].

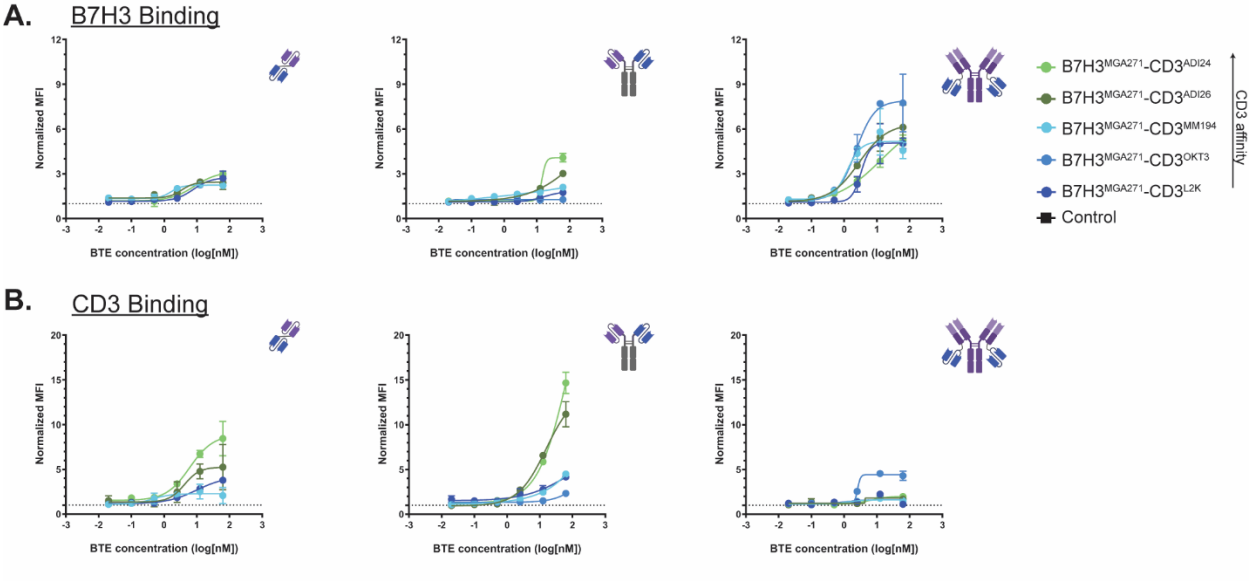

***Figure 2.9**: In vitro evaluation of B7H3-CD3 BTE binding to target cells.*

(A) Representative cell binding activity of generated BTEs to B7H3$^+$ human LAN-1 cells. Geometric mean fluorescence intensity was normalized to that of secondary alone control wells.
(B) Representative cell binding activity of generated BTEs to CD3$^+$ human activated T cells. Geometric mean fluorescence intensity was normalized to that of secondary alone control wells.
In this figure, each curve represents an individual BTE at a single concentration with two technical replicates. Gray dotted lines represent intensity of secondary alone control wells. All data is shown as means +/- SD.

To evaluate whether differences in spatial configuration affect induction of T cell-mediated cytotoxicity, we tested each construct in in vitro co-culture assays in which human activated T cells are co-incubated with human neuroblastoma cells and BTEs (**Figure 2.10A**). Each BiTE mediated similar levels of dose-dependent cytotoxicity against LAN-1 neuroblastoma target cells independently of CD3 binder affinity (Range of maximal cytotoxicity = 57.4% - 78.9%) (**Figure 2.10B**). Unexpectedly, MaxibAb constructs exhibited minimal activity compared to ATC-only controls (Range of maximal cytotoxicity = 7.7% - 41.3%) (**Figure 2.10B**). In the IgG-L-scFv format, increased CD3 affinity correlated with improved cytotoxicity (range = 23.7-70.4%) (**Figure 2.10B**). Similar findings were also observed when SK-N-SH cells, which express higher levels of B7H3, were used as target cells (**Figure 2.10B**). Again, MaxibAb constructs failed to induce

significant T cell-dependent cytotoxicity, while BiTE and IgG-L-scFvs showed clear evidence of T cell-mediated induction of tumor cell death.

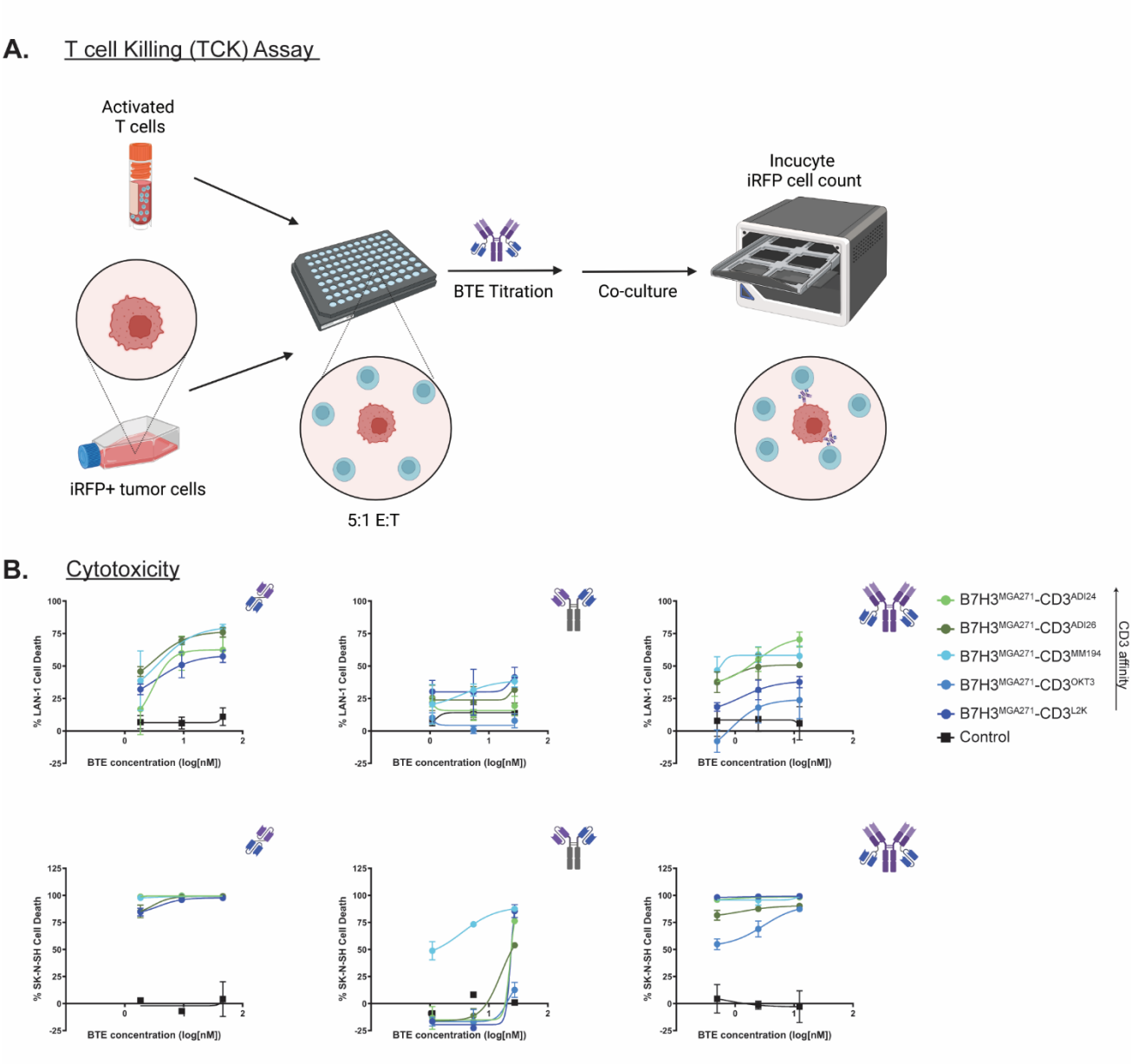

Figure 2.10: *Functional Evaluation of B7H3-CD3 Targeting BTEs.*

(A) Schematic illustrating the set-up of T cell killing (TCK) assays used to evaluate the function of generated BTEs. Previously activated T cells (ATCs) are thawed and incubated with iRFP-expressing adherent neuroblastoma cells and a dose titration of BTEs in a 96-well plate. The number of iRFP positive cells is quantified every 4 hours for up to 5 days by an Incucyte.

(B) T cell-mediated cytotoxicity of generated BTEs against LAN-1 (top) or SK-N-SH (bottom) target cells following 48HR of co-incubation. In this figure, each curve represents an individual BTE at a single concentration with three technical replicates. All data is shown as means +/- SD.

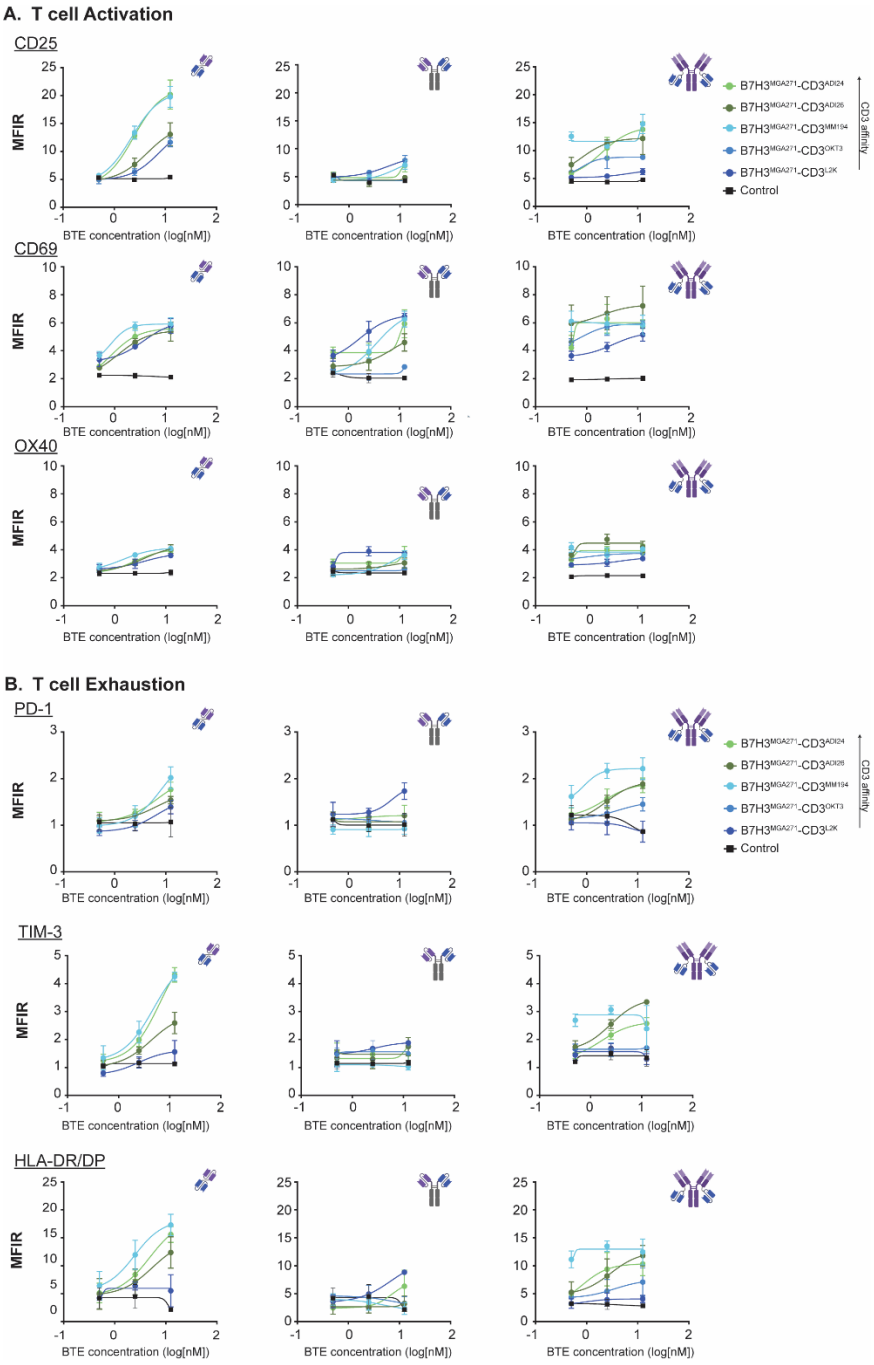

Figure 2.11: *BTEs induce upregulation of T cell activation and exhaustion surface markers.*

(A) Expression of T cell activation markers after 48 hours of co-culture of ATCs with BTE and LAN-1 target cells or tumor cells alone (control).

(B) Expression of T cell exhaustion markers following 120 hours of co-culture of ATCs with BTE and LAN-1 target cells or tumor cells alone (control). Each curve represents an individual BTE construct, and each point represents a distinct concentration of BTE, averaging the results of 3 technical replicates +/- SD.

To further explore how differences in BTE architecture may drive T cell function, we next isolated T cells from the co-culture cytotoxicity assays after 48 hours and evaluated expression of the early activation markers CD25, CD69, and OX40 (**Figure 2.11A**). As expected, BiTEs and IgG-L-scFvs elicited increased upregulation of CD25 compared to MaxibAbs, which failed to induce T cell-mediated cytotoxicity at this timepoint. Interestingly, despite the lack of functional activity mediated by MaxibAbs, they still mediated upregulation of CD69. In the IgG-L-scFv format, increased upregulation of activation markers correlated with increased CD3 binder affinity, suggesting that in this configuration, higher affinity CD3 binders may activate T cells more effectively. Across all BTEs, upregulation of OX40 was dose-dependent and independent of CD3 clone. Next, we analyzed expression of T cell exhaustion markers after 5 days of co-culture (**Figure 2.11B**). Following chronic antigen stimulation, effector T cells may enter a hypofunctional state, indicated by decreased proliferative potential and increased expression of inhibitory receptors such as PD-1 and TIM-3. We hypothesized that increased affinity of CD3 engagement would drive increased exhaustion independently of BTE architecture. Surprisingly, for BiTEs and IgG-L-scFvs, the mid affinity anti-CD3^{MM194} engager was associated with more pronounced upregulation of exhaustion markers, particularly when incorporated into a BiTE. Overall, there were no significant differences in exhaustion marker expression between BiTEs and IgG-L-scFvs. Upregulation of exhaustion markers was not observed in response to MaxibAbs, likely due to a failure to trigger robust T cell activation. Overall, results suggest that spatial configuration had no effect on induction of T cell exhaustion at the evaluated timepoint.

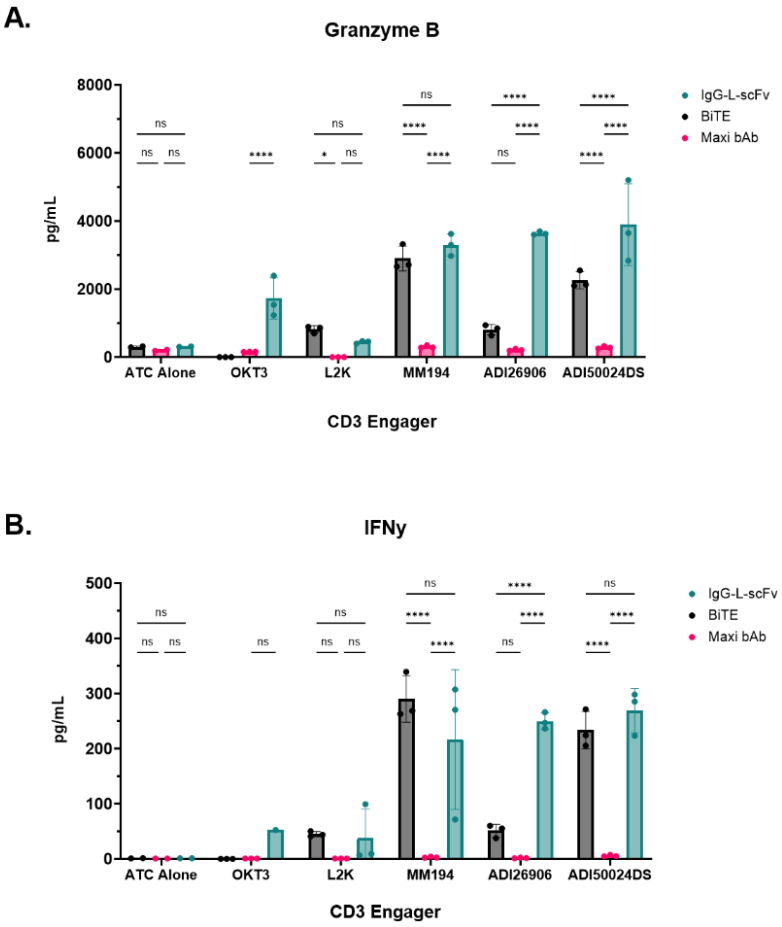

Figure 2.12: *BiTEs and IgG-L-scFvs promote secretion of Granzyme B and IFNγ*

(A) Granzyme B secretion following 48 hours of co-culture of ATCs with 0 nM or 2.5 nM BTE molecules and LAN-1 target cells.
(B) IFNγ release after 48 hours of co-culture of ATCs with 0nM or 2.5nM BTE molecules and LAN-1 target cells.
Each data point represents an individual well (n=3, ordinary two-way ANOVA with Tukey's multiple comparisons correction, **p* <0.05, ***p* <0.01, ****p* < 0.001). Data is shown as mean +/- SD.

T cell-driven cytotoxicity is accomplished through three main mechanisms: release of cytotoxic granules, triggering death receptors, and secretion of IFNγ[177]. CD8+ T cells store cytotoxic granules in secretory vesicles that are released into the immunologic synapse following TCR/CD3 clustering[178]. These granules contain a variety of perforins and granzymes. Perforins create pores throughout tumor cell membranes, permitting the entry of granzymes, which cleave

target peptides and induce apoptosis. This is thought to be a primary mechanism by which BTEs mediate tumor cell death[90]. Following activation, cytotoxic T lymphocytes upregulate expression of a membrane protein termed FAS ligand (FAS-L)[178]. Death via death receptor-ligand systems is mediated by binding of FAS-L or TNF-related apoptosis inducing ligand (TRAIL) to receptors present on tumor cells, triggering apoptotic signaling pathways. Additionally, the release of IFNγ by activated CD4+ and CD8+ cells has been shown to reduce tumor cell proliferation, upregulate FAS and TRAIL ligands on the cell surface, and increase the activity of caspases. When T cells were cultured with tumor cells in the absence of BTEs, release of granzyme B and IFNγ into the supernatant was minimal (**Figure 2.12**). In contrast, BiTEs and IgG-L-scFvs both mediated a significant increase in the production of Granzyme B and IFNγ. Consistent with a decreased ability to induce tumor cell death, BTEs containing $CD3^{OKT3}$ or $CD3^{L2K}$ were less effective inducers of IFNγ and granzyme B secretion (**Figure 2.12**). Interestingly, in the IgG-L-scFv format, increased CD3 affinity was associated with greater release of granzyme B and IFNγ (**Figure 2.12**), suggesting that the IgG-L-scFv format may require high affinity interactions with CD3 for optimal function.

Discussion

Here, we demonstrated the successful high-throughput production of a fully human/cynomolgus cross-reactive B7H3-CD3 BTEs using human host cells. In the presence of B7H3-expressing neuroblastoma cells, B7H3-CD3 BiTEs and IgG-L-scFv BTEs mediated polyclonal activation of human T cells independently of co-stimulation, as evidenced by increased surface expression of CD25, CD69, and OX40 (**Figure 2.11**). These constructs induced T cell-mediated cytotoxicity of B7H3-expressing target cells, shown through functional assays and increased secretion of granzyme B and IFNγ (**Figures 2.10 and 2.12**). In contrast, MaxibAbs were nonfunctional (**Figure 2.10**), despite confirmed binding to both CD3 and B7H3 (**Figure 2.9**).

The unexpected dysfunctionality of the MaxibAb BTEs may be attributed to several factors. The potency of BTEs has been shown to depend on not only the level of antigen expression on target cells, but also biophysical properties of the antigen itself. For instance, the mobility of the target antigen within the plasma membrane[179,180] and the distance between the targeted epitope to CD3 have been documented to influence BTE potency[151,152]. It is possible that the MaxibAbs as designed here resulted in the creation of an immunologic synapse that was not optimal. Given that this design has demonstrated high potency when targeting PD-L1 in previous publications[130], the optimal BTE architecture is likely dependent on the targeted tumor epitope.

In theory, a BTE with bivalent binding to a tumor antigen should exhibit increased avidity for the target antigen, thereby increasing the selectivity and potency of the BTE[165,181,182]. We demonstrate increased binding of IgG-L-scFv constructs to B7H3+ neuroblastoma cells compared to monovalent BTEs (**Figure 2.9**). However, this did not translate to increased potency in cytotoxicity assays compared to BiTEs (**Figure 2.10**). One possible reason is that the 5:1 E:T ratio used masked avidity-driven effects. In contrast to in vitro settings, solid tumors are remarkably heterogeneous, with tumor cells expressing a range of antigen densities, and in this context, the E:T ratio is dramatically lower. The increased avidity of IgG-L-scFvs may be advantageous in this context. While BiTEs and IgG-L-scFvs exhibited similar EC_{50} values in in vitro cytotoxicity assays, IgG-L-scFvs emerged as the more attractive BTE format for further investigation. IgG-L-scFvs consistently exhibited less intensive purification and higher final protein yields in human HEK293 cells compared to BiTEs - primarily due to their lower propensity to form dimers and larger aggregates. Although IgG-L-scFvs incorporate two anti-CD3 scFvs per molecule, preliminary evidence and published works suggest that this bivalency does not induce non-specific activation of T cells. However, further work is needed to thoroughly evaluate the target specificity of these constructs. Compared to BiTEs, the Fc region present on IgG-L-scFvs brings a significant pharmacokinetic advantage. For instance, while blinatumomab is administered as a 28-day continuous infusion that typically requires inpatient admission, currently

approved IgG-like BTEs are administered as weekly intravenous or subcutaneous injections that can be administer in an outpatient setting.

Families of children diagnosed with cancer struggle to maintain a sense of normalcy in the face of frequent hospital visits for treatment, especially when inpatient admissions are required to administer therapies[183]. In an effort to reduce the burden blinatumomab treatment protocols place on families, the Children's Oncology Group ran a clinical trial to evaluate the feasibility of in-home administration[184]. Parents of children with cancer report that in-home chemotherapy treatments are less disruptive to family life, and are associated with reduced cost, less time traveling for care, and lower levels of stress[185]. BTEs that require less arduous dosing protocols are an attractive option in the pediatric setting. Of the 5 B7H3-engaging IgG-L-scFvs evaluated in our screen, the high affinity $B7H3^{MGA271}$-$CD3^{ADI24}$ IgG-L-scFv emerged as the leading therapeutic candidate, as it had the lowest EC_{50} of all the IgG-L-scFvs evaluated and displayed promising manufacturability.

3. A B7H3-CD3 IgG-L-scFv BTE promotes T cell-mediated cytotoxicity of neuroblastoma cells in a target-dependent manner.

Abstract

Patients with relapsed high-risk neuroblastoma have few treatment options and frequently die of their disease. Bispecific T cell engaging antibodies are a growing immunotherapy approach that harnesses the cytolytic capacity of endogenous lymphocytes by bridging a tumor associated antigen and CD3. Although one Bispecific T cell Engager (BTE), blinatumomab, has demonstrated impressive efficacy in treating relapsed pediatric acute lymphoblastic leukemia, the clinical potential of BTEs for the treatment of pediatric solid tumors such as neuroblastoma is an open area of investigation. Using an IgG-L-scFv framework, we engineered and produced a fully human B7H3-CD3 bispecific T cell engaging antibody (BTE) with bivalent binding to both B7H3 (CD276) on neuroblastoma cells and CD3 on T cells. The design of this BTE conferred promising tumor selectivity, inducing preferential activation of T cell activation, proliferation, and selective cytotoxicity against B7H3-expressing cells while leaving B7H3-negative cells unharmed. Despite promising activity in vitro, this BTE failed to mediate an anti-tumor effect in neuroblastoma xenografts. We found that while systemic BTE was able to infiltrate tumors, intravenously administered T cells failed to accumulate within tumor. Within xenografts, T cells were restricted to the inhibitory tumor stroma, surrounded by immunosuppressive cells, and showed evidence of an exhausted phenotype. This work provides insight into the barriers to BTE-based immunotherapies in neuroblastoma and by extension other pediatric solid tumors. A deeper understanding of the mechanisms regulating T cell trafficking may guide future development of immunotherapeutic strategies for children with aggressive neuroblastoma tumors.

Introduction

Although implementation of anti-GD2 monoclonal antibody therapy has markedly extended survival for children with high-risk neuroblastoma, most patients will ultimately relapse and die of their disease[17]. Anti-GD2 antibodies redirect innate immune cells through Fc receptor binding, but do not directly engage with adaptive immune cells. GD2-targeting therapies have been associated with dose-limiting symptoms of pain, due to low levels of the antigen on peripheral nerves.

Bispecific T cell Engagers (BTEs) are a promising class of anti-cancer agents with the potential to eradicate tumors more precisely and efficaciously compared to conventional chemotherapies by redirecting lymphocytes to destroy cancer cells. Despite impressive clinical efficacy of BTEs for the treatment of hematological malignancies, these constructs have largely failed to demonstrate significant anti-tumor activity in solid tumors. The use of BTEs to treat solid tumors has proved challenging, and several have been limited by the presence of target antigens on healthy tissues. For example, a phase 1 trial showed that an EpCAM-CD3 BTE (AMG110, MT110) resulted in severe gastrointestinal and liver dose-limiting toxicities, consistent with EpCAM expression in the gastrointestinal tract and liver[186]. Currently, only one BTE, tebentafusp, a TCR-CD3 scFv fusion protein, is clinically approved for the treatment of a solid tumor (uveal melanoma)(**Supplementary Table 5**)[97]. No BTEs are currently approved for pediatric solid tumors, and only 2 are under active evaluation in clinical trials (**Supplemental Table 1**).

Two clinical trials have been completed evaluating the clinical potential of GD2-CD3 BTEs in neuroblastoma. The first study (NCT02173093), completed in 2019, evaluated a chemically conjugated $GD2^{3F8}$-$CD3^{OKT3}$ BTE. This IgG-IgG BTE was administered in combination with ex vivo expanded and activated autologous T cells, under the hypothesis that “arming” of T cells with BTE prior to infusion would enhance anti-tumor activity[187]. 12 patients were enrolled onto this trial, 7 with neuroblastoma (n=7/12, 58.3%). All patients developed manageable symptoms of cytokine release syndrome (CRS) but notably, no symptoms of pain. Evidence of BTE activity was

observed in several patients, including one patient with osteosarcoma with a PET response and one patient with neuroblastoma who exhibited a complete bone marrow response and remained progression-free for 2.5 years after cessation of treatment[52].

An alternative GD2^{3F8}-CD3^{OKT3} in the IgG-L-scFv format has shown impressive activity in preclinical models of neuroblastoma[165,188]. In 2019, a phase I/II clinical trial evaluating the safety and efficacy of GD2^{3F8}-CD3^{OKT3} IgG-L-scFv BTE in pediatric solid tumor patients was initiated (NCT03860207). However, this study was terminated in 2021 before a maximally tolerated dose could be determined. The design of this study included 6 escalating dose levels ranging from 0.009 mcg/kg/cycle to 9.3 mcg/kg/cycle, administered intravenously over 1-3 hours. 11 subjects were enrolled, including patients with osteosarcoma (4/11, 36.4%) and neuroblastoma (n=7/11, 63.6%). Following BTE treatment, 63.6% of patients reported symptoms of CRS (n=7/11), one of which was categorized as a severe adverse event (n=1/11, 9.1%). 36% of patients (4/11) reported symptoms of pain. Unfortunately, evidence of disease progression was noted in 81.8% (n=9/11) over the course of the study. While these 2 clinical trials have begun to investigate the utility of BTEs for the treatment of neuroblastoma, further trials to evaluate the safety and efficacy of these drugs are needed. As GD2 is already targeted through dinutuximab treatment, and patients may lose GD2 expression following dinutuximab therapy[189], investigation of alternative neuroblastoma targets is valuable.

We identified B7H3 as an attractive target for bispecific T cell engager therapy that is overexpressed in neuroblastoma (**Chapter 1**). A preliminary screen identified a B7H3^{MGA271}-CD3^{ADI24} IgG-L-scFv as a candidate BTE (**Chapter 2**). Here, we aimed to characterize the function and specificity of the generated B7H3^{MGA271}-CD3^{ADI24} IgG-L-scFv in vitro and in vivo.

Methods

Protein Sequences

The B7H3^{MGA271}-CD3^{ADI24} IgG-L-scFv BTE ("BTE") was designed as described in Chapter 2. The sequence for the control B7H3 ^{MGA271} human IgG1 antibody was constructed by removing the anti-CD3 scFvs. The sequence for the CD19-CD3 IgG-L-scFv control BTE was constructed by replacing the V_H and V_L domains with anti-CD19 V_H and V_L domains derived from blinatumomab[46]. Selected protein sequences are denoted in **Supplementary Table 6**. Amino acid sequences were reverse translated using human codons, codon-optimized, and synthesized de novo at GenScript (New Jersey, USA).

Large-scale Expression and Purification of Bispecific T cell Engagers from Human Cells

The Daedalus mammalian expression platform was used to produce and purify BTE proteins[129,130]. HEK 293-ST cells were transfected with lentiviral vectors and DNA plasmids encoding proteins of interest. Each lentiviral vector contained a cis-linked fluorescent protein reporter (iRFP or GFP) driven by an internal ribosome entry site allowing tracking of relative protein expression levels. Light chains or knobs were associated with the iRFP reporter. Heavy chain or holes sequences were associated with the GFP reporter. iRFP and GFP lentiviral vectors were co-transfected into HEK 293-ST cells at an equal ratio. After 3 days, supernatant containing lentivirus was collected and used to transduce suspension-adapted FreeStyle 293-F cells. Transduced FreeStyle 293-F cells were cultured until terminal volume (2.5-4 L) in FreeStyle 293 Expression Medium (Invitrogen, #12338018). Supernatants containing expressed proteins were harvested, 0.22-um sterile filtered, and purified via fast protein liquid chromatography (FPLC) IMAC Ni-affinity chromatography (Cytiva, #17525501). Next, nickel-neat material was spin concentrated using 30 kDa spin columns (Amicon, #UFC901096), centrifuging at 4000 rpm for 1 hours. Next, protein-containing fractions were further purified by size exclusion chromatography (HiLoad Superdex 26/600, Cytiva #28989336) and buffer-exchanged into sterile PBS. Final

protein-containing fractions were identified, pooled, and flash frozen in liquid nitrogen. Aliquots were stored at -80ºC. Proteins were thawed overnight at 4ºC, and then spin filtered through a 0.22uM PVDF filter (Millipore, #UFC30GVNB). Protein concentrations were quantified on a Stunner instrument (Unchained Labs). Endotoxin levels were quantified using Endosafe LAL Cartridges (Charles River, #PTS20F) on a Endosafe nexgen-PTS spectrophotometer (Charles River) according to manufacturer's protocol.

Patient Derived Cell Cultures

LAN-1, IMR-32, SK-N-SH, and SK-N-BE2 cells were obtained from American Type Culture Collection. Cells were cultured in RPMI media supplemented with 10X/20mM GlutaMAX (ThermoFisher, #35050061) and 10% fetal bovine serum (ThermoFisher, #1043806). CHLA-255 cells were generously shared by the laboratory of Dr. Dean Lee (Abigail Wexner Research Institute, Nationwide Children's Hospital). Other patient-derived neuroblastoma cell lines were obtained from Children's Oncology Group and cultured in RPMI media supplemented with 20% fetal bovine serum, 10X/20 mM GlutaMAX, 10X Insulin-Transferrin-Selenium (ThermoFisher, #51500056), 10X and Antibiotic-Antimycotic (ThermoFisher, #15240062). All cultures were maintained in a 5-8% CO_2 buffered incubator at 37ºC. Characterization of all cell lines are described in **Supplementary Table 2.**

T cell Isolation and Expansion

Healthy, unstimulated human donor peripheral blood mononuclear cells (PBMCs) were obtained from Bloodworks NW (Seattle, WA, USA), frozen and stored in liquid nitrogen. T cells were isolated from a thawed PBMC aliquot using a CD3+ magnetic negative selection kit (StemCell Technologies, #7951) according to the manufacturer's instructions. Isolated cells were stained with an anti-CD3 antibody and analyzed by flow cytometry to verify successful T cell isolation, defined as >95% CD3+ population. Isolated naïve T cells were activated and expanded using Human T cell anti-CD3/CD28 activating Dynabeads (ThermoFisher, #11132D) according to the

manufacturer's protocol. Cells were cultured in RPMI media supplemented with 25mM HEPEs (ThermoFisher, #22400105), 10X GlutaMAX (ThermoFisher, #35050061), 1X PenStrep (ThermoFisher, #10378016), 0.5X 2-mercaptoethanol (ThermoFisher, #21-985-023), human recombinant IL-2 (StemCell Technologies, #78036) and 10% heat-inactivated human serum (Valley Biomedical, #HP1022HI). After 14 days of culture, T cells were harvested. Briefly, T225 flasks were placed on a magnetic slab for 5 minutes. Supernatant was decanted into 600mL TPP bottles. Remaining beads were resuspended in media and transferred to a 15mL conical tube placed on a magnetic stand. After 5 minutes, the cell suspension was transferred to a TPP bottle. Cells were spun down at 500xg for 20 minutes at 4ºC. Supernatant was decantated and cell pellet was resuspended and placed on a magnetic rack to remove remaining Dynabeads. After 5 minutes, cells were removed and counted on a ViCell Analyzer (Beckman Coulter). Collected T cells were phenotyped by flow cytometry and subsequently frozen in cell culture solution supplemented with 10% DMSO.

Evaluation of Bispecific T cell Engager Binding by Flow Cytometry

Target binding of BTEs was evaluated by flow cytometry. Neuroblastoma cells or human ATCs were incubated with titrations of BTEs in duplicate for 30 minutes on ice. Then, cells were washed and incubated with an anti-His Tag secondary antibody (GenScript, #A01802, 0.6 ug/mL) for 30 minutes on ice. Cells were washed and resuspended in a final solution of DAPI (ThermoFisher, #D3571, 1 ug/mL). Cells were analyzed on a NovoCyte 3000 Flow Cytometer.

Human Leukocyte Antigen (HLA) Typing

For PBMCs, HLA typing was performed by Bloodworks Northwest (Seattle, WA). For neuroblastoma cultures, genomic DNA (gDNA) was purified using DNeasy Blood and Tissue Kit (Qiagen, 69504). gDNA was submitted to the Geraghty Lab (Fred Hutch Cancer Center, Seattle, WA) for HLA typing.

T cell Cytotoxicity Assays

In a 96-well flat bottom plate (Greiner, #655090) neuroblastoma-luc-iRFP target cells were plated in neuroblastoma culture media and allowed to adhere. Then, serially diluted concentrations of BTEs and purified human activated T cells were added to wells in T cell culture media lacking IL-2. Neuroblastoma-iRFP cells were co-cultured with purified T cells at a 5:1 Effector:Target (E:T) cell ratio unless otherwise noted. All conditions were performed in a minimum of triplicate wells. To evaluate changes in tumor cell death, iRFP+ cells were quantified using the Incucyte SX5 cell analysis system (Sartorius) every 4 hours. iRFP+ cell counts were exported to Excel (Microsoft) and percent cytotoxicity was calculated utilizing the following formula:

% Cytotoxicity = [(Mean Count of iRFP+ cells (no drug) – Mean count of iRFP+ cells (with drug)) / Mean count of iRFP+ cells (no drug)] x 100%

Fitted curves were generated by applying a Sigmoidal, 4PL, x is log(concentration) model or a [Agonist] vs response – variable slope (four parameters) model using GraphPad Prism 10.

Evaluation of T cell Activation and Exhaustion Markers by Flow Cytometry

Human ATCs were incubated with neuroblastoma-iRFP cells (5:1 E:T) and serially diluted equimolar concentrations of BTEs in triplicate. After 48 hours, cells were pelleted, washed and stained with the following antibodies: PE anti-human CD25 (BioLegend, #302606), PE anti-human CD69 (BioLegend, #310906), or PE mouse IgG1k isotype control antibody (BioLegend, #400114) according to manufacturer protocols. For Day 5 analysis, the experiment was repeated, but cells were co-cultured for five days and stained with the following antibodies: PE anti-human PD-1 (BioLegend, #379210), PE anti-human TIM-3 (BioLegend, #379210), PE anti-human LAG-3 (BioLegend, #369306), or PE mouse IgG1k isotype control antibody (BioLegend, #400114) according to manufacturer instructions. Cells were acquired on an iQue Screener Plus Flow Cytometer (Sartorius). Acquired data was analyzed using GraphPad Prism 10. Fitted curves were generated by applying a Sigmoidal, 4PL, x is log(concentration) model.

Cytokine Quantification

For T cell cytotoxicity assays, supernatant was collected by spinning the assay plate at 400xg for 5 minutes, transferring supernatant to a V-bottom 96-well plate (Corning, #3363) and stored at -20ºC. Luminex cytokine detection assays were completed by the Immune Monitoring Core at Fred Hutch Cancer Center (Seattle, WA). Briefly, samples and cytokine standards were incubated with multiplexed microbeads coated with cytokine-specific capture reagents. Beads were washed, incubated with biotinylated detection reagents, washed, and stained with PE-conjugated streptavidin, washed, and analyzed on a Luminex 200 System instrument. Sample concentrations were calculated from best-fit curves generated for each analyte. Acquired data was analyzed using GraphPad Prism 10. Fitted curves were generated by applying a Sigmoidal, 4PL, x is log(concentration) model.

CFSE Proliferation Assay

Activated T cells were labeled with 5-Carboxyfluorescein diacetate succinimidyl ester (CFSE) according to manufacturer's protocol (BioLegend, #423801). In a 96-well round bottom plate (Corning, #3799), CFSE-labeled ATCs were co-cultured with iRFP-labeled neuroblastoma cells at a 5:1 Effector:Target (E:T) cell ratio and dose titration of B7H3-CD3 IgG-L-scFv BTE. All conditions were performed in a minimum of triplicate wells. After 5 days of co-culture, cells were collected and analyzed by flow cytometry using an iQue Screener Plus Flow Cytometer (Sartorius). To evaluate changes in T cell proliferation, iRFP-negative cells were gated and CFSE intensity was evaluated in the FITC channel. Acquired FCS files were analyzed using FlowJo v10.8.1 software (BD Biosciences). Exported data was graphed using GraphPad Prism 9. Fitted curves were generated by applying a Sigmoidal, 4PL, x is log(concentration) model.

Evaluation of Changes in Neuroblastoma Antigen Expression by Flow Cytometry

Neuroblastoma-iRFP cells were incubated with human ATCs (5:1 E:T) and serially diluted equimolar concentrations of BTEs in triplicate. After 48 hours, cells were pelleted, washed and

stained with the following antibodies: PE mouse IgG1k isotype control (BioLegend, #400114), PE anti-human B7H3/CD276 (BioLegend, #351004) or PE anti-human PDL1 (BioLegend, #393608), according to manufacturer protocols. Cells were acquired on an iQue Screener Plus Flow Cytometer (Sartorius). Acquired data was analyzed using GraphPad Prism 10. Fitted curves were generated by applying a Sigmoidal, 4PL, x is log(concentration) model.

Neuroblastoma Xenograft Models

For all in vivo studies, NSG-(K^bD^b)^{null} (NSG-(K^bD^b)^{null} (IA)^{null}, NSG-(K^b D^b)^{null} (IA^{null})) mice were obtained from in-house breeding stocks. All experiments were conducted in accordance with Seattle Children's Research Institute (SCRI) Institutional Animal Care and Use Committee (IACUC) approved protocol #ACUC00682. Study endpoint criteria included weight loss >20%, a body condition score >8, luminescence-based tumor burden >10^{10} RLU, or subcutaneous tumor burden of >2000 mm^3.

Subcutaneous Flank Xenografts

6–8-week-old NSG-MHC-I/II DKO (NSG-(K^bD^b)^{null} (IA)^{null}, NSG-(K^b D^b)^{null} (IA^{null})) mice were subcutaneously injected with 5e6 neuroblastoma cells in 50% Matrigel (Corning, #354248) prepared in PBS to a final volume of 100uL. Purified BTE proteins were administered via tail vein injections in 100uL PBS twice weekly. Tumors were evaluated by caliper measurements twice weekly. Mice were euthanized when any of the pre-defined experimental endpoints were met.

Metastatic Models

For metastatic models, LAN-1 cells co-expressing iRFP firefly luciferase (LAN-1 iRFP-ffluc) cells were harvested as previously described and resuspended at a concentration of 4e6 cells/100uL USP grade PBS. 100uL was injected into the tail vein of NSG-(K^bD^b)^{null} mice. Tumor burden was monitored weekly using an IVIS Spectrum Imaging System (Perkin Elmer).

Para-orthotopic renal capsule xenografts

For para-orthotopic models, LAN-1 cells co-expressing iRFP firefly luciferase were harvested from culture, washed with PBS and resuspended in USP-grade PBS at a concentration of 50e6/mL. 10 uL (0.5e6) of cells were surgically implanted beneath the right renal capsule of 4–6-week-old anesthetized NSG-$(K^bD^b)^{null}$ mice using a 27g needle and 50uL Hamilton syringe. Tumor burden was monitored weekly using an IVIS Spectrum Imaging System (Perkin Elmer).

Tumor Digestion for Flow Cytometry Analysis

Tumor samples were collected and dissociated with a tumor digestion Kit (Miltenyi Biotec, #130-095-929) according to the manufacturers protocol. After dissociation, cell numbers were quantified on a ViCell instrument (Bekman Coulter) and samples were incubated for 30 minutes in 10 ug/mL murine Fc receptor blocking solution (BioLegend, #101302). Following blocking, samples were stained for flow cytometry analysis as previously described. The following antibodies were used for staining: APC anti-human CD47 (BioLegend, #323124), PE anti-human CD45 (BioLegend, #304039), APC anti-human CD8 (BioLegend, #344721), APC anti-human CD69 (BioLegend, #310910), APC anti-human PD-1/CD279 (BioLegend, #379208), APC anti-human PDL1/CD274 (BioLegend, #329708), PE anti-human B7H3/CD276 (BioLegend, #351004), APC mouse IgG1k isotype control (BioLegend, #400142), or PE mouse IgG1k isotype control (BioLegend, #400114). Samples were analyzed on a NovoCyte 3000 Flow Cytometer.

Immunohistochemistry

Tumors from in vivo studies were harvested and immediately immersion-fixed in 10% neutral buffered formalin. After 24 hours, tissue was transferred to 70% ethanol for a minimum of 24 hours. Then, tumors were sectioned and paraffin-embedded for immunohistochemical (IHC) analysis. All IHC was performed by the Experimental Histopathology Core at Fred Hutchinson

Cancer Center (Seattle, WA). Slides were visualized and images were captured using Halo Image Analysis Software (Indica Labs).

Statistical Analysis

Preliminary data analysis was performed using Excel version 16.0.16130.20806 (Microsoft). GraphPad Prism 10.1.0 was used to conduct statistical analysis and generate graphs. For in vitro studies, statistical comparisons were made using either unpaired t-tests when comparing two experimental groups, or one-way ANOVA with multiple comparison correction when comparing three or more conditions. For in vivo studies, Kaplan Meier survival curves were compared using the Log-rank (Mantel-Cox) test. The Mann-Whitney test was used to compare two experimental groups. For all statistical analysis, $p<0.05$ was set as the threshold for statistical significance. P values are denoted with asterisks: $p > 0.05$, non-significant (ns); $*p < 0.05$; $**p < 0.01$; $***p < 0.001$; and $****p < 0.0001$.

Results

Production and characterization of the B7H3-CD3 IgG-L-scFv BTE

Prior work established that a $B7H3^{MGA271}$-$CD3^{ADI24}$ BTE in the IgG-L-scFv architecture was superior to a suite of comparator molecules. Consequently, we focused subsequent experiments on this candidate BTE. We produced a $B7H3^{MGA271}$-$CD3^{ADI24}$ BTE in the IgG-L-scFv format at large scale using transduced FreeStyle HEK-293F cells (**Figure 3.1A**). Under denaturing conditions, we observed a predominant protein band of approximately 200 kDa, indicative of full-length IgG-L-scFv BTE. Under additional reducing conditions, one band at 55 kDa was observed, suggesting expected disruption of disulfide bonds (**Figure 3.1B**). By SEC-HPLC, the desired BTE constituted 42% of the total yield. Aggregates were removed by size exclusion, and the highlighted fraction was isolated (**Figure 3.1C**). This BTE proved stable after a freeze-thaw cycle when assayed by SEC-HPLC (**Figure 3.1D**).

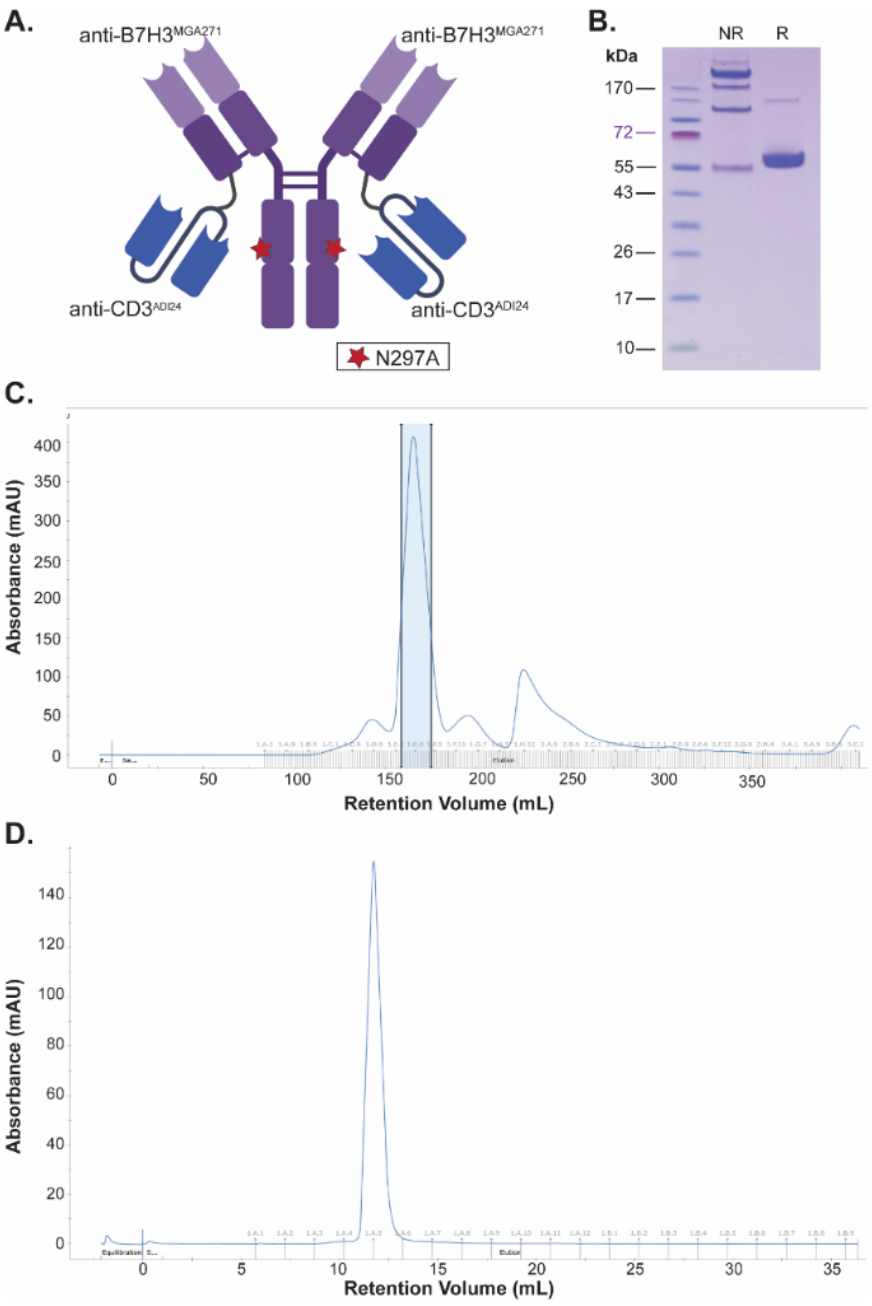

***Figure 3.1**: Large scale expression and purification of B7H3^{MGA271}-CD3^{ADI24} IgG-L-scFv BTE*

(A) Schematic diagram of the B7H3-CD3 IgG-L-scFv BTE produced.
(B) SDS-PAGE gel showing the final purified protein under non-reducing (left) and reducing (right) conditions.
(C) SEC chromatogram showing the elution profile of the protein following NiNTA affinity purification. The blue rectangle represents the final collected fractions.
(D) SEC chromatogram displaying the elution profile of the final purified protein.

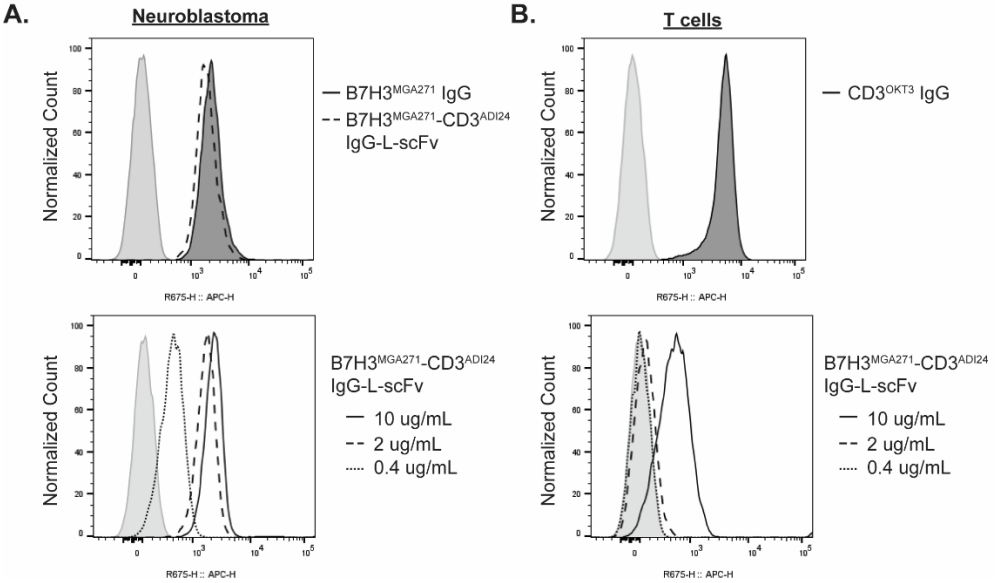

Figure 3.2*: Binding of B7H3-CD3 IgG-L-scFv BTE to target cells.*

(A) FACs histograms of B7H3 IgG (2 ug/mL) or B7H3-CD3 BTE (10, 2, 0.4 ug/mL) binding to neuroblastoma cells. Secondary alone controls are shown in light gray.
(B) FACs histograms of anti-$CD3^{OKT3}$ IgG (2 ug/mL) or B7H3-CD3 BTE (0, 2, 0.4 ug/mL) binding to human activated T cells. Isotype (top) and secondary alone controls (bottom) are shown in light gray.

By flow cytometry, this BTE exhibited comparable binding to B7H3+ neuroblastoma cells as an anti-$B7H3^{MGA271}$ human IgG1 (N297A) antibody (**Figure 3.2A**). The IgG-L-scFv showed diminished binding to CD3+ T cells compared to a conventional anti-$CD3^{OKT3}$ antibody (**Figure 3.2B**). This observation supports the hypothesis that attachment of the anti-CD3 scFv to the IgG light chain lowers avidity and reduces nonspecific binding to T cells.

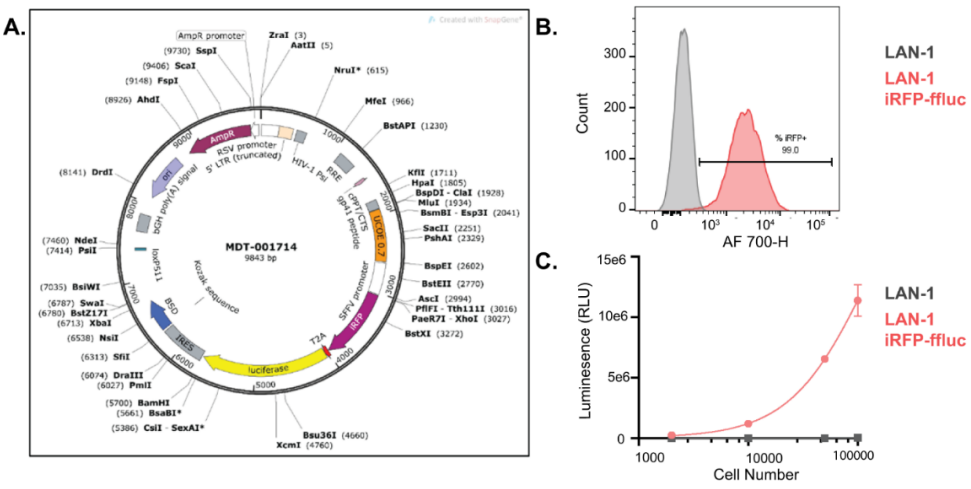

***Figure 3.3**: Lentiviral transduction of neuroblastoma cells.*

(A) Schematic of the lentiviral vector used to generate iRFP -firefly luciferase (ffluc) expressing neuroblastoma cells.
(B) iRFP expression as assessed by flow cytometry.
(C) Firefly luciferase activity was confirmed through a OneGlo Assay.

B7H3-CD3 IgG-L-scFv BTE induces T cell-directed killing of neuroblastoma cells in vitro

To evaluate the ability of the B7H3^{MGA271}-CD3^{ADI24} IgG-L-scFv BTE to promote T cell-mediated neuroblastoma cell death, a panel of neuroblastoma cell lines were transduced to express iRFP-firefly luciferase (**Figure 3.3**). Because donor matched PBMCs are not available for these cultures, T cells were isolated and expanded from four different PBMC donors as described in the methods section. During the expansion process, donors varied in proliferative potential and exhibited distinct CD4:CD8 ratios (**Figure 3.4A,B**). When co-culturing allogeneic lymphocytes and tumor cells, non-BTE mediated cytotoxicity may occur. As clearly illustrated by the field of organ transplantation, HLA mismatches can drive T cell mediated rejection of foreign tissues. HLA typing was performed for neuroblastoma cultures and PBMCs (**Supplemental Tables 7 and 8**). No complete HLA matches were identified. To evaluate whether activated T cells (ATCs) may induce neuroblastoma cell death in the absence of BTE, tumor cells were cultured with or without T cells and monitored for growth. After 72 hours of co-culture, no difference in neuroblastoma cell growth was observed in 3/4 (75%) of donors evaluated (**Figure**

3.4C). These results establish that in the absence of BTE, minimal T cell-directed killing of neuroblastoma tumor cells occurs.

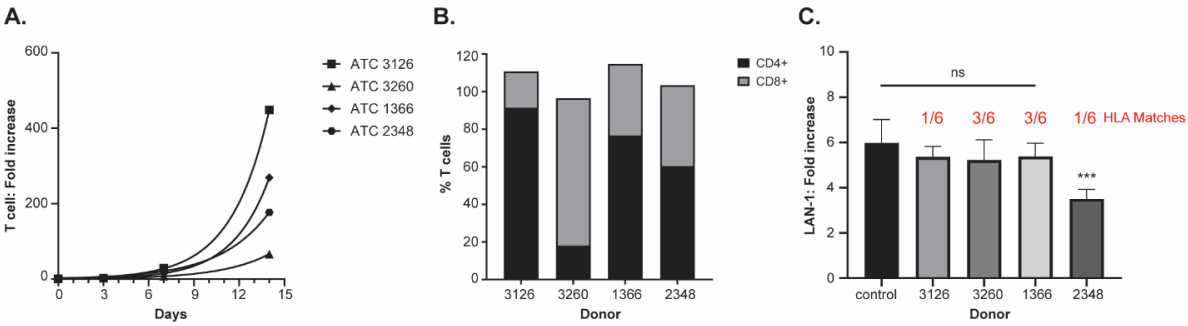

Figure 3.4: *Characterization of T cell donors.*

(A) 14-day expansion of T cells isolated from 4 independent donors. Each curve represents the results observed using a single T cell donor averaged across 1 (ATC 1366, ATC 2348) or 2 (ATC 3126, ATC 3260) independent expansions. Data shown as mean +/- SD.
(B) Ratio of CD4+ to CD8+ cells present in ATC populations following 14 days of expansion.
(C) Increase in the population of LAN-1 tumor cells following 3 days of co-culture with ATCs or media alone (control). Red text indicates the proportion of matched HLA-I alleles. (One-way ANOVA with multiple comparisons correction; ***p<0.001; ns, non-significant) Data is shown as mean +/- SD.

Next, we assessed the efficacy and potency of B7H3-CD3 BTE-directed T cell cytotoxicity against a comprehensive panel of neuroblastoma cultures. As expected, co-incubation of neuroblastoma cells and T cells with the B7H3-CD3 BTE resulted in a dose-dependent increase in neuroblastoma cell death independently of T cell donor (**Figure 3.5A**). Minimal differences in ATC donor EC_{50} were observed in SK-N-SH cell line, which expresses the highest levels of B7H3 of the 4 cultures shown in panel A (B7H3 expression = 60,213)(EC_{50} range = 0.02 – 0.09 nM). In contrast, the greatest variability in BTE efficacy was observed in the presence of IMR-32 cells. Of the 4 cell lines shown in panel A, IMR-32 cells harbor the lowest levels of B7H3 (B7H3 expression = 15,350) (EC_{50} range = 0.01 – 0.14 nM). Thus, T cell donor-dependent differences in efficacy may only become evident when target antigen density is low. Additional in vitro assays confirmed that the BTE was efficacious against a diverse panel of neuroblastoma cell cultures (**Figure 3.5B**)(**Supplemental Table 2**).

We found that the activity of the B7H3-CD3 BTE was attenuated when B7H3 expression was low (**Figure 3.6**), suggesting that B7H3 density may serve as a predictor of response. Further analysis showed a positive correlation between B7H3 surface expression and extent of BTE-driven tumor cell death in vitro (**Figure 3.6**). A linear relationship between target antigen expression and T cell activation has been previously documented for a BTE targeting solid tumors[190].

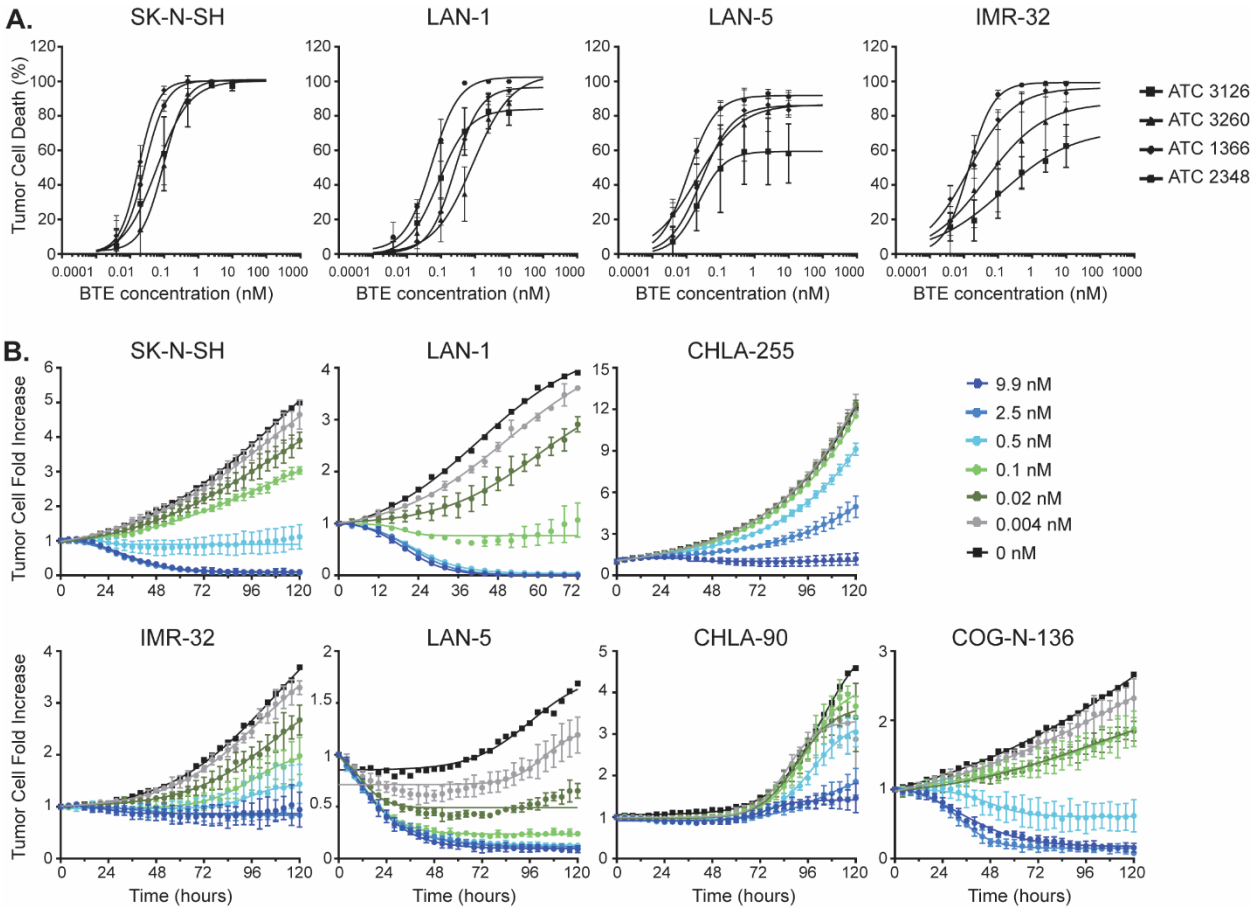

Figure 3.5: *B7H3-CD3 IgG-L-scFv mediates T cell-dependent cytotoxicity of neuroblastoma cells.*

(A) 72-hour cytotoxicity assays evaluating B7H3-CD3 BTE with multiple T cell donors and neuroblastoma cultures. Results are representative of a minimum of two assays using ATCs at a 5:1 E:T ratio. Each curve represents the results observed using a single T cell donor and a dose-titration of BTE, averaged across a minimum of two biological replicates and three technical replicates. Data shown as mean +/- SD.

(B) T cell-mediated cytotoxicity of B7H3-CD3 BTE against a panel of neuroblastoma cell lines. Results are representative of one assay using ATC 3126 effector cells at a 5:1 E:T ratio. Each curve represents a single concentration of BTE, averaged across a minimum of three technical replicates. Data shown as mean +/- SD.

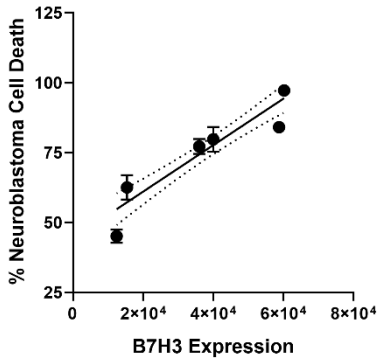

Figure 3.6: *Relationship between B7H3 expression and potency of B7H3-CD3 BTE.*

The X axis represents B7H3 expression as determined through quantitative flow cytometry (**Figure 1.5C**). The Y axis indicates the average cytotoxicity observed following 72-hour co-incubation with 9.9 nM of B7H3-CD3 BTE for each cell line (**Figure 3.5**). Simple linear regression (solid line) and 95% confidence interval (dotted lines) are shown (r^2=0.66, p<0.001, n = 48). Error bars represent the standard error of the mean.

To generate a sufficient quantity of T cells to bank for future experiments, it is necessary to culture isolated T cells with polyclonal activating stimuli to induce population expansion. However, synthetically activated T cells differ phenotypically and functionally from naïve and resting T cells. Endogenously, memory T cells respond to lower concentrations of antigen and mediate effector functions more quickly than naïve T cells[191]. Additionally, memory T cells require less co-stimulation in order to exert effector functions[191,192]. Thus, it is possible that naïve and pre-activated T cells may respond differently to BTE engagement. To evaluate whether the B7H3-CD3 BTE can activate naïve and resting T cells, cytotoxicity assays were repeated using whole PBMCs. In this context, BTE induced dose-dependent tumor cell death (**Figure 3.7**). BTE EC_{50} values for in vitro lysis of LAN-1 cells after 72 hours were slightly lower when purified ATCs (EC_{50} = 0.084 nM) were used as effector cells compared to whole PBMCs (EC_{50} = 0.13 nM) from the same donor. Altogether, these results suggest that the B7H3-CD3 IgG-L-scFv molecule can redirect the activity of both pre-activated and non-activated T cells (**Figure 3.7**).

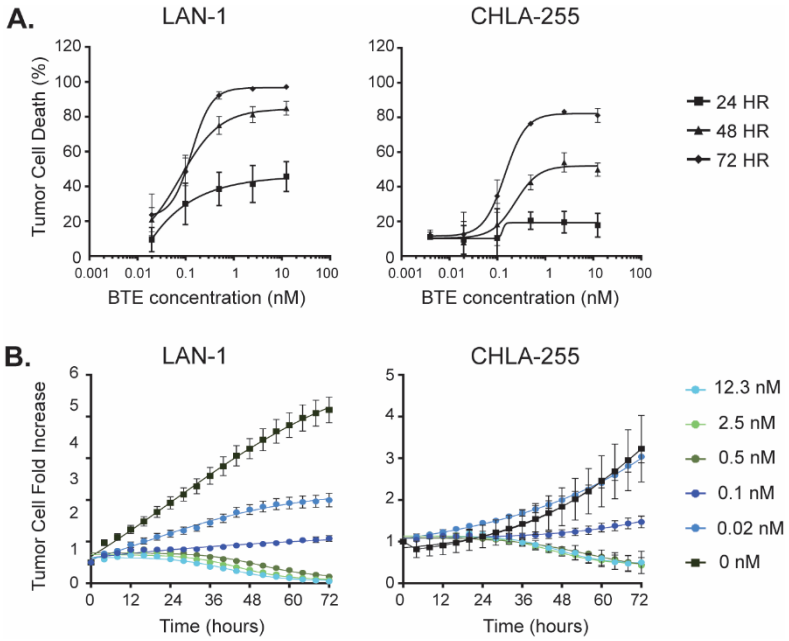

Figure 3.7: *Redirection of naïve and resting T cells by B7H3-CD3 IgG-L-scFv.*

(A) Results of cytotoxicity assays utilizing PBMCs isolated from donor 3126 as effector cells at a 5:1 T cell:tumor cell ratio. Each point along the curve represents an average of at least three technical replicates. Data shown as mean +/- SD.
(B) Naïve T cell-mediated cytotoxicity of B7H3-CD3 BTE against LAN-1 or CHLA-255 cells over time. Results are representative of one assay using PBMCs isolated from donor 3126 cells at a 5:1 T cell:tumor cell ratio.

B7H3-CD3 BTE promotes dose-dependent activation of T cells

In response to antigenic stimulation, T cells undergo “activation”, a process that drives clonal expansion of antigen-specific T cells. Activation is characterized by defined temporal changes in the expression of T cell surface markers. Within a few hours following an activating signal, T cells upregulate expression of CD69, a glycoprotein essential for the proliferation, survival, and migration of activated T cells[192,193]. Next, T cells upregulate CD25 (IL-2Ra), which enables T cells to respond to soluble IL-2[192]. CD25 expression peaks after 24 hours. After this time, $CD4^+$ T cells upregulate CD40L (CD154), which facilitates engagement with antigen presenting cells. After 72 hours, T cells will begin synthesizing and expressing MHC class II molecules (HLA-DR/DQ/DP), which serve as late markers of activation[194,195]. Stimulation-induced

expression of MHC class II may play a role in downregulation of the immune response, inducing apoptosis and anergy[194,196].

In addition to inducing characteristic phenotypic changes, the process of activation triggers T cell-mediated secretion of cytokines. The exact cytokine milieu heavily influences naïve T cell differentiation and finely modulates the overarching immune response. Immediately following stimulation, $CD4^+$ cells begin to secrete IL-2, the predominant mitogen that drives clonal expansion[192]. Secretion of IL-2 is rapid and brief, declining after only 12 hours. IL-12 and IFNy promotes the differentiation of $CD4^+$ T cells towards the pro-inflammatory type 1 helper T (Th1) subset[197,198]. Th1 helper T cells are classically associated with anti-microbial and auto immune responses but have been increasingly shown to play a major role in regulating anti-tumor immunity[197,199,200]. Th1 cells are defined by their production of IL-2, IFNy, and TNFa, which directly enhance effector functions and proliferation of cytotoxic CD8+ T cells. IFNy also indirectly supports anti-tumor immunity though activation of antigen presenting cells. TNFa is produced by both Th1 and CD8+ T cells, and enhances CD25 expression, cytokine production, and lymphocyte proliferation[201]. In addition to promoting inflammation, IFNy and TNFa directly induce apoptosis of tumor cells[177].

In response to co-incubation with BTE and a suite of B7H3-expressing target cells, T cells increased surface expression of CD25 (**Figure 3.8A**). BTE-mediated upregulation of CD25 and CD69 was dose-dependent (**Figure 3.8B**) and associated with secretion of pro-inflammatory cytokines IFNy, IL-2 and TNFa (**Figure 3.8C**). To evaluate T cell proliferation in response to BTE, a CFSE dilution assay was performed. Results showed a clear increase in T cell proliferation in cytotoxicity assays (**Figure 3.8D**). Altogether, this data affirms that in the presence of B7H3 target

cells, B7H3-CD3 BTE mediates T cell activation in a manner analogous to that induced by canonical antigenic stimulation.

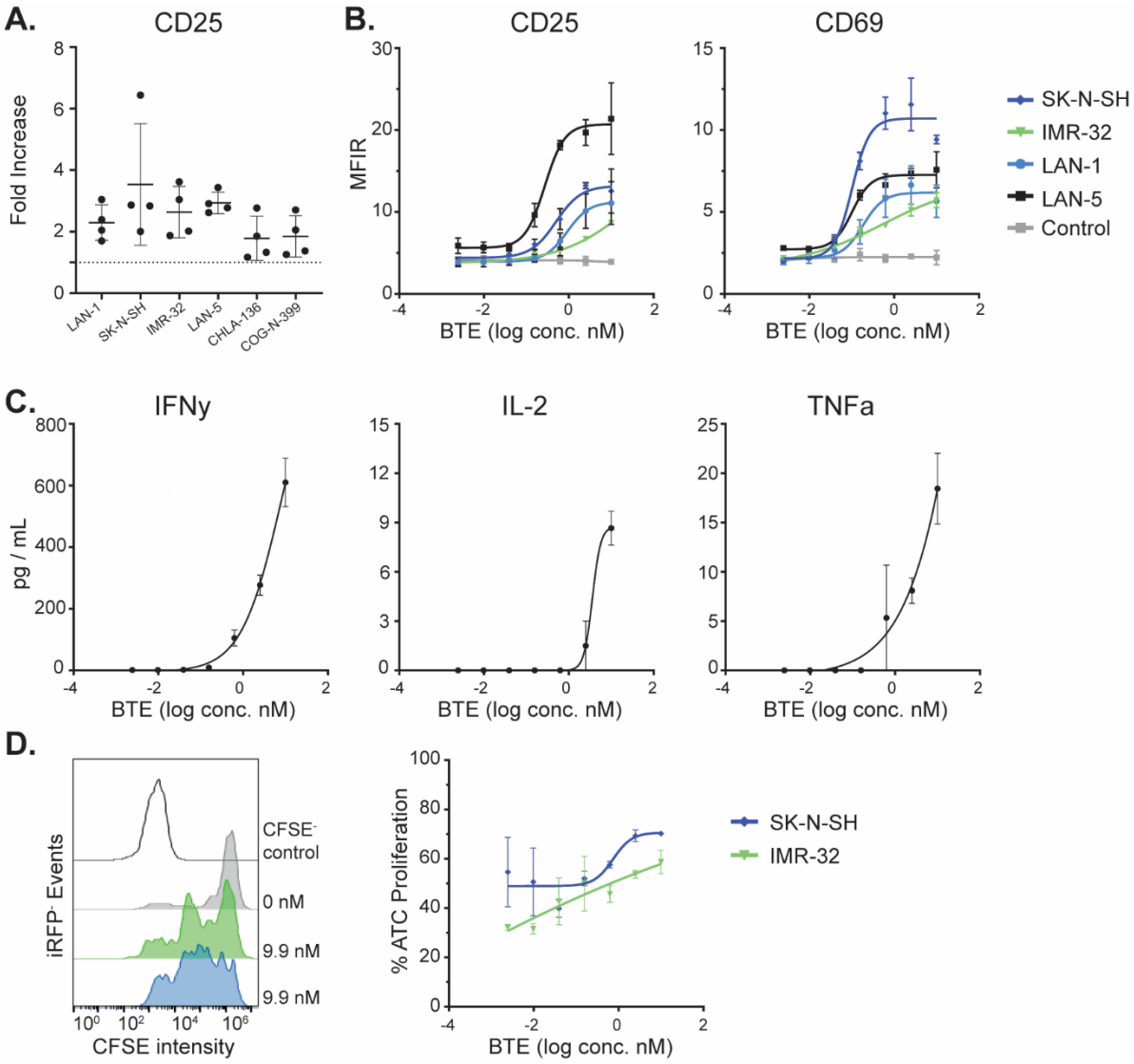

***Figure 3.8**: B7H3-CD3 IgG-L-scFv BTE promotes T cell activation.*

(A) Fold change in CD25 expression of ATCs following 48-hour co-incubation with neuroblastoma cell lines and 9.9 nM BTE. Each point represents the average of 2 technical replicates for an individual T cell donor. Fold increase was calculated by dividing mean fluorescent intensity ratio (MFIR) of the sample by that of the corresponding 0 nM BTE control. For each plot, the mean is indicated by the center line. Error bars represent the standard deviation.

(B) T cell expression of activation markers following 48-hour co-incubation with neuroblastoma cell lines and a dose titration of BTE. As a control, T cells were co-incubated with BTE in the absence of tumor cells. Results are representative of one assay using ATC 3126 effector cells at a 5:1 E:T ratio. MFIR was calculated by dividing geometric mean intensity by that of the corresponding isotype control.

Each curve represents a single target cell line, averaged across a minimum of three technical replicates. Data shown as mean +/- SD.

(C) Cytokine secretion by T cells following 48 hr co-incubation with neuroblastoma cell lines and a dose titration of BTE. Results are representative of one assay using ATC 3126 effector cells at a 5:1 E:T ratio and LAN-1 target cells. Each point along the curve represents the average of three technical replicates. Data shown as mean +/- SD.

(D) (left) Representative histogram overlay illustrating proliferation of CFSE-labeled ATCs after 5 days of co-culture with neuroblastoma cells and 0 or 9.9 nM BTE as measured by dilution of CFSE staining intensity. Unlabeled ATCs are shown as a negative control (black outline). (right) Corresponding graph plotting percent of T cells undergoing proliferation as a function of BTE concentration. Each curve represents a single target cell line, averaged across a minimum of three technical replicates. Data shown as mean +/- SD.

B7H3-CD3 BTE induces target-dependent redirection of T cell cytolysis

Immunomodulatory drugs commonly carry black box warnings for cytokine release syndrome (CRS), a syndrome of intense systemic immune hyperactivation that can be life-threatening[202]. CRS, originally termed “cytokine storm”, was first described in the 1990s, when the anti-CD3^{OKT3} antibody muromonab was used clinically as an immunosuppressive agent for solid organ transplantation[203–205]. Hallmarks of CRS include fever, flu-like symptoms, and dramatic elevations in circulating cytokines. In many cases, symptoms can be managed with supportive care measures[206]. However, the potential severity of CRS came to light during a first-in-human trial of theralizumab (TGN1412), an anti-CD28 monoclonal antibody. Theralizumab was intravenously administered to 6 healthy individuals, triggering severe CRS within minutes of administration. In 4 patients, symptoms progressed to multi-organ failure[207]. The clinical experience with theralizumab highlighted the dangers associated with non-specific T cell activation.

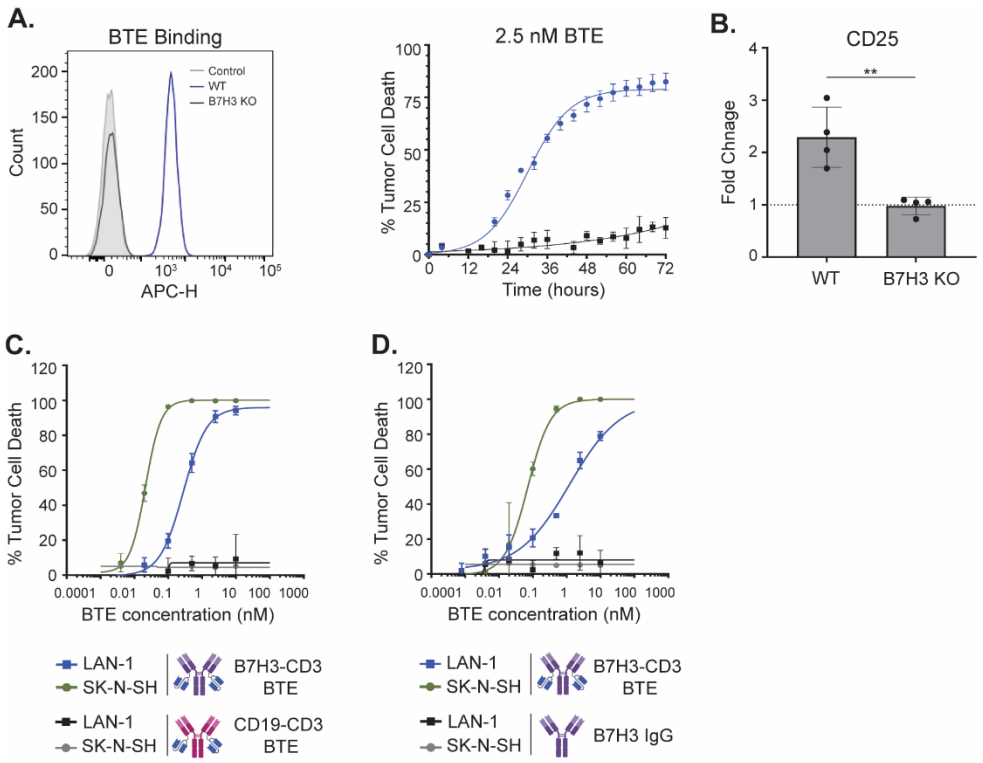

Figure 3.9: *Activity of B7H3-CD3 BTE is target dependent.*

(A) (left) FACs histogram comparing binding of B7H3-CD3 BTE to LAN-1 wildtype (WT) (blue) and LAN-1 B7H3 knock-out (KO) cells (black). Cell staining with the secondary antibody alone was used a control (gray). (right) Graph showing induction of cell death of LAN-1 WT (blue) or LAN-1 B7H3 KO cells (black) over time in the presence of 2.5nM B7H3-CD3 BTE and ATCs (5:1 E:T). Data is shown as mean +/- SD of 3 experimental replicates.

(B) Fold change in CD25 expression by ATCs following 48-hour co-incubation with BTE and either LAN-1 WT or B7H3 KO cells. Fold change was calculated by normalizing to CD25 expression measured in corresponding non-BTE controls. Each point represents the average of 2 technical replicates for an individual T cell donor. (n=4 donors, unpaired, two-tailed Student's *t*-test, $^{**}p$=0.0046). For each plot, the mean is indicated by the center line. Error bars represent the standard deviation.

(C) Quantification of T-cell dependent cytotoxicity of neuroblastoma cell lines in the presence of $B7H3^{MGA271}$-$CD3^{ADI24}$ or $CD19^{Blina}$-$CD3^{ADI24}$ control BTE. ATC 1366 cells were used at a 5:1 E:T ratio. Results are representative of two assays. Each point along the curve represents the average of at least three technical replicates. Data shown as mean +/- SD.

(D) Quantification of T-cell dependent cytotoxicity of neuroblastoma cell lines in the presence of $B7H3^{MGA271}$-$CD3^{ADI24}$ BTE or $B7H3^{MGA271}$ control antibody. ATC 3260 cells were used at a 5:1 E:T ratio. Results are representative of two assays. Each point along the curve represents the average of at least three technical replicates. Data shown as mean +/- SD.

We aimed to ascertain whether the produced B7H3-CD3 BTE mediates strictly target-dependent activation and redirection of T cells in vitro. In a comparative cytotoxicity assay, the B7H3-CD3 BTE induced death of LAN-1 WT but not LAN-1 B7H3 KO cells (**Figure 3.9A**).

Likewise, BTE activated T cells in the presence of B7H3 WT but not B7H3 KO target cells, as evidenced by CD25 expression (**Figure 3.9B**). To confirm that cytotoxicity requires BTE binding to antigen-expressing cells, a CD19^{Blina}-CD3^{ADI24} IgG-L-scFv BTE was generated. This control molecule was designed to be identical in structure to the B7H3-CD3 IgG-L-scFv BTE but bind the surface antigen CD19 in lieu of B7H3 (**Figure 3.10A**) (**Supplementary Table 6**). CD19 expression is restricted to cells of B cell lineage and is not present on neuroblastoma cells (**Figure 3.10B**). The produced CD19-CD3 BTE was confirmed to be functional, inducing cytolysis of Raji cells (**Figure 3.10C**). However, the CD19-CD3 IgG-L-scFv control BTE had no effect on neuroblastoma cells (**Figure 3.9C**), confirming that CD3 ligation in this context is not sufficient to induce target cell death.

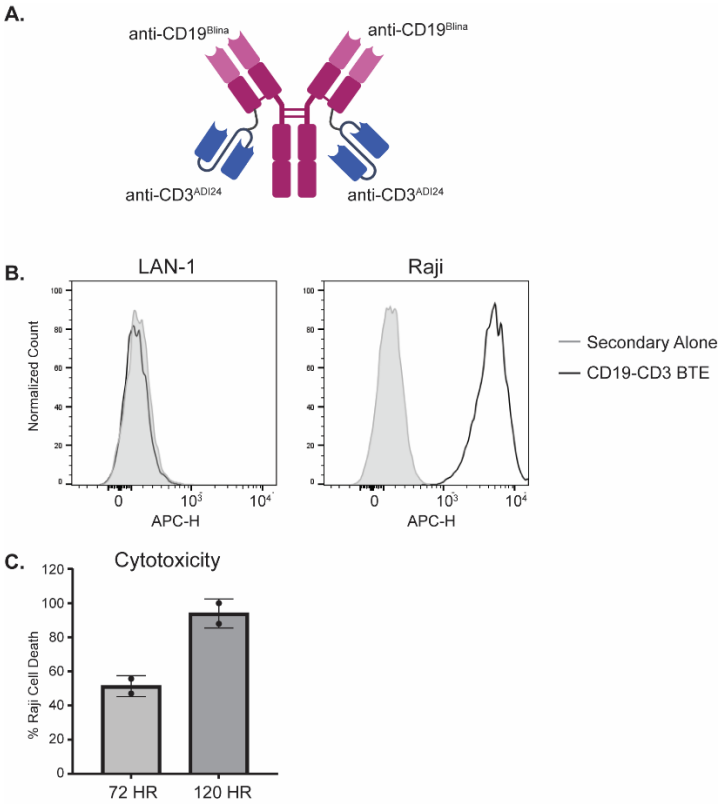

Figure 3.10: *Validation of CD19^{Blina}-CD3^{ADI24} IgG-L-scFv BTE*

(A) Schematic illustrating the structure of the produced CD19^{Blina}-CD3^{ADI24} IgG-L-scFv BTE.
(B) FACs histograms demonstrating BTE (2.5 ug/mL) binding to CD19^{-} LAN-1 and CD19^{+} Raji cells.
(C) Graph showing induction of Raji cell death in the presence of 9.9 nM CD19-CD3 BTE and ATC 3126 cells (5:1 E:T). Data is shown as mean +/- SD of n=2 experimental replicates.

As B7H3 is widely accepted to act as a T cell checkpoint ligand[58,62], we next asked whether blockade of B7H3 is sufficient to induce T cell-driven cytolysis. Anti-B7H3^{MGA271} IgG (**Supplementary Table 6**) failed to elicit cytotoxicity in vitro (**Figure 3.9D**). Altogether, this data suggests that the anti-tumor activity observed is strictly dependent on BTE-driven T cell-tumor cell cross-linking. Essentially, BTE binding to both tumor antigen and CD3 is required for activity.

In summary, this data affirms the target dependency of IgG-L-scFv BTE-mediated activation and redirection of cytotoxic T cells in vitro. While these findings do not eliminate the possibility that this BTE may induce CRS in humans, it provides reassurance that the clinical severity will be lower than what was observed in response to non-specific T cell-activating antibodies. CRS has been documented in response to blinatumomab and adoptive T cell therapies. However, the incidence and severity of CRS continues to decline following implementation of preventative protocols[206,208,209] and treatment with soluble IL-6 receptor (tocilizumab)[206,210].

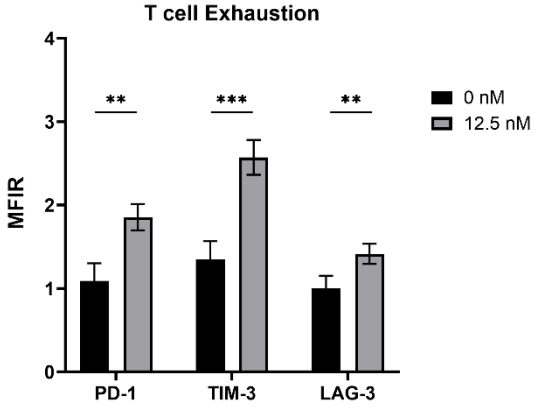

Figure 3.11: *Long-term exposure to B7H3-CD3 IgG-L-scFv upregulates surface markers associated with T cell exhaustion.*

Fold change in expression of exhaustion markers by ATCs following 5-day co-incubation with LAN-1 cells and 12.5 nM BTE. Mean Fluorescence Intensity Ratio (MFIR) was calculated by dividing geometric mean fluorescent intensity of the sample by that of the corresponding isotype control (n=6, Paired, two-tailed Student's *t*-tests, ** $p<0.01$, *** $p<0.001$). Data is shown as mean +/-SD.

Following intense antigenic stimulation, T cells commonly enter a hypofunctional "exhausted" state[178]. This phenomenon has been extensively described in the context of chronic viral infections, and more recently, in the setting of anti-cancer immunotherapies. Unlike immune tolerance, in which T cells fail to develop into effector cells, T cell exhaustion is considered a sequela of activation, and likely evolved to naturally down-regulate host immune responses[178]. Exhaustion is characterized by co-expression of inhibitory immune checkpoints including programmed cell death protein 1 (PD-1), T-cell immunoglobulin and mucin domain-3 (TIM-3) and lymphocyte activation gene-3 (LAG-3). Functionally, exhausted lymphocytes have diminished capacities for cytokine production, proliferation, and effector functions[178].

To mimic the long-term antigenic stimulation associated with exhaustion, ATCs were co-cultured with LAN-1 tumor cells and a high concentration of BTE for 5 days. At this point, T cells exhibited minor but significant upregulation of exhaustion markers (PD-1, LAG-3, and TIM-3) (**Figure 3.11**). T cells collected from patients concurrently receiving blinatumomab showed a decline in ex vivo cytotoxicity and IFNy production, which was restored following cessation of treatment[211]. Therefore, BTE-induced exhaustion may be a temporary, reversible state. Additionally, BTEs which are not administered as a continuous infusion may be less prone to inducing exhaustion.

Evaluation of B7H3-CD3 BTE in neuroblastoma xenograft models

Given the evidence that B7H3-CD3 IgG-L-scFv BTE mediates potent, target-dependent, T-cell mediated killing of neuroblastoma cells in vitro, we next aimed to evaluate the efficacy of this BTE in neuroblastoma xenograft models. For all models, we utilized an established dosing paradigm in which after tumor burden is established, ATCs (ATC 3126, 7.5e6 i.v.) are dosed once weekly, and BTE (B7H3-CD3 IgG-L-scFv, 25-100ug i.v.) is dosed twice weekly until endpoint criteria are met[130]. NSG-$(K^bD^b)^{null}$ mice were utilized in all studies to permit engraftment of human neuroblastoma cells and prevent the development of graft-vs-host disease. Unexpectedly, treatment with B7H3-CD3 BTE had no effect on LAN-1 tumor growth in subcutaneous, metastatic,

and para-orthotopic renal capsular xenograft models (**Figure 3.12A-C**). Flow cytometry analysis of subcutaneous LAN-1 tumors showed limited infiltration of human T cells (**Figure 3.12D**). Parallel analysis of murine bone marrow collected from mice with metastatic disease similarly showed a lack of a human T cell population (**Figure 3.12E**).

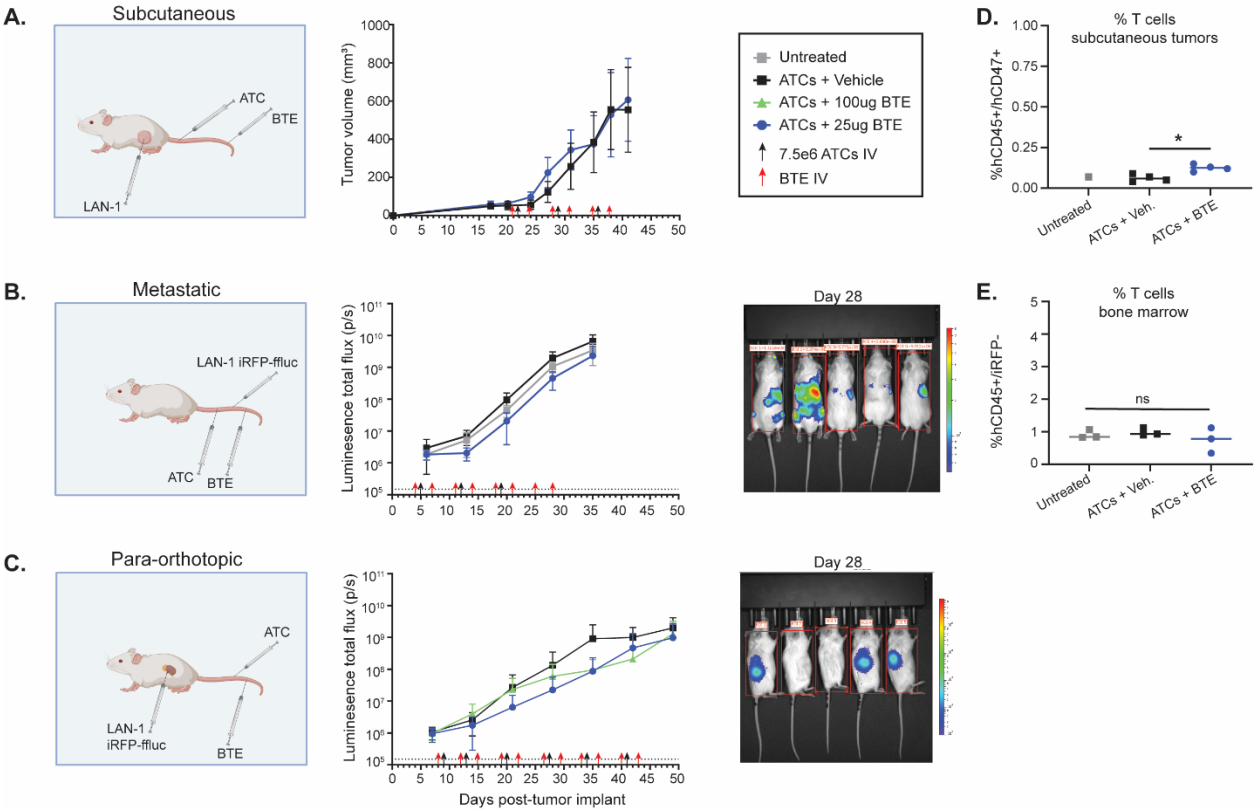

Figure 3.12: *B7H3-CD3 BTE fails to reduce tumor burden in LAN-1 in vivo models.*

Treatment with B7H3-CD3 BTE failed to reduce tumor burden in LAN-1 (A) subcutaneous, (B) metastatic, and (C) para-orthotopic renal capsular tumor models. Following establishment of tumor burden, mice were dosed with intravenous BTE twice weekly and intravenous activated T cells (ATC 3126) as indicated by arrows. Dotted lines denote intensity of background signal. Right, representative BLI images.
(D) Frequency of human T cells (DAPI-,hCD45+,hCD47+) identified in individual LAN-1 subcutaneous tumors (one-way ANOVA with multiple comparisons correction; ns, non-significant). Each line is representative of the group mean.
(E) Frequency of human T cells (DAPI-,hCD45+,iRFP-) identified in individual murine bone marrow samples collected from the study shown in panel B (one-way ANOVA with multiple comparisons correction; ns, non-significant). Each line is representative of the group mean.

These findings drew into question whether the generated BTE or the neuroblastoma tumor microenvironment was the primary barrier to efficacy. To differentiate between these possibilities, a positive control BTE was evaluated in vivo. We recently developed a PDL1-CD3 BTE in the MaxibAb format that mediates potent anti-tumor efficacy in multiple subcutaneous tumor models[130]. We have found that this BTE also significantly extends survival in orthotopic pediatric brain tumor xenografts expressing PD-L1 (data not shown).

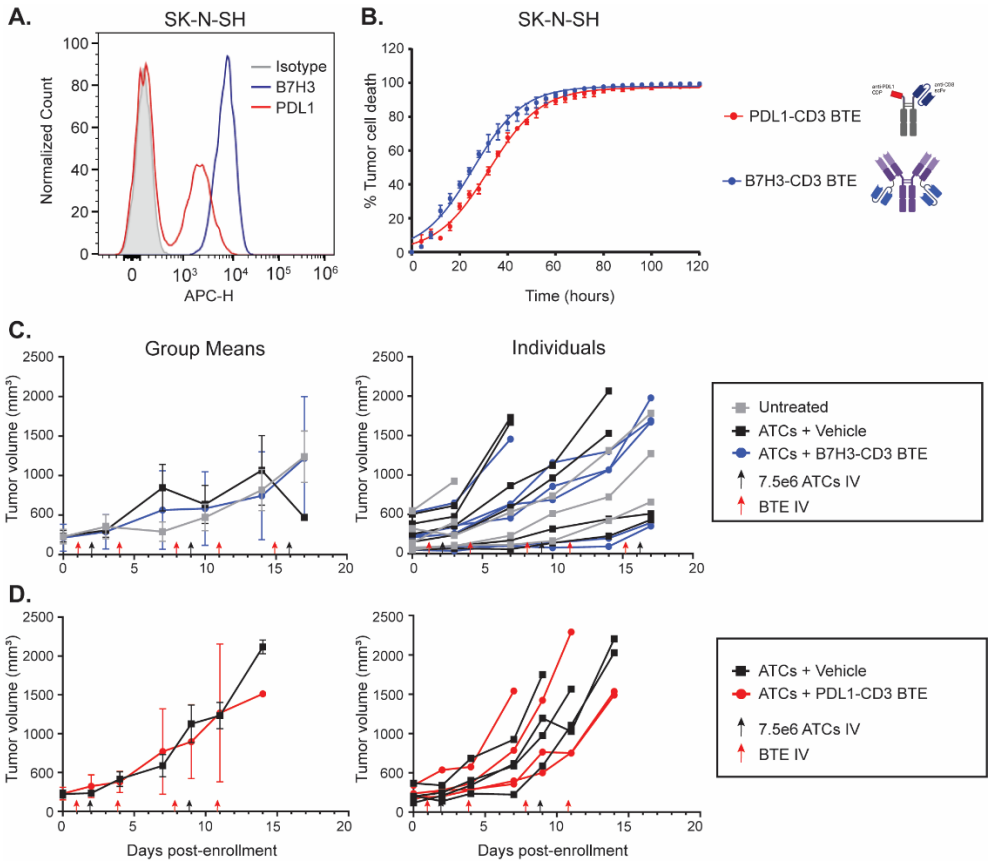

Figure 3.13: *BTEs fail to demonstrate anti-tumor efficacy in the SK-N-SH tumor model.*

(A) Surface expression of B7H3 and PDL1 on the SK-N-SH neuroblastoma cell line as determined by flow cytometry.

(B) T cell-mediated cytotoxicity of PDL1-CD3 MaxibAb and B7H3-CD3 IgG-L-scFv BTEs against SK-N-SH target cells over time. Results are representative of one assay using ATC 3126 effector cells at a 5:1 E:T ratio. BTEs were used at 2 ug/mL. Each data point represents the average of a minimum of three technical replicates. Data shown as mean +/- SD.

(C) The B7H3-CD3 IgG-L-scFv BTE did not demonstrate anti-tumor activity in the SK-N-SH subcutaneous tumor model. Following establishment of tumor burden, mice were dosed with

intravenous BTE twice weekly and intravenous activated T cells (ATCs) as indicated by arrows. Results are representative of two independent studies.

(D) The PDL1-CD3 MaxibAb BTE did not demonstrate anti-tumor efficacy in the SK-N-SH subcutaneous tumor model. Following establishment of tumor burden, mice were dosed with intravenous BTE twice weekly and intravenous activated T cells (ATCs) as indicated by arrows. Results are representative of two independent studies.

To investigate whether the lack of in vivo efficacy observed was due to a shortcoming of the B7H3-CD3 BTE, we compared the efficacy of the B7H3-CD3 IgG-L-scFv and PDL1-CD3 MaxibAb BTE in a neuroblastoma subcutaneous tumor model (**Figure 3.13**). Of all the neuroblastoma cell cultures evaluated by flow cytometry (n=15), SK-N-SH cells were found to express the highest levels of PD-L1 (**Figures 1.3A, 3.13A**). In vitro cytotoxicity assays confirmed the activity of the PDL1-CD3 and B7H3-CD3 BTEs against this cell line (**Figure 3.13B**). The two BTEs were next evaluated in the SK-N-SH subcutaneous tumor model. Again, the B7H3-CD3 BTE again failed to inhibit tumor progression (**Figure 3.13C**). Surprisingly, the PDL1-CD3 BTE was also ineffective (**Figure 3.13D**). Given that the PDL1-CD3 BTE has demonstrated reproducible anti-tumor activity across multiple in vivo xenograft models, we hypothesized that the neuroblastoma tumor microenvironment hinders efficacy of BTE therapy in vivo.

Dearth of T cells in the neuroblastoma microenvironment hampers the anti-tumor activity of B7H3-CD3 BTE

Solid tumors are notoriously hostile environments for immune effector cells. The solid tumor microenvironment (TME) is poorly perfused, driving the accumulation of anti-inflammatory metabolites, lowering of pH, and induction of hypoxia which influences the functions of infiltrating immune cells. Solid tumors have been extensively shown to combat anti-tumor immunity by inhibiting T cell activation, eliciting T cell exhaustion, inducing T cell apoptosis, and promoting differentiation of CD4 cells to inhibitory regulatory phenotypes[212]. Compounding these barriers,

the high interstitial pressure and dense extracellular matrix of solid tumors renders drug delivery and T cell infiltration difficult[213–216].

We postulated that the neuroblastoma microenvironment could hamper the anti-tumor activity of BTEs through several mechanisms including: 1) prevention of BTE accumulation, 2) inhibition of T cell infiltration, or 3) induction of T cell dysfunction. Given that IgG-L-scFv BTEs have demonstrated favorable biodistribution in neuroblastoma xenografts[105,217], we hypothesized that lack of efficacy may be due in part to inadequate trafficking of T cells into neuroblastoma tumors. To test this, SK-N-SH cells were mixed with ATCs at a 1:1 E:T ratio and implanted subcutaneously. After 3 days, intravenous B7H3-CD3 BTE treatment was initiated, and tumor growth was monitored. A dose-dependent reduction in tumor growth rate was evident in groups receiving BTE (**Figure 3.14A**). In the cohort receiving the highest dose (25 ug), only 1/5 (20%) of mice developed measurable tumor burden, which occurred at a delayed timepoint following cessation of BTE treatment. This reduction in tumor development, attributed to BTE-dependent, T-cell mediated clearance, resulted in a significant survival advantage for mice treated with 5 ug and 25 ug doses of BTE (**Figure 3.14B**). Similar results were observed in a second neuroblastoma xenograft model, LAN-1 (**Figure 3.14C**) in which B7H3-CD3 BTE treatment led to prolonged survival (**Figure 3.14D**). These results demonstrate that intravenous B7H3-CD3 BTE reduces tumor burden when T cells are present within the TME. In previous models, T cells were

administered intravenously, and a lack of T cells within the neuroblastoma microenvironment may have prevented BTE efficacy.

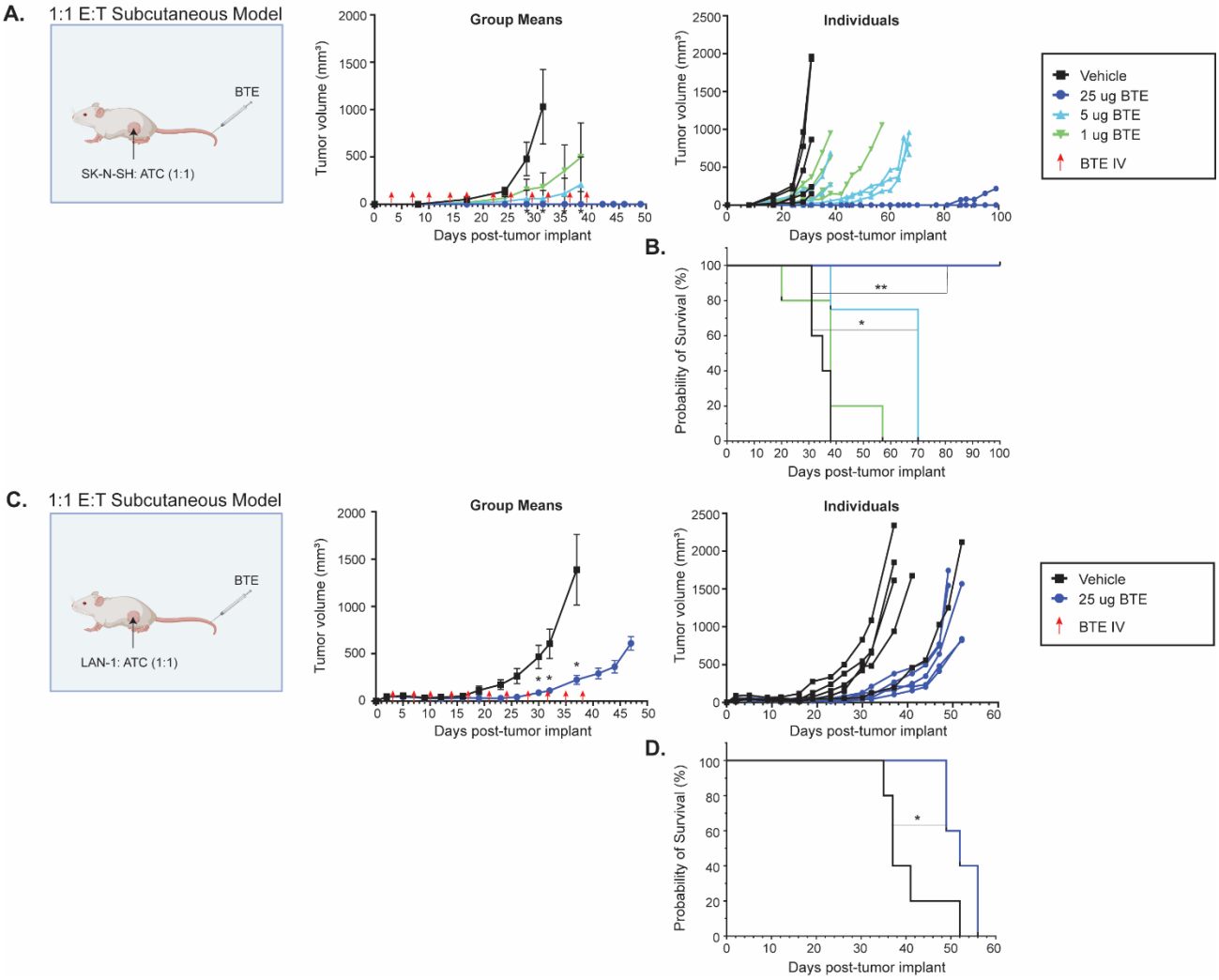

Figure 3.14: *B7H3-CD3 BTE mediates in vivo efficacy in 1:1 E:T subcutaneous neuroblastoma models.*

(A) Efficacy of B7H3-CD3 BTE in 1:1 E:T subcutaneous SK-N-SH model. 4e6 SK-N-SH cells were mixed with 4e6 ATC 3126 cells and injected subcutaneously into the flank of NSG-$(K^bD^b)^{null}$ mice. After 3 days, mice were injected intravenously with either B7H3-CD3 BTE or PBS (vehicle) twice weekly, as indicated by the red arrows. Data is shown as mean +/- SEM.

(B) Survival analysis of mice treated in Panel A. P values were computed by a log-rank (Mantel-Cox) test. (Vehicle, n=5; 25 ug, n=5, $^{**}p$=0.0025; 5 ug, n=5, $^{*}p$=0.022; 1 ug, n=5, non-significant).

(C) Efficacy of B7H3-CD3 BTE in 1:1 E:T subcutaneous LAN-1 model. 4e6 LAN-1 cells were mixed with 4e6 ATC 3126 cells and injected subcutaneously into the flank of NSG-$(K^bD^b)^{null}$ mice. After 3 days, mice were injected intravenously with either B7H3-CD3 BTE or PBS (vehicle) twice weekly as indicated by the red arrows. (Unpaired Student's two-tailed t test, $^{*}p$<0.05). Data is shown as mean +/- SEM.

(D) Survival analysis of mice treated in Panel C. P value was computed by a log-rank (Mantel-Cox) test. (Vehicle, n=5; 25 ug, n=5, $^{*}p$=0.027).

To confirm that intravenously administered B7H3-CD3 BTE can access neuroblastoma xenografts and subsequently activate intra-tumoral T cells, SK-N-SH cells were implanted into the flanks of NSG-$(K^bD^b)^{null}$ mice (**Figure 3.15A**). 4 weeks after tumor establishment, mice were distributed by tumor burden into two equivalent groups before receiving a single intra-tumoral dose of human ATCs (**Figure 3.15B**). On the same day, mice received either one intravenous injection of 25 ug BTE or PBS (vehicle). After 48 hours, tumors were harvested, mechanically and enzymatically digested, and human T cells were identified and characterized by flow cytometry (**Figure 3.15C**). There was no difference in the quantity of intra-tumoral T cells between groups (**Figure 3.15D**). However, mice receiving BTE had a higher proportion of CD8+ T cells compared to mice receiving vehicle and parental ATCs (Parental ATCs, mean percent CD8+ = 12.8%; Vehicle cohort, mean percent CD8+ = 17.5%; BTE cohort, mean percent CD8+ = 28.5%) (**Figure 3.15E**). This difference suggests potential BTE-driven proliferation of cytotoxic CD8+ lymphocytes in the tumor. Preferential expansion of CD8 cells in response to BTE has been shown previously[218,219]. Notable differences in T cell phenotype were also observed between treatment groups. In response to BTE, T cells robustly upregulated CD69 expression (**Figure 3.15F, G**), indicative of T cell activation. Taken together, this data suggests systemically administered BTE is present within neuroblastoma tumors and induces activation and proliferation of cytotoxic lymphocytes.

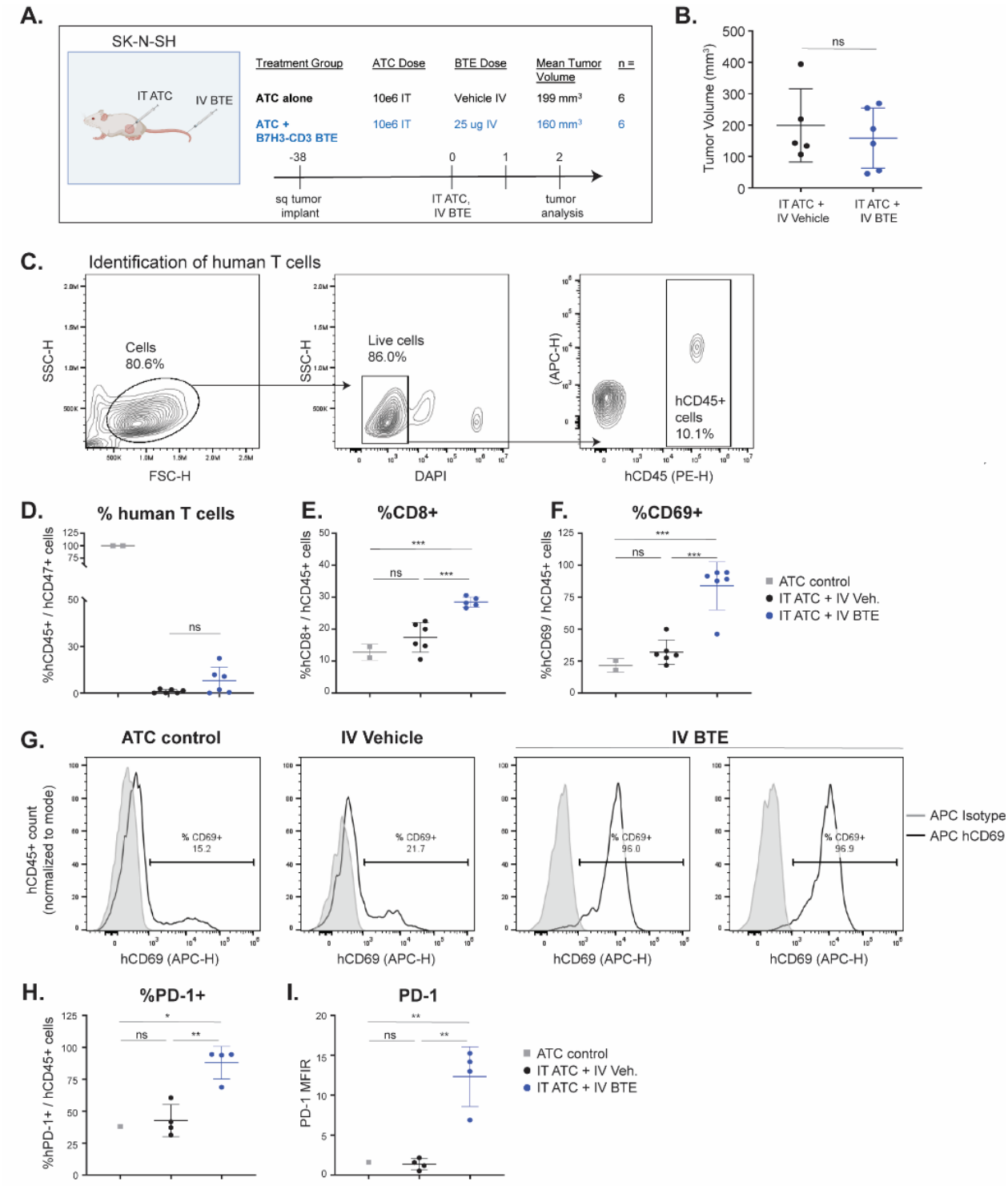

Figure 3.15: *Intravenous BTE activates intra-tumoral human T cells.*

(A) Study overview. 4e6 SK-N-SH cells were injected subcutaneously into the flank of NSG-$(K^bD^b)^{null}$ mice. Once tumors reached a volume of >50 mm^3, mice were injected intra-tumorally with 10e6 ATCs and injected intravenously with either B7H3-CD3 BTE or PBS vehicle control. After 48 hours, tumors were harvested and analyzed by flow cytometry.

(B) 38 days after tumor implantation, tumor volumes were measured, and treatment groups were established. (Unpaired, two-tailed Student's *t*-test with Welch's correction, *P*=0.55; ns, non-significant).
(C) Representative flow cytometry plots depicting gating strategy used to identify human T cells (DAPI-, hCD45+) from SK-N-SH tumors. Plots are representative of n=11 experimental replicates.
(D) Frequency of human T cells (DAPI-,hCD45+,hCD47+) identified in individual SK-N-SH subcutaneous tumors (one-way ANOVA with multiple comparisons correction; ns, non-significant). Data is shown as mean +/- SD.
(E) Frequency of intra-tumoral hCD45+ T cells staining positive for hCD8 as identified by flow cytometry analysis. (one-way ANOVA with multiple comparisons correction; **p<0.01, ***p<0.001; ns, non-significant). Data is shown as mean +/- SD.
(F) Frequency of intra-tumoral hCD45+ T cells staining positive for hCD69 as identified by flow cytometry analysis. (one-way ANOVA with multiple comparisons correction; **p<0.01, ***p<0.001; ns, non-significant). Data is shown as mean +/- SD.
(G) Flow cytometry histograms measuring the percent of intra-tumoral hCD45+ T cells expressing CD69. Cultured activated T cells were used as gating controls (left). ATC control plots are representative of two experimental replicates. IV Vehicle and IV BTE plots are representative of 6 and 5 experimental replicates respectively.
(H) Frequency of intra-tumoral hCD45+ T cells staining positive for the hPD-1 as identified by flow cytometry analysis (one-way ANOVA with multiple comparisons correction; **p<0.01). Data is shown as mean +/- SD.
(I) PD-1 staining intensity of hCD45+ T cells. Mean Fluorescence Intensity Ratio (MFIR) was calculated by dividing geometric mean fluorescent intensity of each sample by that of the corresponding isotype control. (one-way ANOVA with multiple comparisons correction; **p<0.01). Data is shown as mean +/- SD.

Neuroblastoma tumor microenvironment promotes T cell exhaustion

T cells isolated from tumors exposed to BTE were more likely to express the exhaustion marker PD-1 (**Figure 3.15H-I**). We previously showed in a long-term ATC:LAN-1 co-culture assay that BTE induces a moderate 1.7-fold upregulation of PD-1 on ATCs (Control, mean MFIR = 1.09; BTE, mean MFIR = 1.86)(*P* = 0.0012)(**Figure 3.11**). BTE-induced upregulation of PD-1 observed in the context of SK-N-SH xenografts was more dramatic, approximately a 9-fold increase (IV Vehicle group, mean MFIR = 1.38; IV BTE group, mean MFIR = 12.32)(*P* = 0.003)(**Figure 3.15I**). To better correlate this data to an in vitro setting, SK-N-SH cells were co-cultured with ATCs and BTE in vitro. After 48 hours, a dose-dependent upregulation of PD-1 expression was observed, maximizing at a 3.5-fold increase (Control, mean MFIR = 2.85; 9.9nM BTE, mean MFIR = 9.90)(*P* = 0.0009) (**Figure 3.16**). Compared to in vivo findings, in vitro, there was a lower baseline percentage of T cells expressing PD-1 and a less dramatic increase in the percentage of T cells expressing PD-1 in response to BTE, maximizing at 42.5% of cells in vitro

(Control, mean %PD-1+ = 16.4%; BTE, mean %PD-1+ = 42.5%)(*P* = 0.0056)(**Figure 3.16**) compared to 87.9% of cells in vivo (Control, mean %PD-1+ = 42.4%; BTE, mean %PD-1+ = 87.9%)(*P* = 0.0056) (**Figure 3.15H**). The increase in PD-1 expression at baseline and in response to BTE observed in intra-tumoral T cells raises the possibility that the neuroblastoma microenvironment may also drive T cell dysfunction.

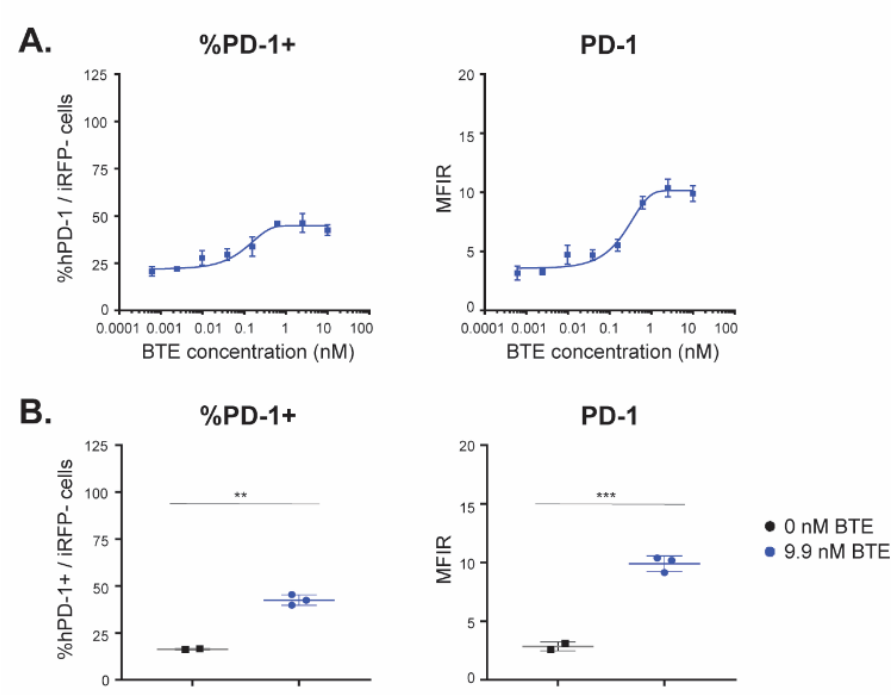

Figure 3.16: *Change in PD-1 expression in response to B7H3-CD3 BTE in vitro.*

(A) SK-N-SH iRFP cells were co-cultured with ATCs in a 5:1 E:T ratio and a dose titration of B7H3-CD3 BTE. After 48 hours, cells were stained for PD-1 expression. T cells were identified as an iRFP- cell population. (left) Graph showing percent of T cells expressing PD-1 as a function of BTE concentration. (right) Graph showing PD-1 staining intensity of T cells as a function of BTE concentration.

(B) Analysis of wells exposed to 9.9nM or 0nM of BTE. (left) Percentage of ATCs expressing PD-1 as identified by flow cytometry analysis. (right) Fold change in PD-1 staining intensity of hCD45+ T cells. Mean Fluorescence Intensity Ratio (MFIR) was calculated by dividing geometric mean fluorescent intensity of the sample by that of the corresponding isotype control. (Unpaired Student's two-tailed *t*-test; ***p*<0.01, ****p*<0.001; ns, non-significant). Data is shown as mean +/- SD.

Tumors commonly exploit the PD-1/PD-L1 axis to evade immune destruction. For example, elevation of PD-L1 on lymphoma cells has been shown to contribute to blinatumomab resistance[220]. We observed that B7H3-CD3 BTE increases expression of PD-1 on lymphocytes

in vitro and in vivo and hypothesized that BTE may also elevate expression of the PD-1 ligand PD-L1 on neuroblastoma cells. As previously discussed, neuroblastoma cells classically lack PD-L1 expression[33,34,221] (**Figure 1.3**). However, human and murine neuroblastoma cultures may upregulate PD-L1 expression in response to IFNγ exposure[33,222,223]. While the underlying mechanism in neuroblastoma has not been defined, studies in adult malignancies point to induction of JAK/STAT and ICAM1-PI3K-AkT signaling pathways[224–227]. One study showed that co-culture of neuroblastoma cells with IFNγ increased expression of the *STAT1* gene[228]. As activation of the Stat1 transcription factor is essential for the transcription of many IFNγ response genes[229,230], neuroblastoma cells may upregulate PD-L1 though IFNγ-JAK-STAT1 signaling. Cells may also develop resistance to targeted immunotherapies though antigen escape[72].

To investigate changes in neuroblastoma cell expression of PD-L1 and B7H3 in response to BTE, surviving tumor cells were collected following a 48-hour in vitro cytotoxicity assay and characterized by flow cytometry. We did not observe any clear changes in B7H3 expression in response to BTE (**Figure 3.17A**). In contrast, a dose-dependent upregulation of PD-L1 in was prominent (**Figure 3.17A**). Given that IFNγ is secreted by BTE-activated lymphocytes, we hypothesized that PD-L1 upregulation may occur in response to this cytokine. Following exposure to exogenous recombinant IFNγ, neuroblastoma cells displayed marked increase in PD-L1 expression (**Figure 3.17B**), consistent with other published works.

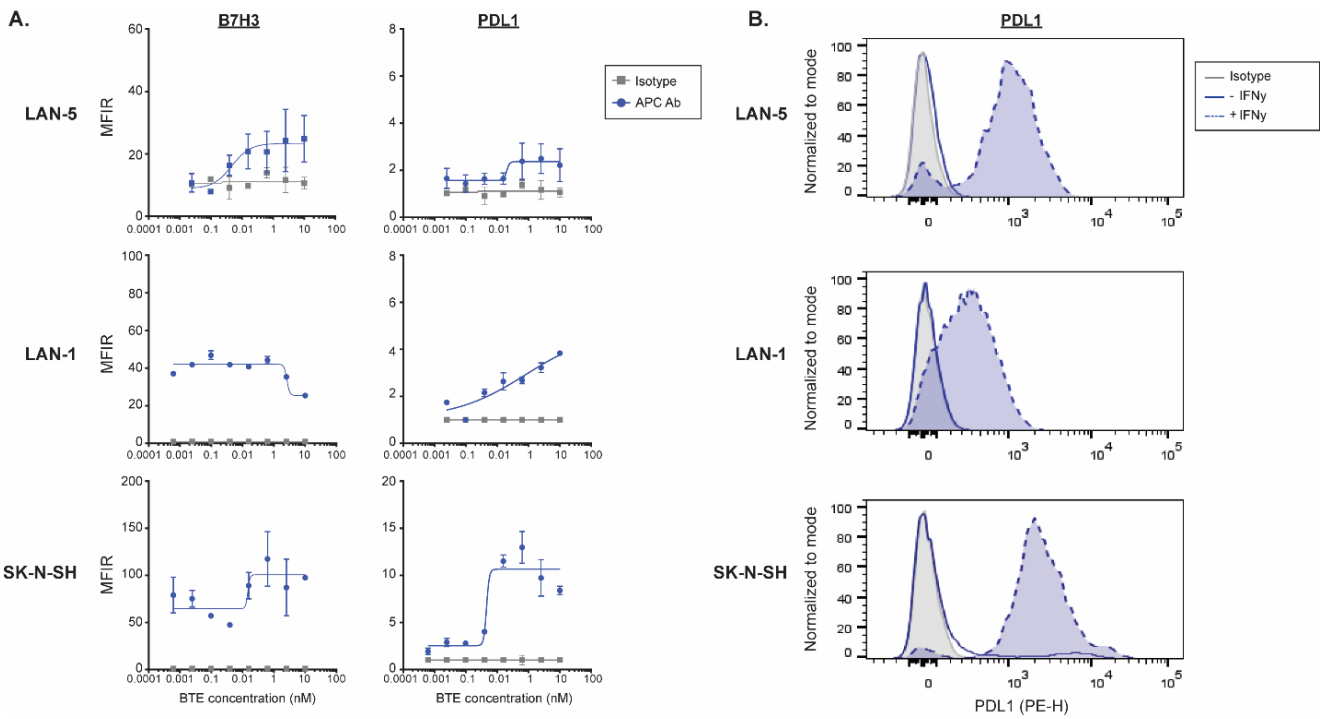

Figure 3.17: *Neuroblastoma cells upregulate surface expression of PD-L1 in response to BTE and IFNy.*

(A) iRFP+ neuroblastoma cells were co-cultured with ATCs in a 5:1 E:T ratio and a dose titration of B7H3-CD3 BTE. After 48 hours, cells were stained with PE-conjugated anti-B7H3, anti-PDL1, or isotype control antibodies. Neuroblastoma cells were identified as an iRFP+ cell population. Graphs show B7H3 (left) and PD-L1 (right) staining intensity of neuroblastoma cells as a function of BTE concentration. Data shown as mean +/- SEM.

(B) Flow cytometry histograms showing the percent of neuroblastoma cells expressing PD-L1. Cells were treated with 50 ng/mL IFNy for 24 hours, collected, and stained with a PE-conjugated PD-L1 antibody. Compared to isotype control (gray), baseline PD-L1 expression (solid blue line) varied across cell lines but cells uniformly upregulated PD-L1 following IFNγ exposure (dotted blue line). Histograms are representative of two experimental replicates.

In neuroblastoma flank xenografts, we observed no difference in PD-L1 or B7H3 expression in neuroblastoma xenografts treated with BTE or vehicle (**Figure 3.18**). Thus, while adaptive expression of PD-L1 in response to T cell activation is observed in vitro, this mechanism does not underly the lack of activity of B7H3-CD3 BTE observed in vivo.

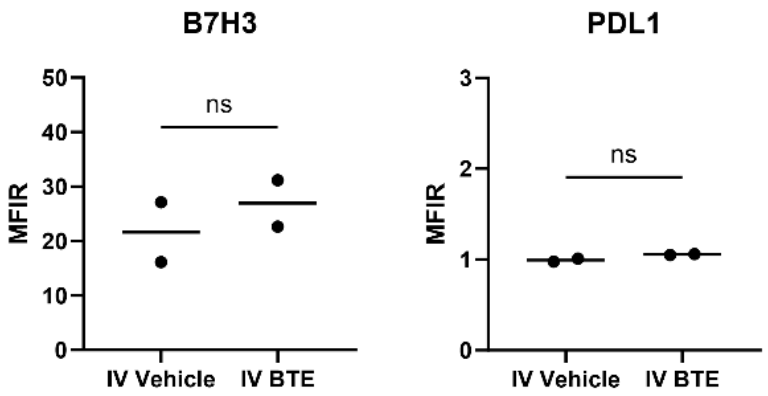

Figure 3.18: *Treatment with B7H3-CD3 BTE has no effect on PDL1 and B7H3 expression in SK-N-SH 1:1 E:T subcutaneous tumors.*

4e6 SK-N-SH cells were mixed with 4e6 ATC 3126 cells and injected subcutaneously into the flank of NSG-(K^bD^b)^{null} mice (1:1 E:T subcutaneous SK-N-SH model). After 3 days, mice were injected intravenously with either B7H3-CD3 BTE or PBS (vehicle) twice weekly, as detailed in **Figure 3.14**. At study endpoints, flank tumors were analyzed by flow cytometry.

(A) B7H3 staining intensity of individual SK-N-SH flank xenografts as determined by flow cytometry. Mean Fluorescence Intensity Ratio (MFIR) was calculated by dividing geometric mean fluorescent intensity of each sample by that of the corresponding isotype control. Horizontal line represents median expression for each group. (unpaired Student's *t* test; ns, non-significant).

(B) PD-L1 staining intensity of individual SK-N-SH flank xenografts as determined by flow cytometry. Mean Fluorescence Intensity Ratio (MFIR) was calculated by dividing geometric mean fluorescent intensity of each sample by that of the corresponding isotype control. Horizontal line represents median expression for each group. (unpaired Student's *t* test; ns, non-significant).

Human T cells co-localize with murine macrophages in neuroblastoma xenografts

So far, we have established that the anti-tumor efficacy of the B7H3-CD3 BTE is limited by poor infiltration of T cells within neuroblastoma xenografts and that when present, these cells may exhibit an exhausted phenotype. Given that tumor-intrinsic changes (upregulation of PD-L1, loss of B7H3 expression) likely do not significantly contribute to resistance in this setting, we turned our attention to surrounding cells in the tumor microenvironment (TME).

To characterize the neuroblastoma TME, immunohistochemistry was performed on tumor tissues collected at endpoint of the SK-N-SH 1:1 E:T subcutaneous efficacy study (**Figure 3.14A**)(**Figure 3.19**). Analysis of mice receiving the highest, most effective, dose of BTE was precluded by a lack of tumor tissue. Hematoxylin and eosin staining revealed the presence of

stromal-rich regions within tumors (**Figure 3.19A,F,K,P**)**.** Tumor stroma is essential for the development and progression of solid tumors, providing a valuable vascular supply that infuses nutrients, facilitates gas exchange, removes metabolic waste, and creates a physical barrier that excludes inflammatory cells[214]. Stroma is primarily composed of a mixture of blood vessels, macrophages, and fibrocollagenous connective tissue[214]. To confirm the presence of stroma, a Trichrome special stain was performed, highlighting variable deposition of collagen in blue (**Figure 3.19B,G,L,Q**). α-Smooth muscle actin (αSMA) immunostaining was performed to identify cancer associated fibroblasts (CAFs), confirming the presence of these cells within stroma. CAFs are responsible for the secretion of extracellular matrix components and are increasingly recognized proponents of the immunosuppressive TME[216]. In neuroblastoma, elevated presence of CAFs has been shown to correlate with established negative prognosticators[231]. F4/80+ murine macrophages were also found throughout analyzed tissue sections but were particularly enriched within stroma adjacent to CAFs (**Figure 3.19D,I,N,S**). Precursory analysis showed no difference in F4/80+ populations in untreated and BTE-treated tumors (data not shown). Next, sections were stained with an anti-human CD3 antibody to locate human T cells. Sparse populations of T cells were identified in tumor stroma, but entirely absent from surrounding areas (**Figure 3.19E,J,O,T**)**.** Co-localization of macrophages and T cells in tumor stroma has been documented in neuroblastoma xenografts treated with a GD2-CD3 BTE, supporting potential crosstalk between these populations[188]. The presence and immunosuppressive roles of macrophages within the neuroblastoma microenvironment has been extensively documented[232,233]. Reflective of the human setting, murine neuroblastoma-associated macrophages may limit infiltration of T cells, increase T cell exhaustion, and promote T cell apoptosis. Further work is needed to elucidate the role of tumor associated macrophages in function of BTEs in vivo.

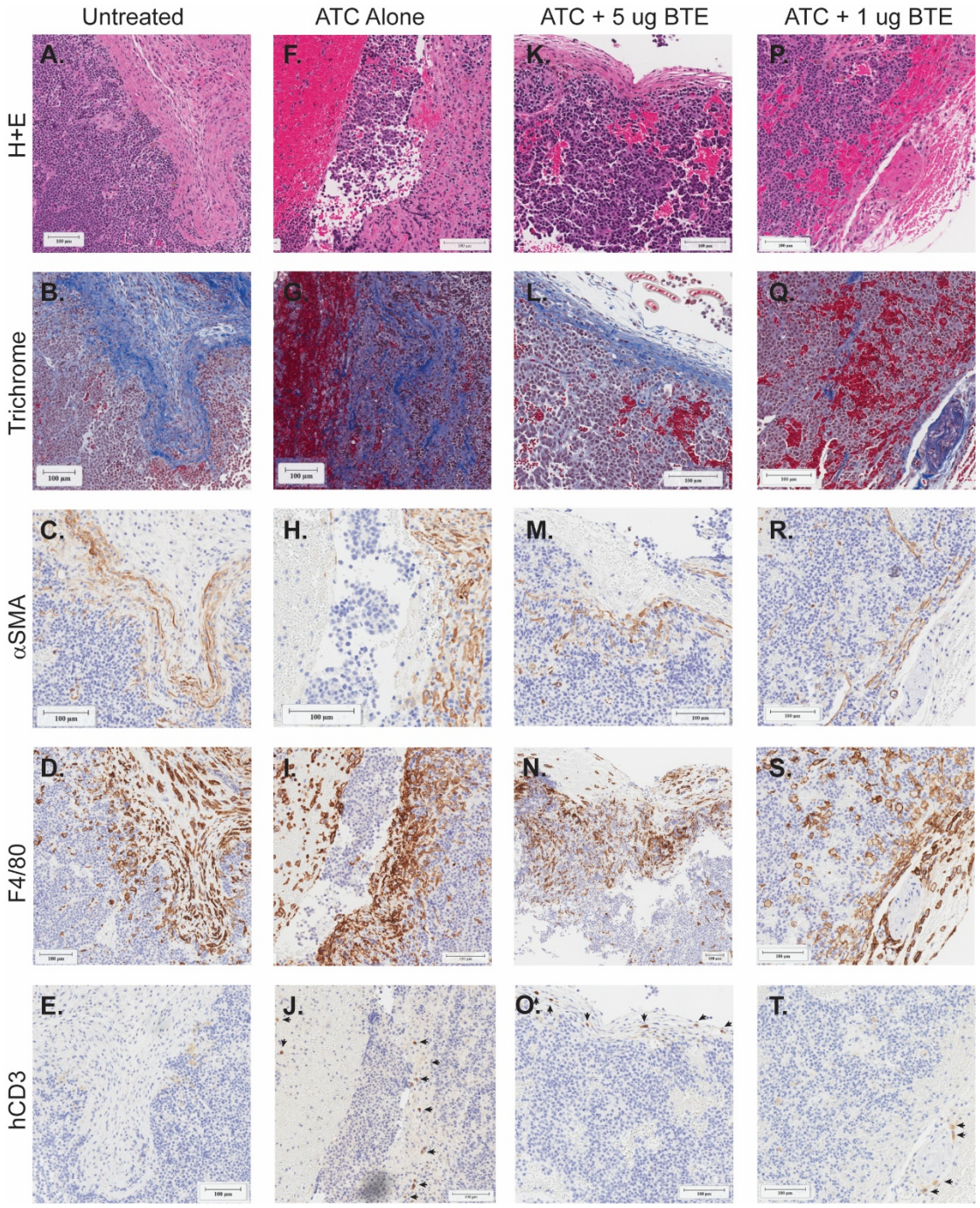

Figure 3.19. *T cells co-localize with murine macrophages within tumor stroma in neuroblastoma flank xenografts.*

Representative sections of SK-N-SH flank tumors collected following no treatment (A-E), vehicle (F-J), 5 ug BTE (K-O), or 1 ug BTE (P-T) in a 1:1 E:T subcutaneous model (**Figure 3.14**). Once endpoint criteria were met (30-38 days post-tumor engraftment), tumors were collected and stained with hematoxylin-eosin (H+E)(A,F,K,P), Trichrome special stain (B,G,L,Q), an anti-human/mouse α-SMA antibody (C,H,M,R), an anti-murine F4/80 antibody to identify macrophages (D,I,N,S), and an anti-human CD3 antibody to identify human T cells (E,J,O,T).

Discussion

Due to their ability to elicit a targeted anti-tumor immune response, BTEs have the potential to improve outcomes for children with high-risk neuroblastoma who have limited treatment options. Although BTEs have shown considerable success in treating hematological malignancies, the effectiveness of BTEs in treating solid tumors remains an open area of investigation. Here, we produced a fully human B7H3-CD3 IgG-L-scFv BTE in human host cells (**Figure 3.1**). In vitro, this BTE directed polyclonal T cell-directed lysis of B7H3+ neuroblastoma cells (**Figure 3.5**). B7H3-CD3 BTE promoted activation of lymphocytes as evidenced by induction of T cell proliferation and production of pro-inflammatory cytokines (**Figure 3.8**). While the efficacy of BTE therapies is dependent on adequate activation of T cells, non-specific lymphocyte activation may trigger life-threatening cytokine release syndrome. We show evidence that the IgG-L-scFv format limits non-specific binding to and activation of T cells (**Figure 3.2**), instead leveraging avidity-based binding to selectively activate T cells in the presence of B7H3-expressing cells. Experiments using a series of BTE variants affirmed the target-dependency of the IgG-L-scFv B7H3-CD3 BTE (**Figure 3.9**). Negligible spontaneous T cell activation was observed in the absence of antigen-expressing cells.

Despite the promising activity of B7H3-CD3 BTE in vitro, this construct failed to reduce tumor burden in neuroblastoma xenografts (**Figure 3.12**). This failure was ultimately attributed to insufficient infiltration of systemically administered T cells (**Figure 3.14**). Further investigations underscored the immunosuppressive nature of the neuroblastoma tumor microenvironment. When present, intra-tumoral T cells were restricted to tumor stroma, surrounded by inhibitory macrophages and cancer associated fibroblasts (**Figure 3.19**). Additionally, intra-tumoral T cells displayed more evidence of exhaustion compared to those collected from in vitro co-cultures (**Figure 3.15**, **Figure 3.16**). These findings suggest that pre-treatment intra-tumoral T cell density may be a predictive biomarker of BTE efficacy in neuroblastoma. Additional measures to

overcome the immunosuppressive neuroblastoma tumor microenvironment are likely necessary to ensure the success of T cell-redirecting therapies.

Clinical evaluation of neuroblastoma tissues suggests that the extent of lymphocyte infiltration is variable, with T cells constituting anywhere from 0-18% of total cells[234,235]. As observed in our murine models, in patients, T cells are often concentrated within fibrovascular rich regions of neuroblastoma tissues[236]. The evident correlations between the quantity of tumor-infiltrating lymphocytes and improved outcomes in high-risk neuroblastoma emphasizes the importance of better understanding the mechanisms governing lymphocyte trafficking in this clinical setting[236–238].

Moreover, one preclinical study demonstrated that pre-treatment intra-tumoral density of lymphocytes is a critical determinant of BTE efficacy[218]. Using a bone marrow chimera system, the authors showed that that anti-tumor effect of BTEs was dependent on local expansion of tumor associated CD8+ cells to a greater degree than recruitment of circulating T cells[218]. In support of this finding, they demonstrated that reducing the number of intra-tumoral T cells rendered a previously BTE-responsive tumor model completely resistant to BTE treatment[218]. Another group showed that BTE efficacy in syngeneic models of breast cancer is dependent on the activation of intra-tumoral T cells that are present prior to treatment initiation. BTE-driven activation of T cells subsequently triggered the release of chemokines which facilitated recruitment of systemic lymphocytes[219]. BTE-resistance caused by a dearth of intra-tumoral T cells may be overcome through addition of immune checkpoint blockade[218]. As neuroblastomas express low levels of PD-L1, alternative combinatorial therapeutic strategies should be investigated to enhance the potency of BTEs.

Multiple mechanisms likely underlie the limited T cell infiltration observed in neuroblastoma. In humans, absent MHC-I expression limits presentation of antigens to specific T cells, preventing subsequent activation and proliferation. The immunosuppressive nature of the neuroblastoma microenvironment also undoubtedly contributes to the exclusion of cytotoxic

lymphocytes. Multiple studies have pinpointed tumor associated macrophages as primary mediators of T cell dysfunction. Indeed, depletion of tumor-infiltrating murine myeloid cells enhanced activity of a GD2-targeting BTE in neuroblastoma patient-derived xenografts[217]. Intriguingly, tumor associated macrophages and stromal cells have been shown to express B7H3[64,239,240]. The B7H3-CD3 BTE evaluated here exclusively recognizes human and cynomolgus B7H3 and does not cross-react with the murine homolog. In humans, B7H3-targeting BTEs could target tumor associated macrophages and tumor stromal cells in addition to neuroblastoma cells, thereby improving infiltration of systemic lymphocytes. Evaluation of murine B7H3-CD3 BTEs in syngeneic models of neuroblastoma or utilization of human B7H3 transgenic mice could be used to address this possibility. On the other hand, syngeneic neuroblastoma models do not faithfully recapitulate the heterogeneity and diversity of human tumors, which could influence responses to BTE in vivo. Furthermore, in mice, B7H3 may exert costimulatory functions[241], further complicating use of syngeneic models.

There are several limitations of this study. Due to the human-selectivity of B7H3-CD3 BTE, our in vivo models are restricted to neuroblastoma xenograft models, which necessitates use of immunocompromised mice. While adoptive transfer of human T cells into NSG mice is a widely accepted system for preclinical evaluation of immunotherapies, these models fail to fully recapitulate human adaptive and innate immune responses. To control for donor-dependent effects, all in vivo studies presented here relied on the use of a single PBMC donor. Re-evaluation of our in vivo models using additional T cell donors should be completed to confirm that our findings are not donor dependent.

In summary, this work is the first demonstration of a B7H3-targeteting, CD3-engaging BTE in the IgG-L-scFv format. In addition, we identified limited recruitment of systemic T cells in circulation as an important mechanism of resistance to BTEs in neuroblastoma. Expression of B7H3 is not restricted to neuroblastomas. Many pediatric solid tumors express B7H3, including high grade gliomas[68,80,81], osteosarcomas[80], Wilms's tumors[80], rhabdomyosarcomas[80] and

Ewing's sarcomas[80]. Therefore, further investigation of B7H3-targeted immunotherapies has potential to impact many children with cancer.

4. Design and Production of Macrophage-Engaging Bispecific Antibodies to Enhance efficacy of Bispecific T cell Engagers in Neuroblastoma

Abstract

Children with high-risk neuroblastoma face a dismal prognosis despite treatment with intensive multi-modal therapies. Neuroblastoma tumors are considered “immunologically cold”, containing few infiltrating cytotoxic lymphocytes and larger populations of immunosuppressive immune cells, including tumor associated macrophages (TAMs). Increased presence of TAMs is predictive of poorer clinical outcomes in neuroblastoma and other malignancies. Growing evidence suggests that these cells may hinder the effectiveness of T-cell directed immunotherapies, including bispecific T cell engagers (BTEs). However, TAM phenotypes are often fluid, and multiple groups have demonstrated that TAMs can be functionally reprogramed to promote anti-tumor immunity. We hypothesized that the efficacy of BTEs could be improved through co-treatment with an additional bispecific antibody that redirects tumor associated macrophages to promote phagocytosis of neuroblastoma cells.

Introduction

As neuroblastomas demonstrate minimal infiltration of T cells[234,236], increasing attention has been placed on harnessing the anti-tumor potential of alternative cells in the neuroblastoma tumor microenvironment. Neuroblastoma tumors are often heavily populated by innate immune cells including macrophages and natural killer cells that may limit the effectiveness of immunotherapies[232,242]. Dinutuximab is an anti-GD2 monoclonal antibody that has improved 2-year event free survival of high-risk neuroblastoma by 20%[22]. The mechanism of action of dinutuximab is in part due to Fc-dependent activation of the innate immune system, specifically by promoting NK cell-mediated antibody-dependent cell-mediated cytotoxicity (ADCC) and macrophage-mediated antibody-dependent cellular phagocytosis (ADCP)[26,27]. Therapies that reduce the immunosuppressive nature of the neuroblastoma microenvironment may enhance the effectiveness of T-cell mediated therapies such as Bispecific T cell Engagers (BTEs).

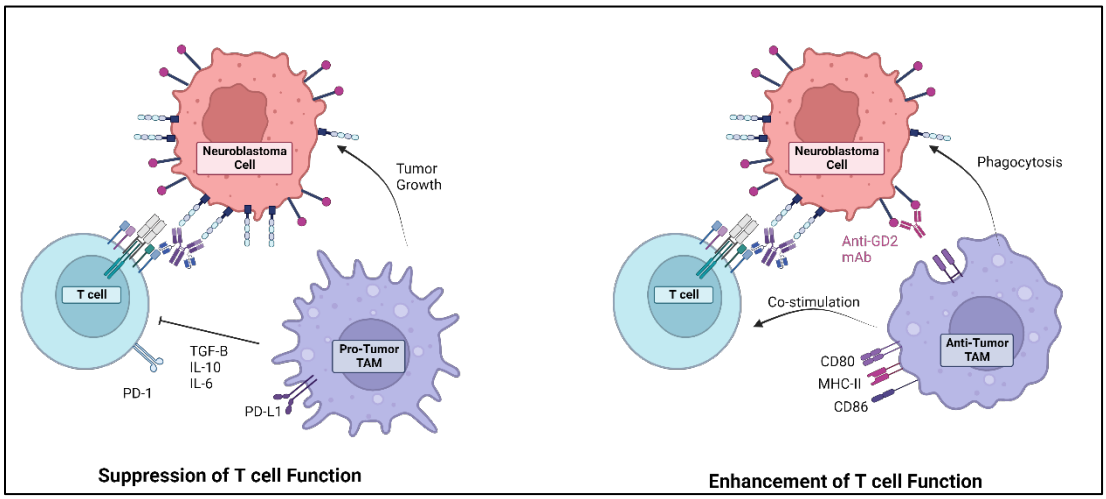

Figure 4.1: *Tumor associated macrophages exhibit a spectrum of functional phenotypes.*

Tumor associated macrophages have been extensively correlated with poor outcomes in neuroblastoma, and have been shown to facilitate tumor growth, invasion, and metastasis[232,233,242,243]. Macrophages are diverse cells whose functional states are heavily influenced by the surrounding environment. While anti-tumor ("M1-like") macrophages are valuable antigen presenting cells and can directly induce tumor cell death through phagocytosis,

pro-tumor tumor-associated macrophages ("M2-like") cells suppress inflammatory signals and promote tumor progression (**Figure 4.1**). Factors within the tumor microenvironment are suspected to push macrophages towards a pro-tumor state, but the exact mechanisms underlying this shift are not well understood.

A growing field of research has highlighted the plasticity of tumor associated macrophages, showing that they can be redirected to exert anti-tumor effects[27,244,245]. Recently, the tumor-associated surface antigens CD47, CD24 and GD2 have been shown to contribute to innate immune evasion[27,244,245]. By binding to inhibitory receptors present on myeloid cells, these "don't eat me signals" inhibit the ability of macrophages to induce phagocytosis. Blocking these signals with monoclonal antibodies has been shown to effectively treat a variety of adult and pediatric solid tumors in preclinical models. In patients, the addition of a monoclonal antibody directed against CD47 was shown to synergize with rituximab, mediated by increased macrophage-mediated phagocytosis of lymphoma cells[246]. Likewise, recent work demonstrated that blocking CD47 enhances the efficacy of anti-GD2 antibodies in preclinical models of neuroblastoma[27]. This combinatorial therapy is currently being evaluated for the treatment of neuroblastoma (NCT04751383). Given the limited efficacy of our B7H3-CD3 BTE in xenograft neuroblastoma models, attributed in part to immunosuppressive tumor associated macrophages in the microenvironment, we wished to evaluate bispecific antibodies targeting TAMs as a combinatorial therapy for T-cell engaging BTEs.

Methods

Protein Design and Production

The B7H3^{MGA271}-CD3^{ADI24} IgG-L-scFv BTE ("BTE") was designed and produced as described in Chapter 3. Anti-GD2^{Dinutux}, Anti-CD24^{SWA11}, and Anti- CD47$^{2.3D11}$ antibodies were produced on human IgG1 frameworks using identical methodology. The sequence of the GD2-CD24 IgG-DEM

BTE was constructed by attaching an anti-CD24 scFv on each V_L domain of an anti-GD2 human IgG1 derived from dinutuximab using a G_3S_3 linker (**Supplementary Table 6**). Amino acid sequences were reverse translated using human codons, codon-optimized, and synthesized de novo at GenScript (New Jersey, USA).

Patient Derived Cell Cultures

LAN-1 and SK-N-SH cells were obtained from American Type Culture Collection. Cells were cultured in RPMI media supplemented with 10X/20mM GlutaMAX (ThermoFisher, #35050061) and 10% fetal bovine serum (ThermoFisher, #1043806). All cultures were maintained in a 5-8% CO_2 buffered incubator at 37ºC. All cell lines are described in **Supplementary Table 2.**

Evaluation of Surface Antigen Expression by Flow Cytometry

Samples were stained with the following APC-conjugated antibodies according to manufacturer's instructions, resuspended in a final solution containing DAPI (ThermoFisher D3571, 1 ug/mL). and analyzed on a NovoCyte 3000 Flow Cytometer: APC mouse IgG1k isotype control (BioLegend, #400142), APC anti-human GD2 (BioLegend, #357306), APC anti-human CD24 (BioLegend, #311118), APC anti-CD47 (BioLegend, #323124), APC anti-human PD-L1/CD274 (BioLegend, #329708), APC anti-human HLA-A,B,C (BioLegend, #311409).

Quantitative Flow Cytometry

Cells were stained with a saturating concentration of PE-conjugated anti-human CD47 antibody (BioLegend, # 323108) or anti-human CD24 antibody (BioLegend, # 311105) per manufacturers instruction. Stained samples were analyzed on a Celesta Flow Cytometer. Cell surface antigen expression was quantified using the BD Quantibrite PE Quantitation kit (BD Biosciences, #340495) following the manufacturers protocol. Cells were washed and resuspended in a final solution of DAPI (ThermoFisher, #D3571, 1 ug/mL).

Macrophage Generation

Healthy, unstimulated human donor peripheral blood mononuclear cells (PBMCs) were obtained from Bloodworks NW (Seattle, WA, USA), frozen and stored in liquid nitrogen. Monocytes were isolated from a thawed PBMC aliquot using a negative selection kit (StemCell Technologies, #19359) according to the manufacturer's instructions. Macrophages were differentiated into macrophages by 7-12 days of culture in RPMI media supplemented with 10% fetal bovine serum (ThermoFisher, #1043806), 80 ng/mL CSF-1 (Peprotech, #300-25) and 20 ng/mL IL-10 (Peprotech, #200-10).

Antibody-Dependent Cellular Phagocytosis Assays

Phagocytosis assays were conducted though flow cytometry. Neuroblastoma cells were labeled with 5-Carboxyfluorescein diacetate succinimidyl ester (CFSE) according to manufacturer's protocol (BioLegend, #423801). CFSE+ neuroblastoma cells and human macrophages were co-cultured at a 1:1 ratio in ultra-low attachment 96-well round bottom plates (Corning, #7007) in serum-free RPMI media. Anti-GD2^{Dinutuximab}, Anti-CD24^{SWA11}, and Anti-CD47$^{2.3D11}$ human IgG1 antibodies were produced in-house and confirmed to lack endotoxins. A non-targeting human IgG1 antibody was used as an isotype control. Antibodies were added at a final concentration of 5 ug/mL and tested in triplicate. Cells were incubated in a 5-8% CO_2 buffered incubator at 37ºC for 2 hours. After this time, plates were spun at 400xg, and stained with an APC anti-human CD11b antibody (BioLegend, #379906). Cells were resuspended in a final solution of DAPI (ThermoFisher, #D3571, 1 ug/mL). Cells were analyzed on a NovoCyte 3000 Flow Cytometer. Phagocytosis was quantified as the proportion of CD11b+CFSE+ macrophages / total CD11b+ macrophages[244]. Results were normalized to media alone conditions.

Immunohistochemistry of Tissue Microarrays

Neuroblastoma tissue microarrays were generously shared by Seattle Children's Hospital Department of Pathology. IHC was performed using the Ventana Discovery Ultra IHC/ISH Auto-

Stainer using anti-CD24 or anti-CD47 rabbit antibodies as previously described. To optimize staining, OVCAR3 flank xenografts were used as a positive control and mouse splenic tissue were used as a negative control.

T cell:Macrophage Cytotoxicity Assays

In a 96-well flat bottom plate (Greiner, #655090), neuroblastoma-iRFP target cells were co-cultured with purified T cells at a 5:1 Effector:Target (E:T) cell ratio and donor-matched macrophages at a 1:1 tumor cell:macrophage ratio. BTE was added at 4X final concentrations. All conditions were performed in a minimum of triplicate wells. To evaluate changes in tumor cell death, iRFP+ cells were quantified using the Incucyte SX5 cell analysis system (Sartorius) every 4 hours. iRFP+ cell counts were exported to Excel (Microsoft) and percent cytotoxicity was calculated utilizing the following formula:

% Cytotoxicity = [(Mean Count of iRFP+ cells (no drug) – Mean count of iRFP+ cells (with drug)) / Mean count of iRFP+ cells (no drug)] x 100%

Fitted curves were generated by applying a [Agonist] vs response – variable slope (four parameters) model using GraphPad Prism 10.

Neuroblastoma Xenograft Models

For all in vivo studies, NSG-$(K^bD^b)^{null}$ (NSG-$(K^bD^b)^{null}$ $(IA)^{null}$, NSG-$(K^b\ D^b)^{null}$ (IA^{null})) mice were obtained from in-house breeding stocks. All experiments were conducted in accordance with Seattle Children's Research Institute (SCRI) Institutional Animal Care and Use Committee (IACUC) approved protocol #ACUC00682. Study endpoint criteria included weight loss >20%, a body condition score >8, luminescence-based tumor burden $>10^{10}$ RLU, or subcutaneous tumor burden of >2000 mm^3.

Metastatic Models

For metastatic neuroblastoma models, LAN-1 iRFP-ffluc cells were harvested and resuspended at a concentration of 4e6 cells/100uL USP grade PBS. 100uL was injected into the tail vein of NSG-(K^bD^b)^{null} mice. Tumor burden was monitored weekly using an IVIS Spectrum Imaging System (Perkin Elmer).

Results

Based on our in vivo observations and published evidence, we hypothesized that macrophages may inhibit the cytolytic capacity of BTE-activated T cells. To test this hypothesis, T cell killing assays were conducted using the B7H3-CD3 BTE in the presence and absence of donor-matched macrophages. Results showed a minor reduction in BTE potency in the presence of macrophages, suggesting that these cells may suppress the function of BTEs in vitro (**Figure 4.2**).

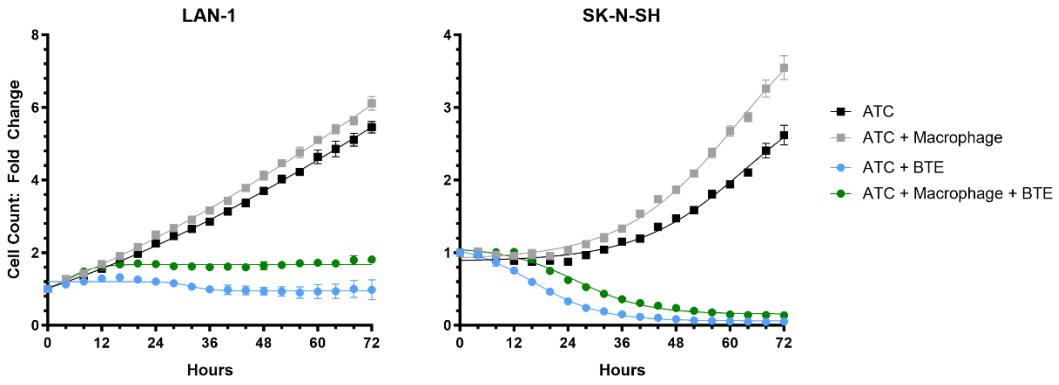

Figure 4.2: *Macrophages inhibit BTE-mediated cytolysis in vitro.*

T cell-mediated cytotoxicity of B7H3-CD3 BTE against a LAN-1 or SK-N-SH iRFP-ffluc neuroblastoma cell lines co-cultured in the presence or absence of donor-matched macrophages. Results are representative of one assay using ATC 3126 effector cells at a 5:1 ratio and Macrophage 3126 cells at a 1:1 ratio. BTE was used at a final concentration of 9.9 nM. Each curve represents a single experimental condition, averaged across a minimum of three technical replicates. Data shown as mean +/- SD.

Blockade of anti-phagocytic signals expressed by tumor cells has been shown by several groups to promote macrophage-mediated phagocytosis of tumor cells[27,244–247]. To evaluate the expression of anti-phagocytic markers on neuroblastoma, we screened a panel of neuroblastoma cell culture lines by flow cytometry, comparing the expression of known "don't eat me signals": CD24[244], CD47[247], GD2[27], MHC-I[248], and PD-L1[249] (**Figure 4.3**). Consistent with previous findings, MHC-I and PD-L1 expression was largely absent. Expression of MHC-I was detected on 23% of cell lines (n=3/13, mean MFIR = 2.0) and PD-L1 was detected on all cells evaluated- albeit at very low levels (mean MFIR = 1.7) Of the 5 antigens evaluated, GD2 was associated with the highest median expression (expression detected on n=11/13, mean MFIR = 188.1), followed by CD24 (expression detected on n=13/13, mean MFIR = 74.7) and CD47 (expression detected on n=13/13, mean MFIR=55.6).

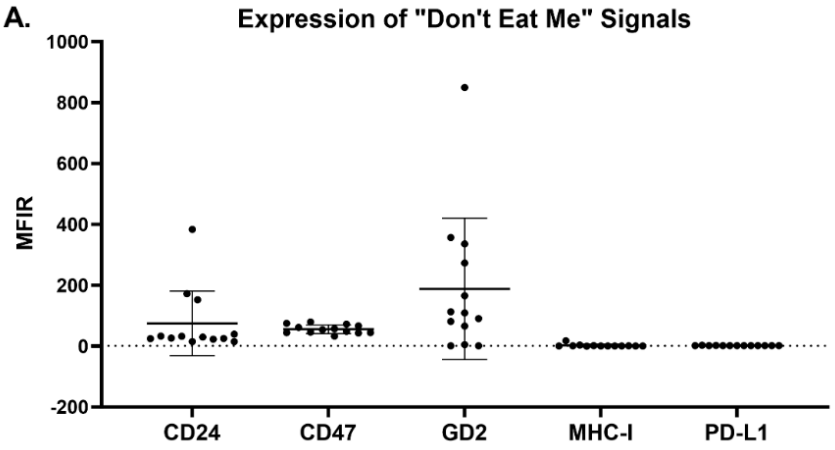

Figure 4.3: *Surface expression of anti-phagocytic "don't eat me" signals on neuroblastoma cell lines.*

(A) Flow cytometry evaluation of a panel of human neuroblastoma cell lines (n=13) was performed to evaluate expression of targetable surface antigens. Each data point represents an individual cell line. MFIR (mean fluorescence intensity ratio) was calculated by dividing mean fluorescent intensity of the sample by that of the corresponding isotype control. For each plot, the median expression is indicated by the center line. Error bars represent the interquartile range (25^{th} and 75^{th} percentiles).

Next, we evaluated phagocytosis of neuroblastoma cells by human macrophages in vitro using a flow-based assay. Anti-GD2, anti-CD47 and anti-CD24 antibodies resulted in significant increases in the phagocytosis of LAN-1 neuroblastoma cells (**Figure 4.4**).

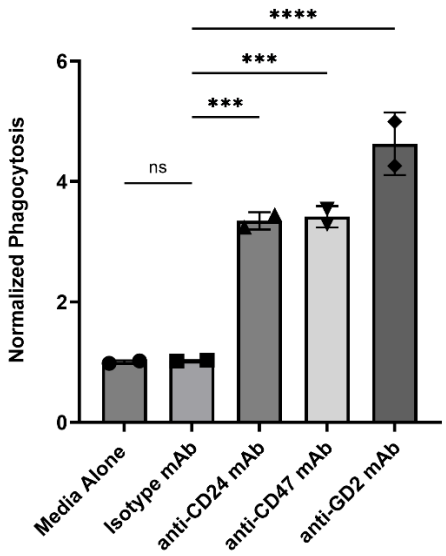

Figure 4.4: *Monoclonal antibody (mAb) targeting of anti-phagocytic signals promotes phagocytosis of neuroblastoma cells.*

Graph showing flow-cytometry-based quantification of phagocytosis of LAN-1 cells in the presence or absence of monoclonal antibodies (5 ug/mL) compared to media-alone control wells; results were normalized to the phagocytosis in untreated wells. Each data point represents results of an independent macrophage donor averaged across triplicate wells (one-way ANOVA, ***$p < 0.001$, ****$p < 0.0001$). Data is shown as mean +/-SD.

Recent work showed that blocking GD2 and CD47 in combination synergically promotes a macrophage-mediated anti-tumor response in neuroblastoma xenograft models[27]; this combination will be investigated in a Phase I/II clinical trial (NCT04751383). Clinical use of anti-GD2 monoclonal antibodies is complicated by GD2 expression on peripheral nerves, which is associated with dose-limiting allodynia[22,55,56]. We hypothesized that a bispecific antibody co-targeting GD2 and an alternative anti-phagocytic signal on neuroblastoma cells could increase the effectiveness of anti-GD2 monoclonal antibodies while simultaneously improving the specificity of this molecule, and by extension, reducing on-target off-tumor toxicities (**Figure 4.5**).

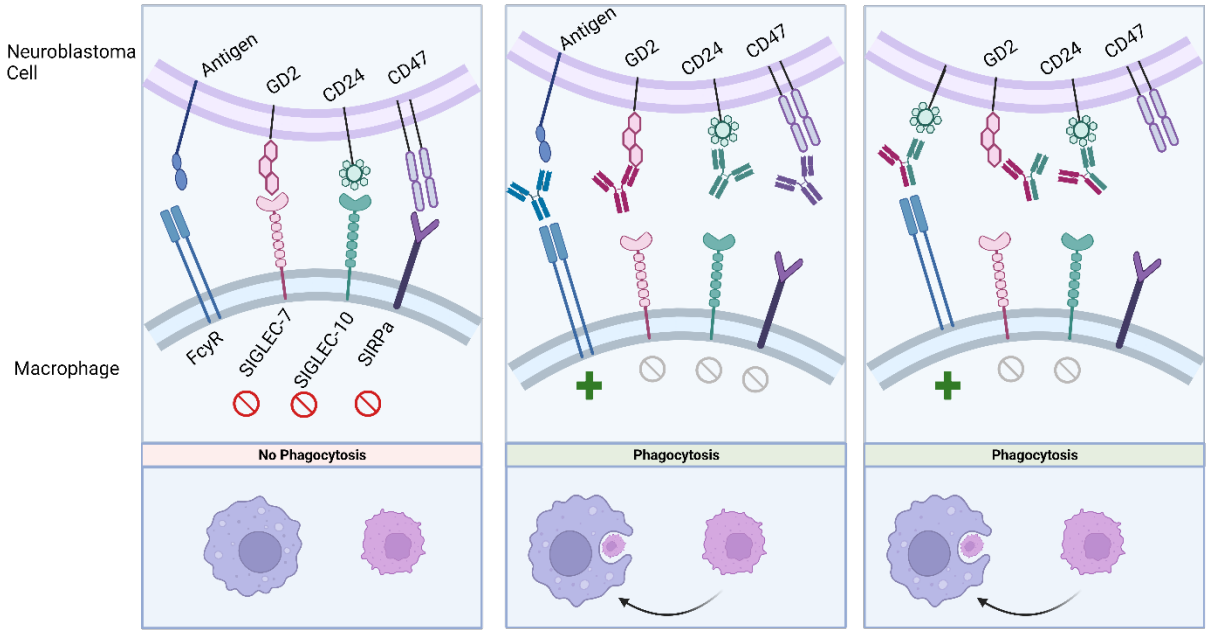

Figure 4.5: *Schematic illustrating proposed model of bispecific macrophage engaging antibodies.*

(left) At baseline, neuroblastoma cells express GD2, CD24, and CD47, which bind to their respective inhibitory receptors on the surface of the macrophages and inhibit phagocytosis. Blockade of these anti-phagocytic signals with monoclonal (middle) or bispecific (right) antibodies promotes tumor cell phagocytosis though alleviation of inhibitory signaling and binding to Fc receptors (FcγR).

Given that GD2 monoclonal antibodies are now part of the standard of care treatment paradigm for high-risk neuroblastoma, and because GD2 blockade elicited the most robust increase in phagocytosis in vitro (**Figure 4.4**), we decided to target GD2 in combination with either CD24 or CD47. To help choose between the two targets, we investigated differences in CD47 and CD24 expression in greater depth. Quantitative flow cytometry analysis of neuroblastoma cell lines demonstrated that CD24 was more highly expressed (**Figure 4.6A**). CD47 expression on neuroblastoma cells was low, similar to that of normal PBMCs (**Figure 4.6A**). Immunohistochemistry analysis of neuroblastoma tissue microarrays supported these findings, demonstrating robust expression of CD24 (**Figure 4.6B**) and minimal expression of CD47 in neuroblastoma tissue samples (**Figure 4.6C**). From this data, we chose to investigate co-targeting of GD2 and CD24 through a novel bispecific macrophage-engaging antibody.

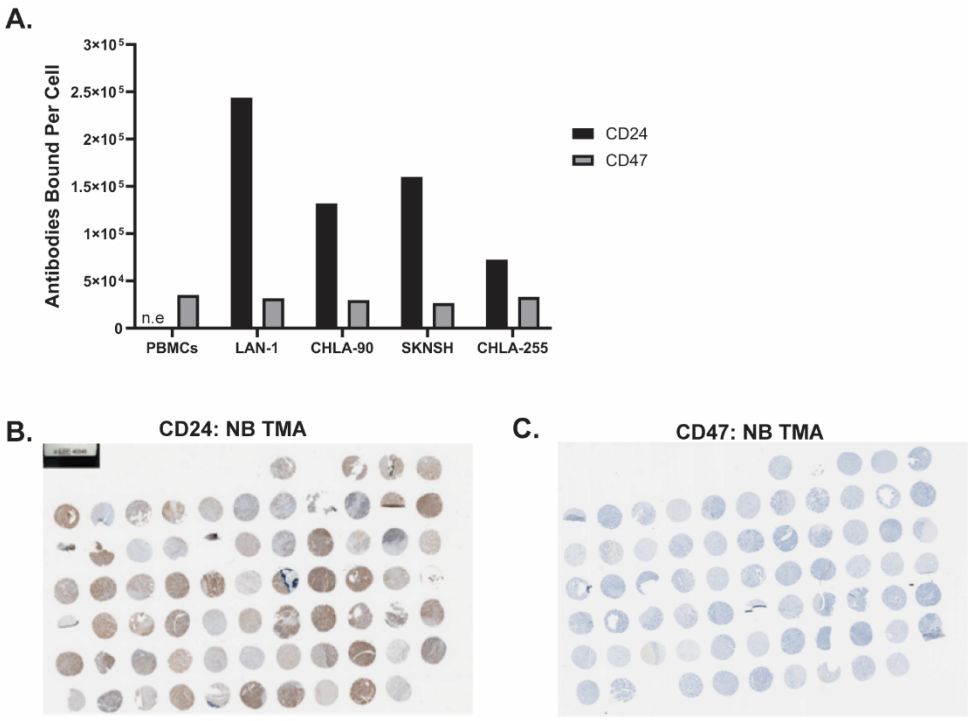

Figure 4.6: *Expression of CD24 and CD47 in neuroblastoma cell lines and patient samples.*

(A) Quantification of CD24 and CD47 surface expression across neuroblastoma cell lines and PBMCs. n.e: not evaluated.
(B) Neuroblastoma tumor microarrays (TMA) were evaluated for CD24 expression by immunohistochemistry (IHC). Representative TMA is shown.
(C) Neuroblastoma tumor microarrays were evaluated for CD47 expression by IHC. Representative TMA is shown.

We produced a $GD2^{Dinutux}$-$CD24^{SWA11}$ human IgG1 bispecific antibody in a novel format we termed “IgG-Don’t Eat Me” (IgG-DEM) using our mammalian expression platform (**Figure 4.7A**). This construct was created by attaching an anti-CD24 scFv to the V_L regions of dinutuximab. The SWA11 anti-CD24 clone was selected for its specificity to the protein core[250]. To evaluate the specificity of this design, we employed two neuroblastoma cell lines, SK-N-SH, which expresses CD24 and lacks GD2 expression, and LAN-1, which expresses both antigens (**Figure 4.7B,C**). Neuroblastoma cells were co-cultured with T cells and donor-matched macrophages in the presence or absence of $GD2^{Dinutux}$-$CD24^{SWA11}$ IgG-DEM. This construct induced rapid LAN-1 cell death, with outgrowth of tumor cells occurring after 36 hours (**Figure 4.7C**). In SK-N-SH cells, only a modest reduction of tumor growth was observed, supporting the specificity of this construct

(**Figure 4.7B**). Next, we evaluated the GD2-CD24 IgG-DEM in combination with our B7H3-CD3 IgG-L-scFv BTE. In both cultures, addition of GD2-CD24 IgG-DEM resulted in more dramatic tumor cell death than B7H3-CD3 BTE alone, highlighting the potential utility of this combination (**Figure 4.7B,C**).

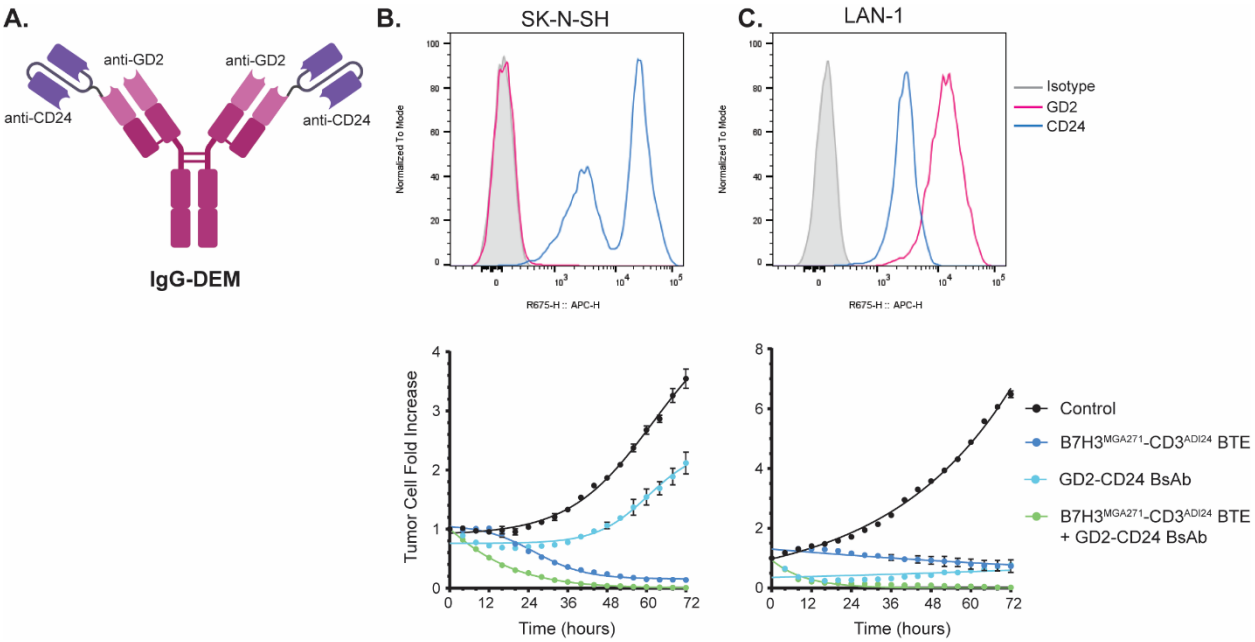

Figure 4.7: *A GD2-CD24 bispecific antibody improves efficacy of B7H3-CD3 IgG-L-scFv BTE in vitro.*

(A) Schematic illustrating the structure of the produced GD2^{Dinutux}-CD24^{SWA11} IgG-Don't Eat Me (IgG-DEM) bispecific antibody.

(B) (top) FACs histogram demonstrating expression of GD2 and CD24 in SK-N-SH cells. (bottom) Growth of SK-N-SH iRFP cells over time in SK-N-SH:T cell:Macrophage co-cultures in the presence or absence of GD2^{Dinutux}-CD24^{SWA11} IgG-DEM (3.5 nM) or B7H3^{MGA271}-CD3^{ADI24} BTE (9.9 nM). Results are representative of one assay using ATC 3126 effector cells at a 5:1 E:T ratio and Macrophage 3126 cells at a 1:1 ratio. Each curve represents a single experimental condition, averaged across a minimum of three technical replicates. Data shown as mean +/- SD.

(C) (top) FACs histogram demonstrating expression of GD2 and CD24 in LAN-1 cells. (bottom) Growth of LAN-1 iRFP cells over time in SK-N-SH:T cell:Macrophage co-cultures in the presence or absence of GD2^{Dinutux}-CD24^{SWA11} IgG-DEM (3.5 nM) or B7H3^{MGA271}-CD3^{ADI24} BTE (9.9 nM). Results are representative of one assay using ATC 3126 effector cells at a 5:1 E:T ratio and Macrophage 3126 cells at a 1:1 ratio. Each curve represents a single experimental condition, averaged across a minimum of three technical replicates. Data shown as mean +/- SD.

In the future, we would like to test whether the GD2-CD24 IgG-DEM is sufficient to improve the activity of B7H3-CD3 BTE in neuroblastoma xenografts. The human IgG1 scaffold utilized in the construction of GD2-CD24 IgG-DEM was confirmed to bind Fc receptors of macrophages

isolated from NSG-(K^bD^b)^{null} mice (data not shown), suggesting that this construct has the potential to also redirect murine macrophages to phagocytose neuroblastoma tumor cells.

Discussion

Increasing evidence suggests that tumor associated macrophages may act as central regulators of neuroblastoma progression and contribute to the resistance to immunotherapies observed clinically. We hypothesized that macrophages may inhibit BTE-directed therapies though multiple mechanisms, including inhibition of lymphocyte recruitment and direct suppression of lymphocyte function. One study reported that myeloid cell depletion enhanced the anti-tumor activity of a GD2-CD3 BTE in neuroblastoma xenografts[217]. We aimed to evaluate the effect of myeloid depletion in our models by employing a similar strategy but found that anti-CSF1R antibodies were not tolerable NSG-(K^bD^b)^{null} mice, precluding further studies (data not shown).

An alternative method to target TAMs is though redirection. Due to the inherent plasticity of macrophages, re-polarization of TAMs has been proposed as an effective strategy to shift these cells to adopt an anti-tumor function and enhance adaptive immunity[232,245,247]. Here, we explored the utility of blocking “don’t eat me” signals expressed by neuroblastoma cells as a potential therapeutic strategy. We showed that monoclonal antibody-mediated targeting of GD2, CD24 and CD47 individually promotes phagocytosis of neuroblastoma cells by macrophages in vitro (**Figure 4.4**). We identified CD24 as a potentially superior anti-phagocytic target compared to CD47, as evidenced by the low CD47 expression present on neuroblastoma patient samples (**Figure 4.6**). A novel bispecific antibody co-targeting GD2 and CD24 elicited potent macrophage-mediated anti-tumor effect against neuroblastoma cells expressing both antigens in vitro, but only mediated a moderate reduction of cell growth in GD2-negative cells (**Figure 4.7**). GD2 is present at low levels on the surface of peripheral neurons[56]. Therefore, any further enhancement of GD2-

targeted immune responses could exacerbate existing on-target off-tumor allodynia. However, preliminary evidence suggests that the GD2-CD24 bispecific antibody created here may have increased specificity for cells expressing both antigens. Expression of CD24 in normal pediatric tissues and overlap with GD2 expression warrants further investigation.

In summary, we show that a novel bispecific antibody recognizing two neuroblastoma-associated anti-phagocytic signals has the potential to induce repolarization of suppressive macrophages and by extension, may improve the efficacy of bispecific T cell engagers in neuroblastoma. Given the complex and dynamic relationship between tumor and immune cells in the tumor microenvironment, immunotherapies which target multiple mechanisms of immune evasion is likely necessary to induce lasting anti-tumor responses in patients.

5. Concluding Remarks

While considerable progress has been made in the treatment of neuroblastoma in recent decades, outcomes for children with relapsed high-risk disease remain dismal[1,17,25]. The natural capability of lymphocytes to mediate antigen-directed cytotoxicity has spearheaded a growing field of research aimed at employing these cells in the fight against cancer. A burgeoning understanding of the mechanisms governing immune evasion in cancer has led to novel therapeutic strategies including checkpoint blockade and adoptive cell therapies that aim to induce tumor regression while avoiding the substantial acute and long-term toxicities induced by conventional therapies. Attempts have been made to integrate T-cell targeting immunotherapies into the treatment of relapsed/refractory high-risk neuroblastoma, but thus far, this approach has failed to significantly improved outcomes. Novel treatment approaches are desperately needed for children and young adults with this disease.

Bispecific T cell engagers (BTEs) are an exciting therapeutic modality that leverages the natural ability of antibody variable regions to bind specific epitopes. BTEs are engineered with antibody-derived domains to enable simultaneous binding of a cancer-specific antigen and CD3 on T cells. BTEs induce polyclonal T cell-mediated lysis of tumor cells independently of MHC-I, avoiding a mechanism of resistance often employed by pediatric solid tumors to evade immune detection[29,30]. The “off-the-shelf” manufacturing of BTEs makes this modality more accessible compared to personalized autologous cellular therapies, which can only be produced at highly specialized centers, <4% of health care centers in the United States[251].

The CD19-CD3 BiTE blinatumomab has shown remarkable efficacy in relapsed/refractory pediatric leukemia[48–50]. Whether BTEs can be successfully applied towards pediatric solid tumors is a growing area of investigation that has been challenged in part by a paucity of targetable surface neoantigens, attributed to low tumor mutational burdens[9].

We and others have screened a range of neuroblastoma cell cultures and identified B7H3 as a candidate BTE target[64,80,252,253]. B7H3 is member of the B7 family of immune checkpoint

ligands and has been increasingly recognized to contribute to immune evasion[62,254]. B7H3 was highly and homogenously express across neuroblastoma cultures. Other groups have described B7H3 expression on pediatric solid tumors including high grade gliomas[68,80,81], Wilms's tumor[80], osteosarcoma[80], rhabdomyosarcoma[80], and Ewing's sarcoma[80]. Furthermore, our data suggests that B7H3 may play a role in neuroblastoma growth, further supporting its candidacy as a target. We show evidence that B7H3 is overexpressed in neuroblastoma patient samples compared to normal pediatric tissues, although low expression was noted in some tissues the adrenal gland and kidney. Other work has similarly reported low levels of B7H3 expression in normal tissues[64]. However, B7H3 monoclonal antibody therapy and B7H3 CAR-T cell therapy in human trials have not reported significant toxicities. Of note, B7H3 expression may be induced on peripheral tissues in response to systemic inflammation[255]. The safety of B7H3 targeting therapies can only be verified though conduction of carefully controlled clinical trials.

We designed, produced, and evaluated a suite of unique B7H3-CD3 BTEs to identify the optimal BTE design. We found that IgG-like BTEs with anti-CD3 scFvs linked to the carboxy-termini of the IgG light chains mediated potent anti-tumor activity in vitro, attributed to their bivalency for both B7H3 and CD3. This format, termed IgG-L-scFv, demonstrated an increase in potency with an increase in CD3 affinity, and yet demonstrated strictly target-dependent activity. IgG-like BTEs exhibit a pharmacokinetic profile similar to that of conventional IgG antibodies, due to their size (above the cut-off for renal excretion) and FcRn-mediated recycling. The potential simplified dosing regimen makes IgG-like BTE formats an attractive option for the treatment of children, potentially reducing the need for inpatient admissions and better preserving a sense of normalcy and quality of life for families.

From our functional screens, we identified a B7H3^{MGA271}-CD3^{ADI24} IgG-L-scFv as the lead candidate BTE. This molecule mediated potent, target-dependent activation and redirection of T cells in vitro and demonstrated efficacy against a variety of neuroblastoma target cells. Antigen density is emerging as an important consideration in BTE design, as it becomes increasingly

evident that a threshold number of target antigens is required to elicit effector functions. The B7H3-CD3 BTE was less effective against tumor cells with lower levels of B7H3 surface expression, suggesting that normal tissues expressing low levels of B7H3 may be spared. Additionally, the B7H3-CD3 BTE was unable to induce cell death of isogenic neuroblastoma cells lacking B7H3 expression, affirming the target dependency of this construct.

Despite the promising activity of the B7H3-CD3 BTE in vitro, systemic administration of BTE and human T cells failed to control tumor growth in multiple neuroblastoma xenograft models. However, when T cells were placed intratumorally, significant tumor control and prolonged survival was observed, raising the possibility that recruitment of systemic lymphocytes may be a barrier to BTE efficacy in neuroblastoma. Defining mechanisms of resistance to BTE therapies and identifying strategies to overcome these challenges is critical to maximizing the potential therapeutic benefit of these drugs. Pediatric solid tumors present numerous challenges to targeted immunotherapies including on-target off tumor toxicity, antigen escape, an immunosuppressive microenvironment, restricted trafficking of lymphocytes, and intrinsic dysfunction of lymphocytes.

Solid tumors exhibit a greater degree of heterogeneity and often express tumor associated antigens at lower levels compared to hematological malignancies[75], which could drive a loss of antigen expression in response to targeted therapies. To avoid antigen escape, targets which are homogenously expressed and have functions essential for tumor progression should be prioritized. Additionally, to combat heterogeneity, use of multiple BTEs targeting separate antigens or the design of novel multi-specific T cell engaging antibodies could be employed. In theory, using a multi-specific BTE may increase the specificity for tumor cells expressing both antigens while minimizing targeting of normal tissues expressing one or the other[256,257]. While this strategy may improve targeting of heterogenous solid tumors, it is important to note that toxicities due to targeting of normal tissues becomes of greater concern as the number of targeted antigens increases.

The low expression of solid tumor antigens on normal tissues creates a risk of inducing on-target, off-tumor toxicities. To overcome this, novel BTE engineering approaches have been employed to enable conditional BTE activation. For example, several unique BTEs have been described that are designed to be administered in an inactive state. After reaching the tumor, the BTE then undergo a conformational change to an active form, triggered by microenvironmental factors such as binding to tumor cells, tumor-specific metalloproteases, or differential pH[258–261]. However, these approaches have yet to show efficacy in human trials.

Another safety concern surrounding BTE therapy is cytokine release syndrome (CRS). CRS is a potentially life-threatening syndrome which occurs when T cells are activated through non-specific CD3 engagement, or when T cells are so robustly activated by a BTE that they secrete an onslaught of proinflammatory cytokines that triggers an inflammatory cascade. Several approaches have been explored to reduce the risk of CRS induced by BTEs including stepwise dosing regimens[206,209], as well as the use of formats that minimize T cell binding in the absence of target cells. Some groups have advocated for the use of low affinity CD3 engagers to minimize cytokine release[154,262]. However, in the context of immunosuppressive solid tumors, it is likely that a minimum threshold of local cytokine production will be required to adequately promote intra-tumoral lymphocyte expansion and ensure recruitment of additional effector cells. Consequently, higher affinity CD3 binders may be necessary for BTEs targeting solid tumors, and steps to manage CRS such as stepwise dosing will be essential.

The lack of efficacy observed in our neuroblastoma xenografts when administering B7H3-CD3 BTE and human T cells systemically draws parallels with the early clinical experience using CAR-T cells to treat neuroblastoma. Initial GD2-targeting CAR-T cell trials showed limited or modest efficacy in neuroblastoma patients[263–265]. Interestingly, multiple studies documented CAR-T cells in peripheral blood of patients following administration but not in concurrent tumor biopsies[263,266], suggestive of impaired CAR-T infiltration into tumors. The correlations between the density of tumor infiltrating lymphocytes and improved clinical outcomes in high-risk

neuroblastoma[236–238] underscore the importance of understanding mechanisms by which neuroblastomas hinder lymphocyte trafficking. Recently, a clinical trial of GD2-CART01 cells showed impressive efficacy in a cohort of children with refractory/relapsed neuroblastoma, inducing clear clinical responses with limited toxicity[40]. Of patients receiving the optimal CAR-T cell dosage, a 60% 3-year overall survival rate was observed. The authors noted that myeloid-derived suppressive cells, which increased in the peripheral blood following CAR-T administration, appeared to inhibit the anti-tumor activity of CAR-T cells[40,267].

The tumor microenvironment (TME) consists of a physical stromal barrier and a milieu of suppressive cell types including tumor associated macrophages, cancer associated fibroblasts, and regulatory T cells that impair efficacy of T-cell directed therapies though distinct mechanisms. To reduce the impact of the TME and by extension improve the effect of BTEs, combinatorial treatment strategies will likely be needed. Depletion of inhibitory macrophages may be accomplished using additional bispecific antibodies that target this population. Anti-GD2 monoclonal antibodies have been shown to shift tumor-associated macrophages to an anti-tumor phenotype[27], and should be explored as a combinatorial therapy for BTEs. We have found the TME impairs the functionality of BTEs in part by restricting trafficking of lymphocytes to solid tumors. While locoregional administration of T cells is currently being explored in some CAR-T cell trials[81], this approach is less suitable for neuroblastoma as the majority of patients present with metastatic disease at the time of relapse[268]. Radiation may enhance the efficacy of cellular immunotherapy by hindering the TME and could be explored in combination with BTEs[269]. Alternatively, BTEs could be modified to transport chemokines into the TME and facilitates lymphocyte recruitment[270,271]. Other payloads could also be used, such as drugs targeting suppressive cells or proteases which degrade components of the extracellular matrix. Here, we show that bispecific antibodies blocking anti-phagocytic signals expressed by neuroblastoma cells may be an effective approach to shift tumor associated macrophages to an anti-tumor phenotype and thereby enhance the efficacy of BTEs.

In order for BTE-directed T cell immunotherapy to be successful, sufficient quantities and quality of lymphocytes are required. There is a growing body of literature emphasizing that children are not small adults- biologic, molecular, and genetic data have clearly demonstrated that pediatric tumors are distinct from those that occur in adults. These differences may also extend to the developing immune system, and it may be important to explore how age-dependent factors may influence responsiveness to BTEs. Studies show that intensive chemotherapy leads to a marked depletion of naïve T cells[272] but memory T cells are relatively unaffected in children[273]. Following cessation of treatment, children demonstrate faster and more complete restoration of naïve T cells compared to adolescents and adults[272]. Moreover, whether the phenotypic and functional properties of systemic lymphocytes reflect those located intratumorally has not been thoroughly explored. One study showed in syngeneic neuroblastoma models that T cells from tumor-bearing mice displayed a reduced capacity for cytokine production compared to T cells isolated from tumor-free mice, suggesting that neuroblastoma development may influence function of systemic lymphocytes[274]. Other studies have shown that tumor infiltrating lymphocytes isolated from neuroblastoma samples demonstrate a spectrum of phenotypes and functions, but largely retain the ability to be activated and exert effector functions[235,275]. The quality of T cells in neuroblastoma patients following intensive standard treatment regimens should be further explored.

In summary, the favorable functional and biophysical properties of BTEs creates opportunities to develop novel therapeutics to treat pediatric malignancies. The flexibility to interchange different binders should invite future investigations into alternative mechanisms of immune cell activation outside of CD3 engagement. Additionally, rapidly evolving high-throughput discovery methods may allow for the identification of novel tumor-associated neoantigens, which should continue to be explored. The IgG-L-scFv BTE format in our hands mediated efficient T cell-directed killing of neuroblastoma cells in vitro, however innovative architectures should continue to be created and explored.

The work presented in this dissertation underscores the challenges facing the application of BTEs and other targeted immunotherapies for the treatment of pediatric solid tumors and provides a foundation for the development of alternative BTEs for the treatment of neuroblastoma. It is my greatest hope that through widespread collaboration and continued technological advancement, these barriers can be addressed and translate into improved outcomes for children with cancer.

Supplemental Tables

Table 1. Clinical trials evaluating CD3-engaging bispecific antibodies in pediatric malignancies[276]

BTE Name	Targets	BTE Format	Selected Indications	Clinical Trial ID	Phase	Status
Flotetuzumab/ MGD006	CD123 x CD3	DART	AML	NCT04158739	Phase I	Active, not recruiting
			B-ALL BPDCN CML Hairy Cell Leukemia Hodgkin Lymphoma T-ALL Systemic Mastocytosis	NCT04681105	Phase I	Active, not recruiting
Blinatumomab	CD19 x CD3	BiTE	B-ALL Mixed Phenotype Acute Leukemia	NCT04556084	Phase II	Recruiting
				NCT01471782	Phase I/II	Completed with results
				NCT02877303	Phase II	Recruiting
				NCT03914625	Phase III	Suspended (FDA partial clinical hold)
				NCT02101853	Phase III	Active, not recruiting
				NCT02879695	Phase I	Active, not recruiting
				NCT04546399	Phase II	Suspended (FDA partial clinical hold)
				NCT03849651	Phase II	Recruiting
CD20Bi	CD20 x CD3	IgG-IgG	CD20+ NHL	NCT00244946	Phase I	Completed

CD30 biAb	CD30 x CD3	IgG-IgG	CD30+ Lymphomas Neuroblastoma Germ Cell Tumors Chondrosarcoma	NCT05544968	Phase I/II	Not yet recruiting
CD33*CD3 BsAb	CD33 x CD3		Relapsed or Refractory Pediatric Acute Myeloid Leukemia	NCT05077423	Phase I	Terminated
UB_TT170	FOLR1a x anti-FITC CAR	BiTE	Osteosarcoma	NCT05312411	Phase I	Recruiting
3F8-BiAb	GD2 x CD3	IgG-IgG Armed T cells	Neuroblastoma, Osteosarcoma	NCT02173093	Phase I/II	Completed
Hu3F8-BsAb	GD2 x CD3	IgG-L-scFv	Neuroblastoma, Osteosarcoma	NCT03860207	Phase I/II	Terminated

Table 2. Characteristics of patient-derived neuroblastoma cell lines.

Cell Line	Stage	Age (months) at diagnosis, at time of collection	Phase of Therapy	Sample Type	MYCN (A = amplified, N=non-amplified)	ALK (WT = wildtype)	p53 (F = functional, NF = Nonfunctional)
LAN-1	unknown	unknown	unknown	unknown	A	unknown	unknown
SK-N-SH	unknown	48	unknown	BM	N	F1174L	unknown
LA-N-5	N/A	5	Dx	BM	A	unknown	unknown
IMR-32	unknown	unknown	unknown	unknown	A	unknown	unknown
SK-N-BE(2)	4		PD	BM	A	unknown	NF
CHLA-122	4	24	Dx	BM	A		F
CHLA-136	4	24, 36	PD-BMT (relapse of CHLA-122)	Blood	A		F
CHLA-90	4	102	PD-BMT	BM	N	F1245V	NF
COG-N-291			PD	BM	N	WT	NF
COG-N-399	4	11	PD-PM	Blood	A		F
COG-N-415	4	17,25	PD	Blood	A	F1174L	NF
COG-N-421	4	32, 118.6	PD-PM	Blood	A	WT	NF
COG-N-440	4	11.2, 18.4	PD-PM	Blood	A	WT	unknown
COG-N-453	4	17,61.3	PD-PM	Liver Tumor	A	WT	F
COG-N-496	4	38.4, 38.4	Dx	BM	A	WT	unknown
COG-N-519	4	25,32	PD-PM	Blood	A	unknown	unknown
COG-N-603	4	266 days	Dx	Adrenal tumor	N	unknown	unknown
COG-N-672	4	615 days	PM	Blood	N	unknown	unknown
COG-N-623	4	266 days	PD (relapse of COG-N-603)	Adrenal tumor	A	unknown	unknown

N/A: not available; Dx: diagnosis; PD: progressive disease; BMT: bone marrow transplant; PM: post-mortem; BM: bone marrow; A: MYCN amplified; N: MYCN non-amplified, WT: wild-type; F: p53 functional; NF: p53 non-functional.

Table 3: B7H3 sgRNA sequences used to generate knock-out cells.

sgRNA name	sgRNA sequence
B7H3_sgRNA_0	gggacagtgattgtggcagt
B7H3_sgRNA_1	gcactgtggttctgcctcac
B7H3_sgRNA_3	ctcacaggaagatgctgcgt

Table 4. PCR primer sequences and conditions.

Gene	Forward PCR Primer	Reverse PCR Primer	WT PCR Product Size	Annealing Temperature	Sequencing Primer	Sequencing Primer Orientation
B7H3/ CD276	CD276_Forw1: GGATATGGGAA TGAGGACCTCC	CD276_Rev1: CACAGTGTATTCAAG AAATAGCACGA	500	65 C	CD276_Seq3: cactctggtccagga gagat	Forward

Table 5. FDA-approved bispecific T cell engaging antibodies (BTEs) for the treatment of cancer[277].

First U.S. approval	Proprietary name	Non-proprietary name	Targets	BTE Format	Expression system	First approved Indications
12/3/2014	Blincyto	blinatumomab	CD19-CD3	BiTE	CHO	Acute lymphoblastic leukemia*
01/25/2022	Kimmtrak	Tebentafusp-tebn	gp100-CD3	IMMTAC	E coli	Metastatic uveal melanoma
10/25/2022	Tecvayli	teclistamab-cqyv	BCMA-CD3	DuoBody	CHO	Multiple myeloma
12/22/2022	Lunsumio	mosunetuzumab-axgb	Cancer	CrossMAb	CHO	Follicular lymphoma
5/19/2023	Epkinly	epcoritamab-bysp	CD20-CD3	DuoBody	CHO	Diffuse large B-cell lymphoma
06/15/2023	Columvi	Glofitamab-gxbm	CD20-CD3	CrossMab	CHO	Diffuse large B-cell lymphoma
08/09/2023	Talvey	talquetamab-tgvs	GPCR5D-CD3	DuoBody	CHO	Multiple myeloma
08/14/2023	Elrexfio	Elranatamab-bcmm	BCMA-CD3	IgG-like	CHO	Multiple myeloma

*Approved for use in pediatric populations

Table 6. Sequences of selected generated proteins.

Molecule	Architecture	Sequence
B7H3[MGA271]-CD3[ADI50024DS]	IgG-L-scFv 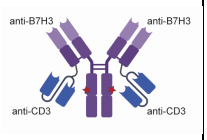	Heavy Chain: METDTLLLWVLLLWVPGSTG**EVQLVESGGGLVQPGGSLRLSCAASGFT FSSFGMHWVRQAPGKGLEWVAYISSDSSAIYYADTVKGRFTISRDNAK NSLYLQMNSLRDEDTAVYYCGRGRENIYYGSRLDYWGQGTTVTVSS**ASTKGPSVFPLAPSSKSTSGGTAALGCLVKDYFPEPVTVSWNSGALTSGVHTFPAVLQSSGLYSLSSVVTVPSSSLGTQTYICNVNHKPSNTKVDKKVEPKSCDKTHTCPPCPAPELLGGPSVFLFPPKPKDTLMISRTPEVTCVVVDVSHEDPEVKFNWYVDGVEVHNAKTKPREEQYASTYRVVSVLTVLHQDWLNGKEYKCKVSNKALPAPIEKTISKAKGQPREPQVYTLPPSRDELTKNQVSLTCLVKGFYPSDIAVEWESNGQPENNYKTTPPVLDSDGSFFLYSKLTVDKSRWQQGNVFSCSVMHEALHNHYTQKSLSLSPGK Light Chain: METDTLLLWVLLLWVPGSTG**DIQLTQSPSFLSASVGDRVTITCKASQNV DTNVAWYQQKPGKAPKALIYSASYRYSGVPSRFSGSGSGTDFTLTISSL QPEDFATYYCQQYNNYPFTFGQGTKLEIK**RTVAAPSVFIFPPSDEQLKSGTASVVCLLNNFYPREAKVQWKVDNALQSGNSQESVTEQDSKDSTYSLSSTLTLSKADYEKHKVYACEVTHQGLSSPVTKSFNRGEC**DIVMSQSPDSLAVSLGERATINCKSSQSLLNARTGKNYLAWY QQKPGQPPKLLIYWASTRSSGVPDRFSGSGSGTDFTLTISSLQAEDVAV YYCVQSYFRRTFGCGTKVEIK****QVQLVQSGAE VKKPGASVKVSCKASGFNIKDYYMHWVRQAPGQCLEWIGWIDLENAN TVYDAKFQGRVTITRDTSASTAYMELSSLRSEDTAVYYCARDAYGRYFY DVWGQGTLVTVSS**HHHHHH
B7H3[MGA271]-CD3[ADI50024DS]	MaxibAb 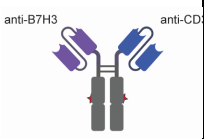	Heavy Chain: METDTLLLWVLLLWVPGSTG**EVQLVESGGGLVQPGGSLRLSCAASGFT FSSFGMHWVRQAPGKGLEWVAYISSDSSAIYYADTVKGRFTISRDNAK NSLYLQMNSLRDEDTAVYYCGRGRENIYYGSRLDYWGQGTTVTVSS****DIQLTQSPSFLSASVGDRVTITCKASQNVDTNV AWYQQKPGKAPKALIYSASYRYSGVPSRFSGSGSGTDFTLTISSLQPED FATYYCQQYNNYPFTFGQGTKLEIK**GSEPKS**S**DKTHTCPPCPAPELLGGPSVFLFPPKPKDTLMISRTPEVTCVVVDVSHEDPEVKFNWYVDGVEVHNAKTKPREEQY**A**STYRVVSVLTVLHQDWLNGKEYKCKVSNKALPAPIEKTISKAKGQPREPQVYTLPPSRDELTKNQVSL**S**C**A**VKGFYPSDIAVEWESNGQPENNYKTTPPVLDSDGSFFL**V**SKLTVDKSRWQQGNVFSCSVMHEALHNHYTQKSLSLSPGKG**SAWSHPQFEK** Light Chain: METDTLLLWVLLLWVPGSTG **DIVMSQSPDSLAVSLGERATINCKSSQSLLNARTGKNYLAWYQQKPGQ PPKLLIYWASTRSSGVPDRFSGSGSGTDFTLTISSLQAEDVAVYYCVQS YFRRTFGCGTKVEIK****QVQLVQSGAEVKKPG ASVKVSCKASGFNIKDYYMHWVRQAPGQCLEWIGWIDLENANTVYDAK FQGRVTITRDTSASTAYMELSSLRSEDTAVYYCARDAYGRYFYDVWGQ GTLVTVSS**GSEPKS**S**DKTHTCPPCPAPELLGGPSVFLFPPKPKDTLMISR TPEVTCVVVDVSHEDPEVKFNWYVDGVEVHNAKTKPREEQY**A**STYRVV SVLTVLHQDWLNGKEYKCKVSNKALPAPIEKTISKAKGQPREPQVYTLPP SRDELTKNQVSL**W**CLVKGFYPSDIAVEWESNGQPENNYKTTPPVLDSD GSFFLYSKLTVDKSRWQQGNVFSCSVMHEALHNHYTQKSLSLSPGKGS HHHHHH

B7H3[MGA271]-CD3[ADI50024DS]	Canonical BiTE 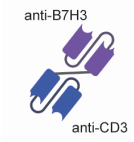	METDTLLLWVLLLWVPGSTG**EVQLVESGGGLVQPGGSLRLSCAASGFT FSSFGMHWVRQAPGKGLEWVAYISSDSSAIYYADTVKGRFTISRDNAK NSLYLQMNSLRDEDTAVYYCGRGRENIYYGSRLDYWGQGTTVTVSS**GGGGSGGGGSGGGGS**DIQLTQSPSFLSASVGDRVTITCKASQNVDTNV AWYQQKPGKAPKALIYSASYRYSGVPSRFSGSGSGTDFTLTISSLQPED FATYYCQQYNNYPFTFGQGTKLEIK**GGGGS**DIVMSQSPDSLAVSLGER ATINCKSSQSLLNARTGKNYLAWYQQKPGQPPKLLIYWASTRSSGVPD RFSGSGSGTDFTLTISSLQAEDVAVYYCVQSYFRRTFGCGTKVEIK**GGG SGGGSGGGSGGGS**QVQLVQSGAEVKKPGASVKVSCKASGFNIKDYY MHWVRQAPGQCLEWIGWIDLENANTVYDAKFQGRVTITRDTSASTAYM ELSSLRSEDTAVYYCARDAYGRYFYDVWGQGTLVTVSSHHHHHH
B7H3[MGA271] IgG	IgG1 	Heavy Chain: METDTLLLWVLLLWVPGSTG**EVQLVESGGGLVQPGGSLRLSCAASGFT FSSFGMHWVRQAPGKGLEWVAYISSDSSAIYYADTVKGRFTISRDNAK NSLYLQMNSLRDEDTAVYYCGRGRENIYYGSRLDYWGQGTTVTVSS**ASTKGPSVFPLAPSSKSTSGGTAALGCLVKDYFPEPVTVSWNSGALTSGVH TFPAVLQSSGLYSLSSVVTVPSSSLGTQTYICNVNHKPSNTKVDKKVEPK SCDKTHTCPPCPAPELLGGPSVFLFPPKPKDTLMISRTPEVTCVVVDVSH EDPEVKFNWYVDGVEVHNAKTKPREEQYASTYRVVSVLTVLHQDWLNG KEYKCKVSNKALPAPIEKTISKAKGQPREPQVYTLPPSRDELTKNQVSLT CLVKGFYPSDIAVEWESNGQPENNYKTTPPVLDSDGSFFLYSKLTVDKS RWQQGNVFSCSVMHEALHNHYTQKSLSLSPGK Light Chain: METDTLLLWVLLLWVPGSTG**DIQLTQSPSFLSASVGDRVTITCKASQNV DTNVAWYQQKPGKAPKALIYSASYRYSGVPSRFSGSGSGTDFTLTISSL QPEDFATYYCQQYNNYPFTFGQGTKLEIK**RTVAAPSVFIFPPSDEQLKS GTASVVCLLNNFYPREAKVQWKVDNALQSGNSQESVTEQDSKDSTYSL SSTLTLSKADYEKHKVYACEVTHQGLSSPVTKSFNRGEC
CD19[Blinatumomab]-CD3[ADI50024DS]	IgG-L-scFv 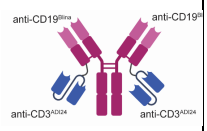	Heavy Chain: METDTLLLWVLLLWVPGSTG**QVQLQQSGAELVRPGSSVKISCKASGYA FSSYWMNWVKQRPGQGLEWIGQIWPGDGDTNYNGKFKGKATLTADE SSSTAYMQLSSLASEDSAVYFCARRETTTVGRYYYAMDYWGQGTTVTV SS**ASTKGPSVFPLAPSSKSTSGGTAALGCLVKDYFPEPVTVSWNSGALT SGVHTFPAVLQSSGLYSLSSVVTVPSSSLGTQTYICNVNHKPSNTKVDKK VEPKSCDKTHTCPPCPAPELLGGPSVFLFPPKPKDTLMISRTPEVTCVVV DVSHEDPEVKFNWYVDGVEVHNAKTKPREEQYASTYRVVSVLTVLHQD WLNGKEYKCKVSNKALPAPIEKTISKAKGQPREPQVYTLPPSRDELTKNQ VSLTCLVKGFYPSDIAVEWESNGQPENNYKTTPPVLDSDGSFFLYSKLTV DKSRWQQGNVFSCSVMHEALHNHYTQKSLSLSPGK Light Chain: METDTLLLWVLLLWVPGSTG**DIQLTQSPASLAVSLGQRATISCKASQSV DYDGDSYLNWYQQIPGQPPKLLIYDASNLVSGIPPRFSGSGSGTDFTLNI HPVEKVDAATYHCQQSTEDPWTFGGGTKLEIK**RTVAAPSVFIFPPSDEQ LKSGTASVVCLLNNFYPREAKVQWKVDNALQSGNSQESVTEQDSKDST YSLSSTLTLSKADYEKHKVYACEVTHQGLSSPVTKSFNRGEC**GGGGSG GGGSGGGGS**DIVMSQSPDSLAVSLGERATINCKSSQSLLNARTGKNYL AWYQQKPGQPPKLLIYWASTRSSGVPDRFSGSGSGTDFTLTISSLQAE DVAVYYCVQSYFRRTFGCGTKVEIK**GGGSGGGSGGGSGGGS**QVQLVQ SGAEVKKPGASVKVSCKASGFNIKDYYMHWVRQAPGQCLEWIGWIDL ENANTVYDAKFQGRVTITRDTSASTAYMELSSLRSEDTAVYYCARDAY GRYFYDVWGQGTLVTVSSHHHHHH
GD2[Dinutuximab]-CD24[SWA11]	IgG-DEM 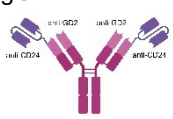	Heavy Chain: METDTLLLWVLLLWVPGSTG**EVQLLQSGPELEKPGASVMISCKASGSSF TGYNMNWVRQNIGKSLEWIGAIDPYYGGTSYNQKFKGRATLTVDKSSS TAYMHLKSLTSEDSAVYYCVSGMEYWGQGTSVTVSS**ASTKGPSVFPLA PSSKSTSGGTAALGCLVKDYFPEPVTVSWNSGALTSGVHTFPAVLQSSG LYSLSSVVTVPSSSLGTQTYICNVNHKPSNTKVDKKVEPKSCDKTHTCPP

		CPAPELLGGPSVFLFPPKPKDTLMISRTPEVTCVVVDVSHEDPEVKFNW YVDGVEVHNAKTKPREEQY**A**STYRVVSVLTVLHQDWLNGKEYKCKVSN KALPAPIEKTISKAKGQPREPQVYTLPPSRDELTKNQVSLTCLVKGFYPS DIAVEWESNGQPENNYKTTPPVLDSDGSFFLYSKLTVDKSRWQQGNVF SCSVMHEALHNHYTQKSLSLSPGK Light Chain: METDTLLLWVLLLWVPGSTG**DIVMSQSPSSLNVSVGEKVTMRCRSSQS** **LLYSSDQKNYLTWYQQKPGQSPKLLISWASTRASGVPDRFTGSGSGTD** **FTLTISSVKAEDLGVYYCQQYFIYPLTFGVGTKLGLK**GGGSGGGSGGGS GGGS**DVHLQESGPDLVKPSQSLSLTCTVTGYSITSGYTWHWIRQFPGN** **TVEWMGYIQYTGSTRYNPALRGRLSISRDTSKNQFFLQLISVTTADTGTY** **FCARGTTASFDYWGQGTTLTVAS**GGGSGGG**EIVMTQSPATLSVSPGER** **ATLSCRSSQSLVHRNGNTYLHWYLQKPGQSPKLLIHKVSNRFSGVPDR** **FSGSGSGTDFTLKISRVEAEDLGVYFCSQSTHVPPLTFGAGTKLELK**RT VAAPSVFIFPPSDEQLKSGTASVVCLLNNFYPREAKVQWKVDNALQSGN SQESVTEQDSKDSTYSLSSTLTLSKADYEKHKVYACEVTHQGLSSPVTK SFNRGECGSHHHHHH

Sequence components include a signal sequence (orange), single chain variable fragments (bolded), glycine-serine linkers (grey), constant regions (black) and a histidine tag (green).

Table 7. HLA types of PBMC donors

Donor ID	HLA Types		
1366	A	A*03:01:01	A*33:01:01
	B	B*07:02:01	B*14:02:01
	C	C*07:02:01	C*08:02:01
3126	A	A*02:01:01	A*32:01:01
	B	B*27:05:02	B*40:01:02
	C	C*01:02:01	C*03:04:01
3260	A	A*02:01:01	A*02:01:01
	B	B*07:02:01	B*15:01:01
	C	C*04:01:01	C*07:02:01
2348	A	A*01:01:01	A*03:01:01
	B	B*08:01:01	B*35:01:01
	C	C*04:01:01	C*07:01:01

Table 8. HLA types of 4 selected neuroblastoma cell cultures

Cell Line	HLA Types		
LAN-1	A	A*02:01:01	A*03:01:01
	B	B*07:02:01	B*58:01:01
	C	C*03:02:02	C*07:02:01
SK-N-SH	A	A*01:01:01	A*24:02:01
	B	B*18:01:01	B*49:01:01
	C	C*07:01:01	C*07:01:01
LAN-5	A	A*24:02:01	A*24:03:01
	B	B*35:04:01	B*48:01:01
	C	C*04:01:01	C*08:03:01
IMR-32	A	A*02:01:01	A*24:02:01
	B	B*07:02:01	B*15:01:01
	C	C*03:03:01	C*07:02:01

References

1. Irwin, M. S. & Park, J. R. Neuroblastoma: paradigm for precision medicine. *Pediatr Clin North Am* **62**, 225–256 (2015).

2. Gurney, J. G. *et al.* Infant cancer in the U.S.: histology-specific incidence and trends, 1973 to 1992. *J Pediatr Hematol Oncol* **19**, 428–432 (1997).

3. Cohn, S. L. *et al.* The International Neuroblastoma Risk Group (INRG) classification system: An INRG task force report. *Journal of Clinical Oncology* **27**, 289–297 (2009).

4. Ponzoni, M. *et al.* Recent advances in the developmental origin of neuroblastoma: an overview. *Journal of Experimental and Clinical Cancer Research* **41**, 1–28 (2022).

5. Gilbert, S. The Neural Crest. *Developmental Biology. 6th Edition.* (2000).

6. Shohet, J. M., Nuchtern, J. G. & Foster, J. H. Clinical presentation, diagnosis, and staging evaluation of neuroblastoma. *UpToDate.* https://www-uptodate-com/contents/clinical-presentation-diagnosis-and-staging-evaluation-of-neuroblastoma.

7. DuBois, S. G. *et al.* Metastatic sites in stage IV and IVS neuroblastoma correlate with age, tumor biology, and survival. *J Pediatr Hematol Oncol* **21**, 181–189 (1999).

8. Liu, S. *et al.* Metastasis pattern and prognosis in children with neuroblastoma. *World J Surg Oncol* **21**, 130 (2023).

9. Pugh, T. J. *et al.* The genetic landscape of high-risk neuroblastoma. *Nature Genetics 2013 45:3* **45**, 279–284 (2013).

10. Valentijn, L. J. *et al.* TERT rearrangements are frequent in neuroblastoma and identify aggressive tumors. *Nature Genetics 2015 47:12* **47**, 1411–1414 (2015).

11. Bordow, S. B., Norris, M. D., Haber, P. S., Marshall, G. M. & Haber, M. Prognostic significance of MYCN oncogene expression in childhood neuroblastoma. *J Clin Oncol* **16**, 3286–3294 (1998).

12. Brodeur, G. M., Seeger, R. C., Schwab, M., Varmus, H. E. & Michael Bishop, J. Amplification of N-myc in Untreated Human Neuroblastomas Correlates with Advanced Disease Stage. *Science (1979)* **224**, 1121–1124 (1984).

13. Seeger, R. C. *et al.* Association of Multiple Copies of the N-myc Oncogene with Rapid Progression of Neuroblastomas. *N Engl J Med* **313**, 1111–1116 (2010).

14. London, W. B. *et al.* Evidence for an age cutoff greater than 365 days for neuroblastoma risk group stratification in the Children's Oncology Group. *Journal of Clinical Oncology* **23**, 6459–6465 (2005).

15. John M. Maris, M. D. Recent Advances in Neuroblastoma. *N Engl J Med* **362**, 2202 (2010).

16. Shohet, J. M. & Nuchtern, J. G. Treatment and prognosis of neuroblastoma. *UpToDate* (2023). https://www-uptodate-com/contents/treatment-and-prognosis-of-neuroblastoma.

17. Moreno, L. *et al.* Outcome of children with relapsed or refractory neuroblastoma: A meta-analysis of ITCC/SIOPEN European phase II clinical trials. *Pediatr Blood Cancer* **64**, 25–31 (2017).

18. Laverdiére, C. *et al.* Long-term Outcomes in Survivors of Neuroblastoma: A Report From the Childhood Cancer Survivor Study. *JNCI: Journal of the National Cancer Institute* **101**, 1131–1140 (2009).

19. Martin, A. *et al.* Secondary malignant neoplasms after high-dose chemotherapy and autologous stem cell rescue for high-risk neuroblastoma. *Pediatr Blood Cancer* **61**, 1350–1356 (2014).

20. Weiner, L. M., Dhodapkar, M. V. & Ferrone, S. Monoclonal Antibodies for Cancer Immunotherapy. *Lancet* **373**, 1033 (2009).

21. Dhillon, S. Dinutuximab: First global approval. *Drugs* **75**, 923–927 (2015).

22. Yu, A. L. *et al.* Anti-GD2 antibody with GM-CSF, interleukin-2, and isotretinoin for neuroblastoma. *N Engl J Med* **363**, 1324–1334 (2010).

23. Wieczorek, A. *et al.* Dinutuximab beta combined with chemotherapy in patients with relapsed or refractory neuroblastoma. *Front Oncol* **13**, 1082771 (2023).

24. Lode, H. N. *et al.* Long-term, continuous infusion of single-agent dinutuximab beta for relapsed/refractory neuroblastoma: an open-label, single-arm, Phase 2 study. *British Journal of Cancer 2023* 1–7 (2023) doi:10.1038/s41416-023-02457-x.

25. Ladenstein, R. *et al.* Investigation of the Role of Dinutuximab Beta-Based Immunotherapy in the SIOPEN High-Risk Neuroblastoma 1 Trial (HR-NBL1). *Cancers (Basel)* **12**, 309 (2020).

26. Sait, S. & Modak, S. Anti-GD2 immunotherapy for neuroblastoma. *Expert Rev Anticancer Ther* **17**, 889–904 (2017).

27. Theruvath, J. *et al.* Anti-GD2 synergizes with CD47 blockade to mediate tumor eradication. *Nature Medicine 2022 28:2* **28**, 333–344 (2022).

28. Gröbner, S. N. *et al.* The landscape of genomic alterations across childhood cancers. *Nature* **555**, 321–327 (2018).

29. Wölfl, M. *et al.* Expression of MHC class I, MHC class II, and cancer germline antigens in neuroblastoma. *Cancer Immunology, Immunotherapy* **54**, 400–406 (2005).

30. Corrias, M. V. *et al.* Lack of HLA-class I antigens in human neuroblastoma cells: analysis of its relationship to TAP and tapasin expression. *Tissue Antigens* **57**, 110–117 (2001).

31. Davis, K. L. *et al.* Nivolumab in children and young adults with relapsed/refractory solid tumors (ADVL1412): A Phase 1 / 2 Trial. *Lancet Oncol* **21**, 541 (2020).

32. Geoerger, B. *et al.* Pembrolizumab in paediatric patients with advanced melanoma or a PD-L1-positive, advanced, relapsed, or refractory solid tumour or lymphoma (KEYNOTE-051): interim analysis of an open-label, single-arm, phase 1-2 trial. *Lancet Oncol* **21**, 121–133 (2020).

33. Dondero, A. *et al.* PD-L1 expression in metastatic neuroblastoma as an additional mechanism for limiting immune surveillance. *Oncoimmunology* **5**, (2016).

34. Melaiu, O. *et al.* PD-L1 is a therapeutic target of the bromodomain inhibitor JQ1 and, combined with HLA class I, a promising prognostic biomarker in neuroblastoma. *Clinical Cancer Research* **23**, 4462–4472 (2017).

35. Saletta, F. *et al.* Programmed Death-Ligand 1 Expression in a Large Cohort of Pediatric Patients With Solid Tumor and Association With Clinicopathologic Features in Neuroblastoma. *JCO precision oncology* 1–12 (2017) doi:10.1200/PO.16.00049.

36. Gardner, R. A. *et al.* Intent-to-treat leukemia remission by CD19 CAR T cells of defined formulation and dose in children and young adults. *Blood* **129**, 3322–3331 (2017).

37. Lee, D. W. *et al.* T cells expressing CD19 chimeric antigen receptors for acute lymphoblastic leukaemia in children and young adults: a phase 1 dose-escalation trial. *Lancet* **385**, 517 (2015).

38. June, C. H., O'Connor, R. S., Kawalekar, O. U., Ghassemi, S. & Milone, M. C. CAR T cell immunotherapy for human cancer. *Science* **359**, 1361–1365 (2018).

39. Richards, R. M., Sotillo, E. & Majzner, R. G. CAR T Cell Therapy for Neuroblastoma. *Front Immunol* **9**, 2380 (2018).

40. Del Bufalo, F. *et al.* GD2-CART01 for Relapsed or Refractory High-Risk Neuroblastoma. *New England Journal of Medicine* **388**, 1284–1295 (2023).

41. Elsallab, M. & Maus, M. V. Expanding access to CAR T cell therapies through local manufacturing. *Nature Biotechnology 2023* 1–11 (2023) doi:10.1038/s41587-023-01981-8.

42. Hoffmann, P. *et al.* Serial killing of tumor cells by cytotoxic T cells redirected with a CD19-/CD3-bispecific single-chain antibody construct. *Int J Cancer* **115**, 98–104 (2005).

43. Dreier, T. *et al.* Extremely potent, rapid and costimulation-independent cytotoxic T-cell response against lymphoma cells catalyzed by a single-chain bispecific antibody. *Int J Cancer* **100**, 690–697 (2002).

44. Brischwein, K. *et al.* Strictly target cell-dependent activation of T cells by bispecific single-chain antibody constructs of the BiTE class. *J Immunother* **30**, 798–807 (2007).

45. Offner, S., Hofmeister, R., Romaniuk, A., Kufer, P. & Baeuerle, P. A. Induction of regular cytolytic T cell synapses by bispecific single-chain antibody constructs on MHC class I-negative tumor cells. *Mol Immunol* **43**, 763–771 (2006).

46. Blinatumomab: Uses, Interactions, Mechanism of Action | DrugBank Online. https://go.drugbank.com/drugs/DB09052.

47. FDA Approves BLINCYTO™ (Blinatumomab) Immunotherapy for the Treatment of Relapsed or Refractory B-Cell Precursor Acute Lymphoblastic Leukemia| Amgen. https://www.amgen.com/newsroom/press-releases/2014/12/fda-approves-blincyto-blinatumomab-immunotherapy-for-the-treatment-of-relapsed-or-refractory-bcell-precursor-acute-lymphoblastic-leukemia.

48. Locatelli, F. *et al.* Blinatumomab in pediatric relapsed/refractory B-cell acute lymphoblastic leukemia: RIALTO expanded access study final analysis. *Blood Adv* **6**, 1004 (2022).

49. Schlegel, P. *et al.* Pediatric posttransplant relapsed/refractory B-precursor acute lymphoblastic leukemia shows durable remission by therapy with the T-cell engaging bispecific antibody blinatumomab. *Haematologica* **99**, 1212 (2014).

50. Gore, L. *et al.* Survival after blinatumomab treatment in pediatric patients with relapsed/refractory B-cell precursor acute lymphoblastic leukemia. *Blood Cancer Journal 2018 8:9* **8**, 1–7 (2018).

51. Locatelli, F. *et al.* Improved survival and MRD remission with blinatumomab vs. chemotherapy in children with first high-risk relapse B-ALL. *Leukemia 2022 37:1* **37**, 222–225 (2023).

52. Yankelevich, M. *et al.* Phase I study of OKT3 x hu3F8 bispecific antibody (GD2Bi) armed T cells (GD2BATs) in GD2-positive tumors. *Journal of Clinical Oncology* **37**, 2533–2533 (2019).

53. Ellenberg, L. *et al.* Neurocognitive status in long-term survivors of childhood CNS malignancies: a report from the Childhood Cancer Survivor Study. *Neuropsychology* **23**, 705–717 (2009).

54. Elitzur, S. *et al.* Blinatumomab as a bridge to further therapy in cases of overwhelming toxicity in pediatric B-cell precursor acute lymphoblastic leukemia: Report from the Israeli Study Group of Childhood Leukemia. *Pediatr Blood Cancer* **66**, (2019).

55. Blom, T. *et al.* Treatment-Related Toxicities During Anti-GD2 Immunotherapy in High-Risk Neuroblastoma Patients. *Front Oncol* **10**, (2021).

56. Marconi, S. *et al.* Expression of gangliosides on glial and neuronal cells in normal and pathological adult human brain. *J Neuroimmunol* **170**, 115–121 (2005).

57. Hsiau, T. *et al.* Inference of CRISPR Edits from Sanger Trace Data. *bioRxiv* 251082 (2019) doi:10.1101/251082.

58. Collins, M., Ling, V. & Carreno, B. M. The B7 family of immune-regulatory ligands. *Genome Biol* **6**, 223 (2005).

59. CD276 CD276 molecule [Homo sapiens (human)] - Gene - NCBI. https://www.ncbi.nlm.nih.gov/gene/80381.

60. Steinberger, P. *et al.* Molecular Characterization of Human 4Ig-B7-H3, a Member of the B7 Family with Four Ig-Like Domains. *The Journal of Immunology* **172**, 2352–2359 (2004).

61. Sun, M. *et al.* Characterization of Mouse and Human B7-H3 Genes. *The Journal of Immunology* **168**, 6294–6297 (2002).

62. Kontos, F. *et al.* B7-H3: An attractive target for antibody-based immunotherapy. *Clinical Cancer Research* **27**, 1227–1235 (2021).

63. Chen, J. T. *et al.* Glycoprotein B7-H3 overexpression and aberrant glycosylation in oral cancer and immune response. *Proc Natl Acad Sci U S A* **112**, 13057–13062 (2015).

64. Du, H. *et al.* Antitumor Responses in the Absence of Toxicity in Solid Tumors by Targeting B7-H3 via Chimeric Antigen Receptor T Cells. *Cancer Cell* **35**, 221-237.e8 (2019).

65. Majzner, R. G. *et al.* CAR T cells targeting B7-H3, a pan-cancer antigen, demonstrate potent preclinical activity against pediatric solid tumors and brain tumors. *Clinical Cancer Research* (2019) doi:10.1158/1078-0432.CCR-18-0432.

66. Modak, S., Kramer, K., Gultekin, S. H., Guo, H. F. & Cheung, N. K. V. Monoclonal antibody 8H9 targets a novel cell surface antigen expressed by a wide spectrum of human solid tumors. *Cancer Res* **61**, 4048–4054 (2001).

67. Castriconi, R. *et al.* Identification of 4Ig-B7-H3 as a neuroblastoma-associated molecule that exerts a protective role from an NK cell-mediated lysis. *Proc Natl Acad Sci U S A* **101**, 12640 (2004).

68. Zhou, Z. *et al.* B7-H3, a potential therapeutic target, is expressed in diffuse intrinsic pontine glioma. *J Neurooncol* **111**, 257–264 (2013).

69. Zhang, H. *et al.* Survival Association and Cell Cycle Effects of B7H3 in Neuroblastoma. *J Korean Neurosurg Soc* **63**, 707–716 (2020).

70. Tan, W. Q., Chen, G., Ye, M. & Jia, B. Artemether Regulates Chemosensitivity to Doxorubicin via Regulation of B7-H3 in Human Neuroblastoma Cells. *Med Sci Monit* **23**, 4252–4259 (2017).

71. Sokol, E. & Desai, A. V. The Evolution of Risk Classification for Neuroblastoma. *Children (Basel, Switzerland)* **6**(2), 27 (2019).

72. Mejstríková, E. *et al.* CD19-negative relapse of pediatric B-cell precursor acute lymphoblastic leukemia following blinatumomab treatment. *Blood Cancer J* **7**, (2017).

73. Orlando, E. J. *et al.* Genetic mechanisms of target antigen loss in CAR19 therapy of acute lymphoblastic leukemia. *Nat Med* **24**, 1504–1506 (2018).

74. Maude, S. L. *et al.* Tisagenlecleucel in Children and Young Adults with B-Cell Lymphoblastic Leukemia. *N Engl J Med* **378**, 439 (2018).

75. Majzner, R. G. & Mackall, C. L. Tumor Antigen Escape from CAR T-cell Therapy. *Cancer Discov* **8**, 1219–1226 (2018).

76. Dondero, A. *et al.* Original research: Multiparametric flow cytometry highlights B7-H3 as a novel diagnostic/therapeutic target in GD2neg/low neuroblastoma variants. *J Immunother Cancer* **9**, 2293 (2021).

77. Kramer, K. *et al.* Compartmental intrathecal radioimmunotherapy: Results for treatment for metastatic CNS neuroblastoma. *J Neurooncol* **97**, 409–418 (2010).

78. Loo, D. *et al.* Development of an Fc-enhanced anti-B7-H3 monoclonal antibody with potent antitumor activity. *Clinical Cancer Research* **18**, 3834–3845 (2012).

79. Powderly, J. *et al.* Interim results of an ongoing Phase I, dose escalation study of MGA271 (Fc-optimized humanized anti-B7-H3 monoclonal antibody) in patients with refractory B7-H3-expressing neoplasms or neoplasms whose vasculature expresses B7-H3. *J Immunother Cancer* **3**, O8 (2015).

80. Majzner, R. G. *et al.* CAR T Cells Targeting B7-H3, a Pan-Cancer Antigen, Demonstrate Potent Preclinical Activity Against Pediatric Solid Tumors and Brain Tumors. *Clin Cancer Res* **25**, 2560–2574 (2019).

81. Vitanza, N. A. *et al.* Intraventricular B7-H3 CAR T Cells for Diffuse Intrinsic Pontine Glioma: Preliminary First-in-Human Bioactivity and Safety. *Cancer Discov* **13**, 114–131 (2023).

82. Vidarsson, G., Dekkers, G. & Rispens, T. IgG Subclasses and Allotypes: From Structure to Effector Functions. *Front Immunol* **5**, (2014).

83. Schroeder, H. W. & Cavacini, L. Structure and Function of Immunoglobulins. *J Allergy Clin Immunol* **125**, S41 (2010).

84. de Taeye, S. W., Rispens, T. & Vidarsson, G. The Ligands for Human IgG and Their Effector Functions. *Antibodies,* **8**(2), 30 (2019).

85. Ryman, J. T. & Meibohm, B. Pharmacokinetics of Monoclonal Antibodies. *CPT Pharmacometrics Syst Pharmacol* **6**, 576 (2017).

86. Liu, L. Pharmacokinetics of monoclonal antibodies and Fc-fusion proteins. *Protein Cell* **9**, 15 (2018).

87. Lighaam, L. C. & Rispens, T. The Immunobiology of Immunoglobulin G4. *Semin Liver Dis* **36**, 200–215 (2016).

88. Kolfschoten, M. V. D. N. *et al.* Anti-inflammatory activity of human IgG4 antibodies by dynamic Fab arm exchange. *Science* **317**, 1554–1557 (2007).

89. Rispens, T. *et al.* Dynamics of inter-heavy chain interactions in human immunoglobulin G (IgG) subclasses studied by kinetic Fab arm exchange. *J Biol Chem* **289**, 6098–6109 (2014).

90. Brischwein, K. *et al.* MT110: A novel bispecific single-chain antibody construct with high efficacy in eradicating established tumors. *Mol Immunol* **43**, 1129–1143 (2006).

91. Schenk, S., Schoenhals, G. J., de Souza, G. & Mann, M. A high confidence, manually validated human blood plasma protein reference set. *BMC Medical Genomics* **1**, 1–28 (2008).

92. Klinger, M. *et al.* Immunopharmacologic response of patients with B-lineage acute lymphoblastic leukemia to continuous infusion of T cell–engaging CD19/CD3-bispecific BiTE antibody blinatumomab. *Blood* **119**, 6226–6233 (2012).

93. Lee, K. J. *et al.* Clinical use of blinatumomab for B-cell acute lymphoblastic leukemia in adults. *Ther Clin Risk Manag* **12**, 1301 (2016).

94. Moore, P. A. *et al.* Application of dual affinity retargeting molecules to achieve optimal redirected T-cell killing of B-cell lymphoma. *Blood* **117**, 4542–4551 (2011).

95. Campagne, O. *et al.* Integrated pharmacokinetic/pharmacodynamic model of a bispecific cd3xcd123 dart molecule in nonhuman primates: Evaluation of activity and impact of immunogenicity. *Clinical Cancer Research* **24**, 2631–2641 (2018).

96. Liddy, N. *et al.* Monoclonal TCR-redirected tumor cell killing. *Nat Med* **18**, 980–987 (2012).

97. FDA approves tebentafusp-tebn for unresectable or metastatic uveal melanoma | FDA. https://www.fda.gov/drugs/resources-information-approved-drugs/fda-approves-tebentafusp-tebn-unresectable-or-metastatic-uveal-melanoma.

98. Nathan, P. *et al.* Overall Survival Benefit with Tebentafusp in Metastatic Uveal Melanoma. *N Engl J Med* **385**, 1196–1206 (2021).

99. Hua, G., Carlson, D. & Starr, J. R. Tebentafusp-tebn: A Novel Bispecific T-Cell Engager for Metastatic Uveal Melanoma. *J Adv Pract Oncol* **13**, 717–723 (2022).

100. Olivier, T., Haslam, A., Tuia, J. & Prasad, V. Eligibility for Human Leukocyte Antigen–Based Therapeutics by Race and Ethnicity. *JAMA Netw Open* **6**, e2338612–e2338612 (2023).

101. Reusch, U. *et al.* A tetravalent bispecific TandAb (CD19/CD3), AFM11, efficiently recruits T cells for the potent lysis of CD19+ tumor cells. *MAbs* **7**, 584 (2015).

102. Molloy, M. E. *et al.* Preclinical Characterization of HPN536, a Trispecific, T-Cell-Activating Protein Construct for the Treatment of Mesothelin-Expressing Solid Tumors. *Clin Cancer Res* **27**, 1452–1462 (2021).

103. Linke, R., Klein, A. & Seimetz, D. Catumaxomab: Clinical development and future directions. *MAbs* **2**, 129 (2010).

104. Saunders, K. O. Conceptual Approaches to Modulating Antibody Effector Functions and Circulation Half-Life. *Front Immunol* **10**, 1296 (2019).

105. Wang, L., Hoseini, S. S., Xu, H., Ponomarev, V. & Cheung, N. K. Silencing Fc Domains in T cell-Engaging Bispecific Antibodies Improves T-cell Trafficking and Antitumor Potency. *Cancer Immunol Res* **7**, 2003–2024 (2019).

106. Moreau, P. *et al.* Teclistamab in Relapsed or Refractory Multiple Myeloma. *N Engl J Med* **387**, 495–505 (2022).

107. Chari, A. *et al.* Talquetamab, a T-Cell-Redirecting GPRC5D Bispecific Antibody for Multiple Myeloma. *N Engl J Med* **387**, 2232–2244 (2022).

108. Budde, L. E. *et al.* Safety and efficacy of mosunetuzumab, a bispecific antibody, in patients with relapsed or refractory follicular lymphoma: a single-arm, multicentre, phase 2 study. *Lancet Oncol* **23**, 1055–1065 (2022).

109. FDA D.I.S.C.O. Burst Edition: FDA approval of Lunsumio (mosunetuzumab-axgb) for adult patients with relapsed or refractory follicular lymphoma after two or more lines of

systemic therapy | FDA. https://www.fda.gov/drugs/resources-information-approved-drugs/fda-disco-burst-edition-fda-approval-lunsumio-mosunetuzumab-axgb-adult-patients-relapsed-or.

110. FDA grants accelerated approval to glofitamab-gxbm for selected relapsed or refractory large B-cell lymphomas | FDA. https://www.fda.gov/drugs/drug-approvals-and-databases/fda-grants-accelerated-approval-glofitamab-gxbm-selected-relapsed-or-refractory-large-b-cell.

111. FDA grants accelerated approval to epcoritamab-bysp for relapsed or refractory diffuse large B-cell lymphoma and high-grade B-cell lymphoma | FDA. https://www.fda.gov/drugs/drug-approvals-and-databases/fda-grants-accelerated-approval-epcoritamab-bysp-relapsed-or-refractory-diffuse-large-b-cell.

112. Mazor, Y., Blarcom, T. Van, Mabry, R., Iverson, B. L. & Georgiou, G. Isolation of engineered, full-length antibodies from libraries expressed in Escherichia coli. *Nature Biotechnology* **25**, 563–565 (2007).

113. Vendel, M. C. *et al.* Secretion from bacterial versus mammalian cells yields a recombinant scFv with variable folding properties. *Arch Biochem Biophys* **526**, 188–193 (2012).

114. Guglielmi, L. & Martineau, P. Expression of single-chain Fv fragments in E. coli cytoplasm. *Methods Mol Biol* **562**, 215–224 (2009).

115. Wang, R. *et al.* Engineering production of functional scFv antibody in E. coli by co-expressing the molecule chaperone Skp. *Front Cell Infect Microbiol* **3**, (2013).

116. Sonoda, H., Kumada, Y., Katsuda, T. & Yamaji, H. Functional expression of single-chain Fv antibody in the cytoplasm of Escherichia coli by thioredoxin fusion and co-expression of molecular chaperones. *Protein Expr Purif* **70**, 248–253 (2010).

117. Sonoda, H., Kumada, Y., Katsuda, T. & Yamaji, H. Effects of cytoplasmic and periplasmic chaperones on secretory production of single-chain Fv antibody in Escherichia coli. *J Biosci Bioeng* **111**, 465–470 (2011).

118. Mamat, U. *et al.* Detoxifying Escherichia coli for endotoxin-free production of recombinant proteins. *Microb Cell Fact* **14**, (2015).

119. Luo, S. & Zhang, B. Benchmark Glycan Profile of Therapeutic Monoclonal Antibodies Produced by Mammalian Cell Expression Systems. *Pharm Res* **1**, 1–9 (2023).

120. Full Prescribing Information: KIMMTRACK (tebentafusp-tebn) injection, for intravenous use. https://www.accessdata.fda.gov/drugsatfda_docs/label/2022/761228s000lbl.pdf.

121. Kunert, R. & Reinhart, D. Advances in recombinant antibody manufacturing. *Appl Microbiol Biotechnol* **100**, 3451 (2016).

122. Goh, J. B. & Ng, S. K. Impact of host cell line choice on glycan profile. *Crit Rev Biotechnol* **38**, 851–867 (2018).

123. Chung, C. H. *et al.* Cetuximab-Induced Anaphylaxis and IgE Specific for Galactose-α-1,3-Galactose. *N Engl J Med* **358**, 1109 (2008).

124. Bosques, C. J. *et al.* Chinese hamster ovary cells can produce galactose-α-1,3-galactose antigens on proteins. *Nature Biotechnology 2010 28:11* **28**, 1153–1156 (2010).

125. Tan, E., Chin, C. S. H., Lim, Z. F. S. & Ng, S. K. HEK293 Cell Line as a Platform to Produce Recombinant Proteins and Viral Vectors. *Front Bioeng Biotechnol* **9**, (2021).

126. Bandaranayake, A. D. & Almo, S. C. Recent advances in mammalian protein production. *FEBS Lett* **588**, 253 (2014).

127. Segaliny, A. I. *et al.* A high throughput bispecific antibody discovery pipeline. *Communications Biology 2023 6:1* **6**, 1–14 (2023).

128. Misorin, A. K., Chernyshova, D. O. & Karbyshev, M. S. State-of-the-Art Approaches to Heterologous Expression of Bispecific Antibodies Targeting Solid Tumors. *Biochemistry (Moscow) 2023 88:9* **88**, 1215–1231 (2023).

129. Bandaranayake, A. D. *et al.* Daedalus: a robust, turnkey platform for rapid production of decigram quantities of active recombinant proteins in human cell lines using novel lentiviral vectors. doi:10.1093/nar/gkr706.

130. Crook, Z. R. *et al.* Ex silico engineering of cystine-dense peptides yielding a potent bispecific T cell engager. *Sci. Transl. Med* **14**, 402 (2022).

131. Gopalakrishnapillai, A. *et al.* Immunotherapeutic targeting of mesothelin positive pediatric aml using bispecific t cell engaging antibodies. *Cancers (Basel)* **13**, 5964 (2021).

132. Dumont, J., Euwart, D., Mei, B., Estes, S. & Kshirsagar, R. Human cell lines for biopharmaceutical manufacturing: history, status, and future perspectives. *Crit Rev Biotechnol* **36**, 1110 (2016).

133. Krah, S., Kolmar, H., Becker, S. & Zielonka, S. Engineering IgG-Like Bispecific Antibodies—An Overview. *Antibodies* **7**, 28 (2018).

134. Sen, M. *et al.* Use of anti-CD3 x anti-HER2/neu bispecific antibody for redirecting cytotoxicity of activated T cells toward HER2/neu+ tumors. *J Hematother Stem Cell Res* **10**, 247–260 (2001).

135. Gall, J. M., Davol, P. A., Grabert, R. C., Deaver, M. & Lum, L. G. T cells armed with anti-CD3 x anti-CD20 bispecific antibody enhance killing of CD20+ malignant B cells and bypass complement-mediated rituximab resistance in vitro. *Exp Hematol* **33**, 452–459 (2005).

136. Ridgway, J. B. B., Presta, L. G. & Carter, P. 'Knobs-into-holes' engineering of antibody CH3 domains for heavy chain heterodimerization. *Protein Eng* **9**, 617–621 (1996).

137. Merchant, A. M. *et al.* An efficient route to human bispecific IgG. *Nat Biotechnol* **16**, 677–681 (1998).

138. Harris, K. E. *et al.* Sequence-Based Discovery Demonstrates That Fixed Light Chain Human Transgenic Rats Produce a Diverse Repertoire of Antigen-Specific Antibodies. *Front Immunol* **9**, (2018).

139. Bönisch, M. *et al.* Novel CH1:CL interfaces that enhance correct light chain pairing in heterodimeric bispecific antibodies. *Protein Eng Des Sel* **30**, 685–696 (2017).

140. Lewis, S. M. *et al.* Generation of bispecific IgG antibodies by structure-based design of an orthogonal Fab interface. *Nat Biotechnol* **32**, 191–198 (2014).

141. Schaefer, W. *et al.* Immunoglobulin domain crossover as a generic approach for the production of bispecific IgG antibodies. *Proc Natl Acad Sci U S A* **108**, 11187–11192 (2011).

142. Klein, C., Schaefer, W. & Regula, J. T. The use of CrossMAb technology for the generation of bi- and multispecific antibodies. *MAbs* **8**, 1010 (2016).

143. Labrijn, A. F. *et al.* Controlled Fab-arm exchange for the generation of stable bispecific IgG1. *Nat Protoc* **9**, 2450–2463 (2014).

144. Schanzer, J. *et al.* Development of tetravalent, bispecific CCR5 antibodies with antiviral activity against CCR5 monoclonal antibody-resistant HIV-1 strains. *Antimicrob Agents Chemother* **55**, 2369–2378 (2011).

145. Robert, R. *et al.* A fully humanized IgG-like bispecific antibody for effective dual targeting of CXCR3 and CCR6. *PLoS One* **12**, e0184278 (2017).

146. Klein, C. *et al.* Epitope interactions of monoclonal antibodies targeting CD20 and their relationship to functional properties. *MAbs* **5**, 22 (2013).

147. Shim, H. One target, different effects: a comparison of distinct therapeutic antibodies against the same targets. *Exp Mol Med* **43**, 539 (2011).

148. Nami, B., Maadi, H. & Wang, Z. Mechanisms Underlying the Action and Synergism of Trastuzumab and Pertuzumab in Targeting HER2-Positive Breast Cancer. *Cancers (Basel)* **10**, (2018).

149. von Minckwitz, G. *et al.* Adjuvant Pertuzumab and Trastuzumab in Early HER2-Positive Breast Cancer. *N Engl J Med* **377**, 122–131 (2017).

150. Alvarez-Rueda, N. *et al.* A Monoclonal Antibody to O-Acetyl-GD2 Ganglioside and Not to GD2 Shows Potent Anti-Tumor Activity without Peripheral Nervous System Cross-Reactivity. *PLoS One* **6**, e25220 (2011).

151. Bluemel, C. *et al.* Epitope distance to the target cell membrane and antigen size determine the potency of T cell-mediated lysis by BiTE antibodies specific for a large melanoma surface antigen. *Cancer Immunol Immunother* **59**, 1197–1209 (2010).

152. Li, J. *et al.* Membrane-Proximal Epitope Facilitates Efficient T Cell Synapse Formation by Anti-FcRH5/CD3 and Is a Requirement for Myeloma Cell Killing. *Cancer Cell* **31**, 383–395 (2017).

153. Poussin, M. *et al.* Original research: Dichotomous impact of affinity on the function of T cell engaging bispecific antibodies. *J Immunother Cancer* **9**, 2444 (2021).

154. Staflin, K. *et al.* Target arm affinities determine preclinical efficacy and safety of anti-HER2/CD3 bispecific antibody. *JCI Insight* **5**, (2020).

155. Mount, C. W. *et al.* Potent antitumor efficacy of anti-GD2 CAR T-cells in H3K27M+ diffuse midline gliomas. *Nat Med* **24**, 572 (2018).

156. Majzner, R. G., Weber, E. W., Lynn, R. C., Xu, P. & Mackall, C. L. Neurotoxicity Associated with a High-Affinity GD2 CAR—Letter. *Cancer Immunol Res* **6**, 494–495 (2018).

157. Richman, S. A. *et al.* High-Affinity GD2-specific CAR T cells induce fatal encephalitis in a preclinical neuroblastoma model. *Cancer Immunol Res* **6**, 36–46 (2018).

158. Rudnick, S. I. *et al.* Influence of affinity and antigen internalization on the uptake and penetration of Anti-HER2 antibodies in solid tumors. *Cancer Res* **71**, 2250–2259 (2011).

159. Liu, C. Y. *et al.* Structure-based engineering of a novel CD3ε-targeting antibody for reduced polyreactivity. *MAbs* **15**, (2023).

160. Oostindie, S. C., Lazar, G. A., Schuurman, J. & Parren, P. W. H. I. Avidity in antibody effector functions and biotherapeutic drug design. *Nature Reviews Drug Discovery 2022 21:10* **21**, 715–735 (2022).

161. Harms, B. D., Kearns, J. D., Iadevaia, S. & Lugovskoy, A. A. Understanding the role of cross-arm binding efficiency in the activity of monoclonal and multispecific therapeutic antibodies. *Methods* **65**, 95–104 (2014).

162. Slaga, D. *et al.* Avidity-based binding to HER2 results in selective killing of HER2-overexpressing cells by anti-HER2/CD3. *Sci Transl Med* **10**, 5775 (2018).

163. Bacac, M. *et al.* CD20-TCB with Obinutuzumab Pretreatment as Next-Generation Treatment of Hematologic Malignancies. *Clin Cancer Res* **24**, 4785–4797 (2018).

164. Hutchings, M. *et al.* Glofitamab, a Novel, Bivalent CD20-Targeting T-Cell–Engaging Bispecific Antibody, Induces Durable Complete Remissions in Relapsed or Refractory B-Cell Lymphoma: A Phase I Trial. *Journal of Clinical Oncology* **39**, 1959 (2021).

165. Santich, B. H. *et al.* Interdomain spacing and spatial configuration drive the potency of IgG-[L]-scFv T cell bispecific antibodies. *Sci Transl Med* **12**, 1315 (2020).

166. Kjer-Nielsen, L. *et al.* Crystal structure of the human T cell receptor CD3 epsilon gamma heterodimer complexed to the therapeutic mAb OKT3. *Proc Natl Acad Sci U S A* **101**, 7675–7680 (2004).

167. Adair, J. R. *et al.* Humanization of the murine anti-human CD3 monoclonal antibody OKT3. *Hum Antibodies Hybridomas* **5**, 41–7 (1994).

168. Law, C. L. *et al.* Expression and characterization of recombinant soluble human CD3 molecules: presentation of antigenic epitopes defined on the native TCR–CD3 complex. *Int Immunol* **14**, 389–400 (2002).

169. Segaliny, A. I. *et al.* A high throughput bispecific antibody discovery pipeline. *Commun Biol* **6**, (2023).

170. Dreier, T. *et al.* Extremely potent, rapid and costimulation-independent cytotoxic T-cell response against lymphoma cells catalyzed by a single-chain bispecific antibody. *Int J Cancer* **100**, 690–697 (2002).

171. Xu, H. *et al.* Retargeting T cells to GD2 pentasaccharide on human tumors using bispecific humanized antibody. *Cancer Immunol Res* **3**, 266 (2015).

172. Park, J. A. & Cheung, N. K. V. GD2 or HER2 targeting T cell engaging bispecific antibodies to treat osteosarcoma. *J Hematol Oncol* **13**, (2020).

173. Lopez-Albaitero, A. *et al.* Overcoming resistance to HER2-targeted therapy with a novel HER2/CD3 bispecific antibody. *Oncoimmunology* **6**, (2017).

174. Hoseini, S. S., Guo, H., Wu, Z., Hatano, M. N. & Cheung, N. K. V. A potent tetravalent T-cell-engaging bispecific antibody against CD33 in acute myeloid leukemia. *Blood Adv* **2**, 1250–1258 (2018).

175. Wu, Z., Guo, H. F., Xu, H. & Cheung, N. K. V. Development of a Tetravalent Anti-GPA33/Anti-CD3 Bispecific Antibody for Colorectal Cancers. *Mol Cancer Ther* **17**, 2164–2175 (2018).

176. Boune, S., Hu, P., Epstein, A. L. & Khawli, L. A. Principles of N-Linked Glycosylation Variations of IgG-Based Therapeutics: Pharmacokinetic and Functional Considerations. *Antibodies* **9**, 1–20 (2020).

177. Hay, Z. L. Z. & Slansky, J. E. Granzymes: The Molecular Executors of Immune-Mediated Cytotoxicity. *Int J Mol Sci* **23**, 1833 (2022).

178. Abbas, A. K., Lichtman, A. H. & Pillai, S. Differentiation and Functions of CD8 + Effector T Cells. *Cellular and Molecular Immunology* 251–259 (Elsevier Inc., 2022).

179. Pfosser, A., Brandl, M., Salih, H., Grosse-Hovest, L. & Jung, G. Role of Target Antigen in Bispecific-Antibody-Mediated Killing of Human Glioblastoma Cells: A Pre-Clinical Study. *J. Cancer* **80**, 612–616 (1999).

180. Fukuda, N. *et al.* Role of the mobility of antigen binding site in high affinity antibody elucidated by surface plasmon resonance. *The Journal of Biochemistry* **161**, 37–43 (2017).

181. Ahmedy, M., Chengy, M., Cheung, I. Y. & Cheung, N. K. V. Human derived dimerization tag enhances tumor killing potency of a T-cell engaging bispecific antibody. *Oncoimmunology* **4**, (2015).

182. Slaga, D. *et al.* Avidity-based binding to HER2 results in selective killing of HER2-overexpressing cells by anti-HER2/CD3. *Sci Transl Med* **10**, (2018).

183. Abrams, H. R., Leeds, H. S., Russell, H. V. & Hellsten, M. B. Factors Influencing Family Burden in Pediatric Hematology/Oncology Encounters. *J Patient Cent Res Rev* **6**, 243 (2019).

184. Bojilova-Dor, L. *et al.* Successful Outpatient Administration of Blinatumomab Infusion in Pediatric Patients with Acute Lymphoblastic Leukemia. *Blood* **138**, 4028–4028 (2021).

185. McCall, C. *et al.* Administration of Home Intravenous Chemotherapy to Children by their Parents. *J Pediatr Oncol Nurs* **34**, 122–129 (2017).

186. Kebenko, M. *et al.* A multicenter phase 1 study of solitomab (MT110, AMG 110), a bispecific EpCAM/CD3 T-cell engager (BiTE®) antibody construct, in patients with refractory solid tumors. *Oncoimmunology* **7**, (2018).

187. Park, J. A., Santich, B. H., Xu, H., Lum, L. G. & Cheung, N.-K. V. Potent ex vivo armed T cells using recombinant bispecific antibodies for adoptive immunotherapy with reduced cytokine release. *J Immunother Cancer* **9**, 2222 (2021).

188. Xu, H. *et al.* Retargeting T cells to GD2 pentasaccharide on human tumors using Bispecific humanized antibody. *Cancer Immunol Res* **3**, 266–277 (2015).

189. Schumacher-Kuckelkorn, R. *et al.* Lack of immunocytological GD2 expression on neuroblastoma cells in bone marrow at diagnosis, during treatment, and at recurrence. *Pediatr Blood Cancer* **64**, 46–56 (2017).

190. Sapski, S., Beha, N., Kontermann, R. E. & Müller, D. Influence of antigen density and immunosuppressive factors on tumor-targeted costimulation with antibody-fusion proteins and bispecific antibody-mediated T cell response. *Cancer Immunology, Immunotherapy* **69**, 2291 (2020).

191. Berard, M. & Tough, D. F. Qualitative differences between naïve and memory T cells. *Immunology* **106**, 127 (2002).

192. Abbas, A. K., Lichtman, A. H. & Pillai, S. Activation of T Lymphocytes. *Cellular and Molecular Immunology* 217–232 (Elsevier, 2022).

193. López-Cabrera, M. *et al.* Molecular cloning, expression, and chromosomal localization of the human earliest lymphocyte activation antigen AIM/CD69, a new member of the C-type animal lectin superfamily of signal-transmitting receptors. *J Exp Med* **178**, 537–548 (1993).

194. Holling, T. M., Schooten, E. & Van Den Elsen, P. J. Function and regulation of MHC class II molecules in T-lymphocytes: Of mice and men. *Hum Immunol* **65**, 282–290 (2004).

195. Rea, I. M., McNerlan, S. E. & Alexander, H. D. CD69, CD25, and HLA-DR activation antigen expression on CD3+ lymphocytes and relationship to serum TNF-alpha, IFN-gamma, and sIL-2R levels in aging. *Exp Gerontol* **34**, 79–93 (1999).

196. Taams, L. S., Van Eden, W. & Wauben, M. H. M. Antigen presentation by T cells versus professional antigen-presenting cells (APC): differential consequences for T cell activation and subsequent T cell-APC interactions. *Eur J Immunol* **29**, 1543-50 (1999) doi:10.1002/(SICI)1521-4141(199905)29:05<1543::AID-IMMU1543>3.0.CO;2-R.

197. Tay, R. E., Richardson, E. K. & Toh, H. C. Revisiting the role of CD4+ T cells in cancer immunotherapy—new insights into old paradigms. *Cancer Gene Therapy 2020 28:1* **28**, 5–17 (2020).

198. Abbas, A. K., Lichtman, A. H. & Pillai, S. Differentiation and Functions of CD4 + Effector T Cells. *Cellular and Molecular Immunology* 233–250 (Elsevier Inc., 2022).

199. Knutson, K. L. & Disis, M. L. Tumor antigen-specific T helper cells in cancer immunity and immunotherapy. *Cancer Immunol Immunother* **54**, 721–728 (2005).

200. Haabeth, O. A. W. *et al.* Inflammation driven by tumour-specific Th1 cells protects against B-cell cancer. *Nature Communications 2011 2:1* **2**, 1–12 (2011).

201. Mehta, A. K., Gracias, D. T. & Croft, M. TNF activity and T cells. *Cytokine* **101**, 14–18 (2018).

202. Fajgenbaum, D. C. & June, C. H. Cytokine Storm. *New England Journal of Medicine* **383**, 2255–2273 (2020).

203. L, C. *et al.* Systemic reaction to the anti-T-cell monoclonal antibody OKT3 in relation to serum levels of tumor necrosis factor and interferon-gamma [corrected]. *N Engl J Med* **320**, 1420–1421 (1989).

204. Chatenoud, L., Ferran, C. & Bach, J. F. The anti-CD3-induced syndrome: A consequence of massive in vivo cell activation. *Curr Top Microbiol Immunol* **174**, 121–134 (1991).

205. Gaston, R. S. *et al.* OKT3 first-dose reaction: Association with T cell subsets and cytokine release. *Kidney Int* **39**, 141–148 (1991).

206. Lee, D. W. *et al.* Current concepts in the diagnosis and management of cytokine release syndrome. *Blood* **124**, 188–195 (2014).

207. Suntharalingam, G. *et al.* Cytokine Storm in a Phase 1 Trial of the Anti-CD28 Monoclonal Antibody TGN1412. *New England Journal of Medicine* **355**, 1018–1028 (2006).

208. Topp, M. S. *et al.* Safety and activity of blinatumomab for adult patients with relapsed or refractory B-precursor acute lymphoblastic leukaemia: a multicentre, single-arm, phase 2 study. *Lancet Oncol* **16**, 57–66 (2015).

209. Teachey, D. T. *et al.* Cytokine release syndrome after blinatumomab treatment related to abnormal macrophage activation and ameliorated with cytokine-directed therapy. *Blood* **121**, 5154–5157 (2013).

210. FDA approval brings first gene therapy to the United States. https://www.fda.gov/news-events/press-announcements/fda-approval-brings-first-gene-therapy-united-states?source=govdelivery&utm_medium=email&utm_source=govdelivery (2017).

211. Philipp, N. *et al.* T-cell exhaustion induced by continuous bispecific molecule exposure is ameliorated by treatment-free intervals. *Blood* **140**, 1104–1118 (2022).

212. Giraldo, N. A. *et al.* The clinical role of the TME in solid cancer. *British Journal of Cancer* **120**, 45–53 (2018).

213. Paresishvili, T. & Kakabadze, Z. Challenges and Opportunities Associated With Drug Delivery for the Treatment of Solid Tumors. *Oncol Rev* **17**, 10577 (2023).

214. Dvorak, H. F. Tumors: Wounds That Do Not Heal. *New England Journal of Medicine* **315**, 1650–1659 (1986). *doi:10.1056/NEJM198612253152606*

215. Salmon, H. *et al.* Matrix architecture defines the preferential localization and migration of T cells into the stroma of human lung tumors. *J Clin Invest* **122**, 899–910 (2012).

216. Labani-Motlagh, A., Ashja-Mahdavi, M. & Loskog, A. The Tumor Microenvironment: A Milieu Hindering and Obstructing Antitumor Immune Responses. *Front Immunol* **11**, 940 (2020).

217. Park, J. A., Wang, L. & Cheung, N.-K. V. Modulating tumor infiltrating myeloid cells to enhance bispecific antibody-driven T cell infiltration and anti-tumor response. *J Hematol Oncol* **14**, 142 (2021).

218. Belmontes, B. *et al.* Immunotherapy combinations overcome resistance to bispecific T cell engager treatment in T cell–cold solid tumors. *Sci Transl Med* **13**, 1524 (2021).

219. Li, J. *et al.* IFNγ-induced Chemokines Are Required for CXCR3-mediated T-Cell Recruitment and Antitumor Efficacy of Anti-HER2/CD3 Bispecific Antibody. *Clin Cancer Res* **24**, 6447–6458 (2018).

220. Köhnke, T., Krupka, C., Tischer, J., Knösel, T. & Subklewe, M. Increase of PD-L1 expressing B-precursor ALL cells in a patient resistant to the CD19/CD3-bispecific T cell engager antibody blinatumomab. *J Hematol Oncol* **8**, (2015).

221. Majzner, R. G. *et al.* Assessment of programmed death-ligand 1 expression and tumor-associated immune cells in pediatric cancer tissues. *Cancer* **123**, 3807–3815 (2017).

222. Bruno, G. *et al.* β3-adrenergic receptor on tumor-infiltrating lymphocytes sustains IFN-γ-dependent PD-L1 expression and impairs anti-tumor immunity in neuroblastoma. *Cancer Gene Therapy 2023 30:6* **30**, 890–904 (2023).

223. Heczey, A. *et al.* CAR T Cells Administered in Combination with Lymphodepletion and PD-1 Inhibition to Patients with Neuroblastoma. *Mol Ther* **25**, 2214–2224 (2017).

224. Jorgovanovic, D., Song, M., Wang, L. & Zhang, Y. Roles of IFN-γ in tumor progression and regression: a review. *Biomarker Research 2020 8:1* **8**, 1–16 (2020).

225. Garcia-Diaz, A. *et al.* Interferon Receptor Signaling Pathways Regulating PD-L1 and PD-L2 Expression. *Cell Rep* **19**, 1189 (2017).

226. Crane, C. A. *et al.* PI(3) kinase is associated with a mechanism of immunoresistance in breast and prostate cancer. *Oncogene* **28**, 306–312 (2009).

227. Doi, T. *et al.* The JAK/STAT pathway is involved in the upregulation of PD-L1 expression in pancreatic cancer cell lines. *Oncol Rep* **37**, 1545–1554 (2017).

228. Tekautz, T. M. *et al.* Evaluation of IFN-γ effects on apoptosis and gene expression in neuroblastoma—Preclinical studies. *Biochimica et Biophysica Acta (BBA) - Molecular Cell Research* **1763**, 1000–1010 (2006).

229. Hu, X. & Ivashkiv, L. B. Cross-regulation of Signaling and Immune Responses by IFN-γ and STAT1. *Immunity* **31**, 539 (2009).

230. Krause, C. D., He, W., Kotenko, S. & Pestka, S. Modulation of the activation of Stat1 by the interferon-γ receptor complex. *Cell Research 2006 16:1* **16**, 113–123 (2006).

231. Zeine, R. *et al.* Presence Of Cancer-Associated Fibroblasts Inversely Correlates With Schwannian Stroma In Neuroblastoma Tumors. *Mod Pathol* **22**, 950 (2009).

232. Liu, K. X. & Joshi, S. “Re-educating” Tumor Associated Macrophages as a Novel Immunotherapy Strategy for Neuroblastoma. *Front Immunol* **11**, 1947 (2020).

233. Asgharzadeh, S. *et al.* Clinical significance of tumor-associated inflammatory cells in metastatic neuroblastoma. *J Clin Oncol* **30**, 3525–3532 (2012).

234. Coughlin, C. M. *et al.* Immunosurveillance and survivin-specific T-cell immunity in children with high-risk neuroblastoma. *J Clin Oncol* **24**, 5725–34 (2006).

235. Carlson, L.-M. *et al.* The microenvironment of human neuroblastoma supports the activation of tumor-associated T lymphocytes. *Oncoimmunology* **2**, e23618 (2013).

236. Mina, M. *et al.* Tumor-infiltrating T lymphocytes improve clinical outcome of therapy-resistant neuroblastoma. *Oncoimmunology* **4**, e1019981 (2015).

237. Martin, R. F. & Beckwith, J. B. Lymphoid infiltrates in neuroblastomas: their occurrence and prognostic significance. *J Pediatr Surg* **3**, 161–4 (1968).

238. Lauder, I. & Aherne, W. The significance of lymphocytic infiltration in neuroblastoma. *Br J Cancer* **26**, 321–30 (1972).

239. Inamura, K. *et al.* Tumor B7-H3 (CD276) expression and smoking history in relation to lung adenocarcinoma prognosis. *Lung Cancer* **103**, 44–51 (2017).

240. Mao, Y. *et al.* Cancer cell-expressed B7-H3 regulates the differentiation of tumor-associated macrophages in human colorectal carcinoma. *Oncol Lett* **14**, 6177 (2017).

241. Chapoval, A. I. *et al.* B7-H3: a costimulatory molecule for T cell activation and IFN-gamma production. *Nat Immunol* **2**, 269–274 (2001).

242. Vitale, C., Bottino, C. & Castriconi, R. Monocyte and Macrophage in Neuroblastoma: Blocking Their Pro-Tumoral Functions and Strengthening Their Crosstalk with Natural Killer Cells. *Cells* **12**, 885 (2023).

243. Asgharzadeh, S. *et al.* Prognostic significance of gene expression profiles of metastatic neuroblastomas lacking MYCN gene amplification. *J Natl Cancer Inst* **98**, 1193–1203 (2006).

244. Barkal, A. A. *et al.* CD24 signalling through macrophage Siglec-10 is a target for cancer immunotherapy. *Nature* **572** 392-396 (2019). doi:10.1038/s41586-019-1456-0.

245. Gholamin, S. *et al.* Disrupting the CD47-SIRPα anti-phagocytic axis by a humanized anti-CD47 antibody is an efficacious treatment for malignant pediatric brain tumors. *Sci Transl Med* **9**, (2017).

246. Advani, R. *et al.* CD47 Blockade by Hu5F9-G4 and Rituximab in Non-Hodgkin’s Lymphoma. *N Engl J Med* **379**, 1711–1721 (2018).

247. Majeti, R. *et al.* CD47 Is an Adverse Prognostic Factor and Therapeutic Antibody Target on Human Acute Myeloid Leukemia Stem Cells. *Cell* **138**, 286–299 (2009).

248. Barkal, A. A. *et al.* Engagement of MHC class I by the inhibitory receptor LILRB1 suppresses macrophages and is a target of cancer immunotherapy. *Nat Immunol* **19**, 76–84 (2018).

249. Gordon, S. R. *et al.* PD-1 expression by tumour-associated macrophages inhibits phagocytosis and tumour immunity. *Nature* **545**, 495–499 (2017).

250. Majores, M. *et al.* Membranous CD24 expression as detected by the monoclonal antibody SWA11 is a prognostic marker in non-small cell lung cancer patients. *BMC Clin Pathol* **15**, 19 (2015).

251. Odstrcil, M. S., Lee, C. J., Sobieski, C., Weisdorf, D. & Couriel, D. Access to CAR T-cell therapy: Focus on diversity, equity and inclusion. *Blood Rev* **64**,101136 (2023) doi:10.1016/J.BLRE.2023.101136.

252. Kendsersky, N. M. *et al.* The B7-H3-Targeting Antibody-Drug Conjugate m276-SL-PBD Is Potently Effective Against Pediatric Cancer Preclinical Solid Tumor Models. *Clin Cancer Res* **27**, 2938–2946 (2021).

253. Modak, S., Kramer, K., Gultekin, S. H., Guo, H. F. & Cheung, N. K. Monoclonal antibody 8H9 targets a novel cell surface antigen expressed by a wide spectrum of human solid tumors. *Cancer Res* **61**, 4048–54 (2001).

254. Pulido, R. & Nunes-Xavier, C. E. Hopes on immunotherapy targeting B7-H3 in neuroblastoma. *Transl Oncol* **27**, 101580 (2023).

255. Veenstra, R. G. *et al.* B7-H3 expression in donor T cells and host cells negatively regulates acute graft-versus-host disease lethality. *Blood* **125**, 3335–3346 (2015).

256. Runcie, K., Budman, D. R., John, V. & Seetharamu, N. Bi-specific and tri-specific antibodies- the next big thing in solid tumor therapeutics. *Mol Med* **24**, (2018).

257. Huang, S., van Duijnhoven, S. M. J., Sijts, A. J. A. M. & van Elsas, A. Bispecific antibodies targeting dual tumor-associated antigens in cancer therapy. *J Cancer Res Clin Oncol* **146**, 3111–3122 (2020).

258. Chang, C. *et al.* Abstract 356: Novel conditionally active biologic (CAB) antibody targeting EpCAM demonstrates anti-tumor efficacy in vivo. *Cancer Res* **79**, 356–356 (2019).

259. Minogue, E. *et al.* Redirecting T-Cells Against AML in a Multidimensional Targeting Space Using T-Cell Engaging Antibody Circuits (TEAC). *Blood* **134**, 2653–2653 (2019).

260. Panchal, A. *et al.* COBRA™: a highly potent conditionally active T cell engager engineered for the treatment of solid tumors. *MAbs* **12**, (2020).

261. Santich, B. H. *et al.* A Self-Assembling and Disassembling (SADA) Bispecific Antibody (BsAb) Platform for Curative Two-step Pretargeted Radioimmunotherapy. *Clin Cancer Res* **27**, 532–541 (2021).

262. Haber, L. *et al.* Generation of T-cell-redirecting bispecific antibodies with differentiated profiles of cytokine release and biodistribution by CD3 affinity tuning. *Scientific Reports 2021 11:1* **11**, 1–17 (2021).

263. Straathof, K. *et al.* Antitumor activity without on-target off-tumor toxicity of GD2-chimeric antigen receptor T cells in patients with neuroblastoma. *Sci Transl Med* **12**, (2020).

264. Louis, C. U. *et al.* Antitumor activity and long-term fate of chimeric antigen receptor-positive T cells in patients with neuroblastoma. *Blood* **118**, 6050–6056 (2011).

265. Heczey, A. *et al.* CAR T Cells Administered in Combination with Lymphodepletion and PD-1 Inhibition to Patients with Neuroblastoma. *Mol Ther* **25**, 2214–2224 (2017).

266. Pule, M. A. *et al.* Virus-specific T cells engineered to coexpress tumor-specific receptors: persistence and antitumor activity in individuals with neuroblastoma. *Nat Med* **14**, 1264–1270 (2008).

267. Tumino, N. *et al.* Polymorphonuclear myeloid-derived suppressor cells impair the anti-tumor efficacy of GD2.CAR T-cells in patients with neuroblastoma. *J Hematol Oncol* **14**, 1–7 (2021).

268. Li, F. *et al.* Factors of Recurrence After Complete Response in Children with Neuroblastoma: A 16-Year Retrospective Study of 179 Cases. *Cancer Manag Res* **14**, 107 (2022).

269. Pocaterra, A., Catucci, M. & Mondino, A. Adoptive T cell therapy of solid tumors: time to team up with immunogenic chemo/radiotherapy. *Curr Opin Immunol* **74**, 53–59 (2022).

270. Lechner, M. G., Russell, S. M., Bass, R. S. & Epstein, A. L. Chemokines, costimulatory molecules and fusion proteins for the immunotherapy of solid tumors. *Immunotherapy* **3**, 1317 (2011).

271. Challita-Eid, P. M. *et al.* A RANTES-antibody fusion protein retains antigen specificity and chemokine function. *J Immunol* **161**, 3729–36 (1998).

272. Mackall, C. L. *et al.* Age, thymopoiesis, and CD4+ T-lymphocyte regeneration after intensive chemotherapy. *N Engl J Med* **332**, 143–149 (1995).

273. Haining, W. N. *et al.* Antigen-specific T-cell memory is preserved in children treated for acute lymphoblastic leukemia. *Blood* **106**, 1749–1754 (2005).

274. Barr, K. M., Jing, W., Hallett, W. H. D., Gershan, J. A. & Johnson, B. D. Examining T cells at vaccine sites of tumor-bearing hosts provides insights to dysfunctional T-cell immunity. *J Immunother* **36**, 41–51 (2013).

275. Ollé Hurtado, M. *et al.* Tumor infiltrating lymphocytes expanded from pediatric neuroblastoma display heterogeneity of phenotype and function. *PLoS One* **14**, e0216373 (2019).

276. ClinicalTrials.gov. https://clinicaltrials.gov (December 1, 2023).

277. The Antibody Society. Therapeutic monoclonal antibodies approved or in regulatory review. (December 10, 2023); www.antibodysociety.org/resources/approved-antibodies.